Journal of
Polymer Materials

Tech Science Press

http://doi.org/10.32604/jpm.2026.084908

REVIEW

# Ion-Imprinted Polymer and Hydrogel for Lithium and Uranium Recovery from Seawater: Fabrication, Properties and Applications

**Jianrui Wang[1], Mahshab Sheraz[1], Rui Wang[1,*], Martin Pipíška[2] and Vladimír Frišták[2]**

[1]School of Environmental Science & Engineering, Shandong University, Qingdao, China
[2]Department of Chemistry, Faculty of Education, Trnava University in Trnava, Priemyselná 4, Trnava, Slovak Republic
*Corresponding Author: Rui Wang. Email: wangrui@sdu.edu.cn

Received: 01 May 2026; Accepted: 27 July 2026; Published: 24 September 2026

**ABSTRACT:** The selective recovery of lithium and uranium from seawater has attracted growing attention due to their strategic importance in energy storage (lithium) and nuclear power (uranium), as well as the vast yet underutilized marine reserves of these elements. However, their extraction remains highly challenging because of their ultra-low concentrations, the overwhelming abundance of competing ions, and the complexity of seawater chemistry. In this context, ion-imprinted polymers (IIPs) and ion-imprinted hydrogels (IIHs) have emerged as promising platforms owing to their target-specific recognition sites, tunable structures, and potential for selective adsorption in complex aqueous systems. This review provides a comprehensive overview of recent advances in IIPs and IIHs for lithium and uranium recovery from seawater, with emphasis on fabrication principles, structure-performance relationships, and practical applications. The fundamental concepts of ion imprinting are first discussed, including template selection, functional monomers and ligands, cross-linkers, initiators, porogens, and advanced strategies such as surface imprinting, stimuli-responsive imprinting, multi-component imprinting, click chemistry, and microwave-assisted synthesis. The review then examines the unique characteristics of ion-imprinted hydrogels, particularly their hydrated networks, diffusion-friendly structures, and stimuli-responsive behavior. Subsequently, lithium- and uranium-selective imprinted materials are critically analyzed in terms of preparation conditions, adsorption mechanisms, selectivity, regeneration, and performance under realistic seawater conditions. Current limitations, including insufficient selectivity in high-salinity environments, structural instability, limited real seawater validation, and lack of standardized evaluation protocols, are also highlighted. Finally, future perspectives are proposed, focusing on advanced ligand design, multifunctional and anti-fouling materials, intelligent responsive systems, and interdisciplinary approaches to accelerate the development of efficient and scalable seawater resource recovery technologies.

**KEYWORDS:** Ion-imprinted polymers; ionic hydrogels; lithium extraction from seawater; uranium extraction from seawater; selective adsorption

## 1 Introduction

The growing demand for strategic metal resources has intensified interest in unconventional and sustainable feedstocks for metal recovery. Among these, seawater represents an enormous yet underutilized reservoir of valuable ions, including lithium and uranium, whose secure supply is increasingly important for energy storage technologies and nuclear energy systems, respectively. Lithium is indispensable formodern rechargeable batteries, electric vehicles, and grid-scale energy storage, whereas uranium remains the cornerstone fuel for nuclear power generation. Although terrestrial ores and continental brines remain the primary commercial sources, geopolitical constraints, uneven resource distribution, environmental

burdens of mining, and rising demand have driven the search for alternative resources [1]. In this context, seawater has emerged as a particularly attractive long-term resource because of its vast volume, continuous replenishment, and globally distributed availability.

However, direct extraction of lithium at 0.1–0.2 ppm and uranium at about 3.3 ppb from seawater is extremely challenging. Uranium predominantly exists as stable carbonate complexes under marine conditions [2]. Seawater also contains a large excess of competing ions such as $Na^+$, $K^+$, $Mg^{2+}$, $Ca^{2+}$, together with dissolved organic matter and fluctuating pH and salinity [3]. These factors severely limit conventional adsorbents, which suffer from insufficient selectivity, slow kinetics, poor regeneration and strong interference from coexisting ions. Therefore, the key challenge is not simply to adsorb a target ion, but to selectively recognize and recover it from an extremely dilute and chemically complex matrix.

Ion-imprinted materials have attracted increasing attention as a promising solution to this challenge because they provide target-specific recognition sites generated through template-directed synthesis [4]. In ion-imprinted polymers (IIPs), the target ion is used as a template during polymerization to organize functional monomers and ligands into a complementary coordination environment; after template removal, the resulting cavities possess structural and chemical affinity toward the target ion in terms of size, charge, and coordination geometry [5]. This feature enables IIPs to achieve higher selectivity than conventional adsorbents, particularly in systems where the target ion must compete with a large excess of chemically similar species. More recently, ion-imprinted hydrogels (IIHs) have emerged as an important extension of this concept [6,7]. By combining ion imprinting with a hydrated and stimuli-responsive polymer network, IIHs can offer additional advantages, including enhanced ion diffusion, tunable swelling behavior, easier regeneration, and, in some cases, direct coupling between ion recognition and macroscopic responses such as volume change or optical signaling [8]. As a result, IIPs and IIHs are increasingly regarded as two complementary material platforms for selective ion capture, separation, and sensing in complex aqueous systems [9].

Considerable progress has been made in the design of ion-imprinted materials for metal-ion separation, including advances in functional monomer design, ligand selection, crosslinking chemistry, polymerization routes, surface imprinting, stimuli-responsive systems, and hybrid architectures [4]. Nevertheless, several major limitations still hinder practical deployment for seawater lithium and uranium recovery [10]. For lithium systems, key issues include low adsorption capacity in real seawater, incomplete discrimination against high-concentration competing ions, and insufficient understanding of how preparation variables and operating conditions jointly affect selectivity [11]. For uranium systems, additional complexity arises from the fact that uranium in seawater mainly exists as carbonate-coordinated species rather than simple uranyl cations, which fundamentally changes the recognition problem and imposes stricter requirements on template design, ligand chemistry, and matrix stability. Moreover, differences in testing protocols, performance metrics, regeneration criteria, and simulated versus real seawater conditions often make it difficult to compare materials across studies and to identify genuinely promising systems [4].

Although a number of reviews have discussed ion-imprinted polymers in general metal-ion recovery, a focused and comparative analysis of ion-imprinted polymers and ion-imprinted hydrogels for lithium and uranium recovery from seawater remains limited. In particular, the relationships among fabrication strategy, structural design, ion-recognition mechanism, adsorption behavior, selectivity, regeneration, and real-system applicability have not yet been systematically integrated across these two target metals and the two major classes of imprinted materials. A critical review is therefore needed to clarify how imprinting concepts are being adapted to seawater conditions, where the recognition chemistry for lithium and uranium

differs substantially, and where hydrogels may offer both opportunities and additional constraints relative to conventional polymer matrices [4,12–15].

In this review, we summarize the fundamental principles, fabrication strategies, and representative architectures of ion-imprinted polymers and ion-imprinted hydrogels, with particular emphasis on their application to lithium and uranium recovery from seawater. We first discuss the preparation basis of ion-imprinted materials, including template selection, functional monomers and ligands, crosslinkers, initiators, porogens, and advanced imprinting strategies. We then examine the fundamentals and fabrication routes of ion-imprinted hydrogels as an emerging class of selective recognition media. Subsequently, we critically evaluate lithium- and uranium-selective imprinted materials in terms of preparation conditions, adsorption mechanisms, operating parameters, selectivity toward competing ions, elution behavior, regeneration performance, and current limitations in real seawater systems. Finally, we identify technical and economic feasibility and commercial prospects major controversies, unresolved issues, and future directions for the rational design of next-generation imprinted materials capable of efficient, selective, and scalable metal recovery from seawater.

## 2 Fundamentals of Ion-Imprinted Polymers and Ion-Imprinted Hydrogels: Fabrication Strategies

Ion-imprinted polymers (IIPs) and ion-imprinted hydrogels (IIHs) are advanced artificial recognition media that are carefully designed to exhibit selective affinity for specific metal ions via template-dependent polymerization [11]. These materials, by crippling the spatial arrangement of coordinating functional groups in the immediate surroundings of a target ion, form ion-specific binding cavities which tightly recapitulate the size, coordination, and charge density of the template ion [16]. This outstanding structural specificity makes ion-imprinting highly appealing for the selective recovery of trace levels of lithium and uranium in the complex seawater environment, where alkali, alkaline-earth, and transition-metal ions are much more common [17,18].

### *2.1 Fundamental Principles of Ion Imprinting*

The interaction of the monomer functional groups with the template is one of the major factors that contributes to a metal ion's successful binding and its ability to remain selective for the imprinted material. The template interaction mechanism depends on the type of bonding between the monomers. It involves two main strategies: covalent and non-covalent. Imprinted ion-selective polymers (IIPs) are produced using a template, functional monomers, crosslinking agents, porogens, and initiators [19]. The selective decisions and proportional correlations of these parts are crucial for maximizing selectivity and binding capacity, and they ultimately determine the physical and chemical properties of the final IIP [20,21].

In the pre-organization phase, the target ion interacts with functional monomers via coordination bonds, electrostatic interactions, hydrogen bonding, or chelation. The interactions delineate the spatial configuration of binding sites in proximity to the ion. The subsequent polymerization stabilizes this configuration within a rigid or semi-flexible matrix. Upon template extraction, ion-specific cavities remain, which selectively rebind the target ion despite the presence of excess competing species. In the context of seawater extraction applications, the efficacy of ion imprinting depends on several critical factors, including selectivity, binding kinetics, diffusion efficiency, and structural stability. These parameters are significantly affected by the chosen fabrication strategy [22–24].

### *2.2 IIP Preparation Components*

To achieve optimal IIPs, it is essential to optimize various components and reagents, particularly templates, functional monomers and ligands, cross-linkers, initiators, and porogens. Their classifications and corresponding ratios may influence recognition selectivity and binding capacities. The subsequent sections will provide a brief introduction to certain general characteristics of the IIPs.

#### *2.2.1 Templates*

Template selection is critical for IIP synthesis. Key requirements include the following [4,25,26]: the template must be non-reactive during polymerization and cross-linking; its functional groups must not interfere with monomer reactivity; it should be cost-effective for scalability; and it must remain stable under synthesis conditions such as elevated temperature or ultraviolet radiation.

#### *2.2.2 Ligand-Based Functional Monomers for Ion Imprinting*

The selection of an appropriate functional monomer aims to provide a functional group capable of covalently or non-covalently binding to template ions, while ensuring the presence of end groups for linkage to cross-linkers to achieve three-dimensional pore-structured polymers. The molar ratio between monomer and template directly influences the affinity of imprinted polymers (IIPs) [27,28]. This determines the precision and specificity of recognition sites. Fig. 1 presents the structures of several typical functional monomers, including acrylic acid (AA), methacrylic acid (MAA), and vinyl pyridine (VP) [28].

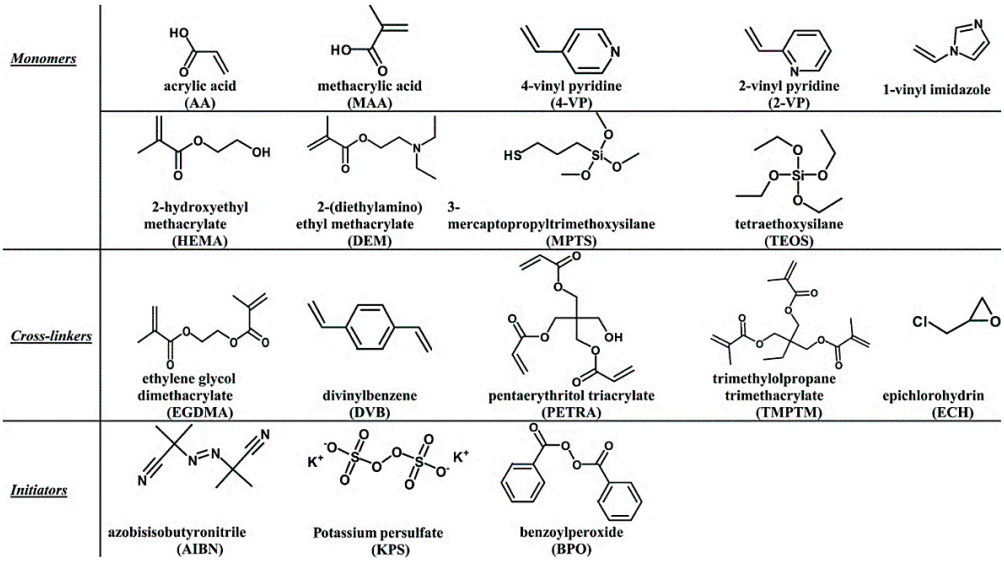


**Figure 1:** Structures of common functional monomers, cross-linkers and initiators. Reprinted with permission from reference [16]. Copyright 2012, RSC.

Nonetheless, numerous functional monomers struggle to satisfy imprinting criteria or exhibit insufficient bonding capacity. Recent investigations have concentrated significantly on novel self-synthetic monomers, including thymine 3 isocyanatopropyl 3 ethoxysilane (T-IPTS) [29], ethylenediaminetetra-N-(3-pyrrole1-yl)propylacetamide (monomer L) [30], (4-ethenylphenyl)-4-formate-6-phenyl-2,2-bipyridine, (2Z)-N,N-bis(2-aminoethylic)but-2-enediamide [31], 8-HQ–APTS [32], and N-(o-carboxyphenyl)maleamic acid (CPMA) [33], and 2,4-dioxopentan-3-yl methacrylate [34]. Karim et al. [35] and Fu et al. [16] have

conducted extensive evaluations of various strategies for optimizing MIP design, which could serve as valuable references.

Ligands and functional monomers differ but often work together. Ligands provide specific chelation, while monomers enable cross-linked network formation. Fig. 2 illustrates three working modes: ligand as an auxiliary monomer, monomer alone, and a composite of both. The monomer-only mode is most common, but the composite mode offers enhanced selectivity and is increasingly used in IIP preparation [35,36].

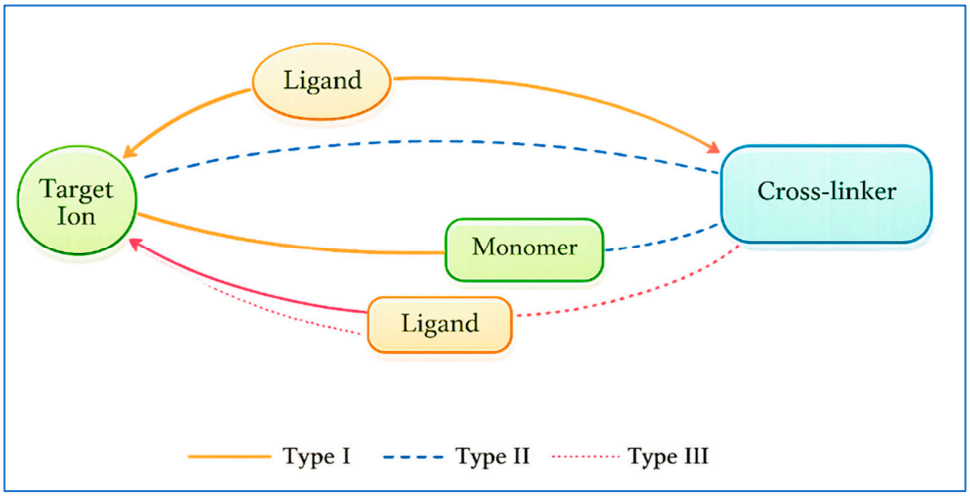


**Figure 2:** A schematic depiction showing three different modes relating to monomer and ligand.

*2.2.3 Role of Cross-Linkers, Initiators, and Porogens in Polymer Network Formation*

The construction of a strong and selective ion-imprinted polymer (IIP) network is not only dependent on the selection of functional monomers and ligands but is also sensitive to interactions between cross-linkers, initiators, and porogenic media. Together, these elements define the structural integrity, pore structure, and accessibility of the imprinted recognition sites, which directly affect adsorption capacity, selectivity, and reusability [36].

Cross-Linkers

Cross-linkers play a crucial role in stabilizing the spatial arrangement of functional groups relative to the template ion throughout the polymerization process. The formation of a three-dimensional network via cross-linking agents enhances mechanical strength and chemical stability while maintaining the geometry of the imprinted cavity after template removal [11]. Traditionally utilized cross-linking agents, including ethylene glycol dimethacrylate (EGDMA), divinylbenzene (DVB) [11], trimethylolpropane trimethacrylate (TMPTM) [37], pentaerythritol triacrylate (PETRA), tetraethoxysilane (TEOS) [38], and epichlorohydrin (ECH) [39], facilitate precise modulation of polymer rigidity and porosity as shown in Fig. 1. Nevertheless, it is imperative to meticulously optimize the cross-linker content: inadequate cross-linking may lead to poorly defined recognition sites and structural failure, while excessive cross-linking can produce excessively rigid networks that hinder mass transfer and diminish the accessibility of effective binding sites. Thus, an optimal monomer-to-crosslinker ratio is essential for achieving a balance between structural stability and adsorption performance [11].

## Initiators

Initiators regulate the kinetics of polymer network formation by modulating radical generation and chain propagation [4]. The selection process is closely linked to the polymerization methodology, the properties of the reaction medium, and the thermal or photochemical stability of the template–monomer complex [40]. Azo-based initiators, including azobisisobutyronitrile (AIBN), and peroxide-based initiators, such as benzoyl peroxide (BPO), are extensively used in bulk, solution, and suspension polymerization systems [4]. In contrast, persulfate salts are more appropriate for aqueous and emulsion polymerization processes. The initiator concentration is critical for determining the size of polymer particles and the uniformity of the network; an excessive radical flux can promote chain termination, resulting in heterogeneous structures and diminished imprinting efficiency [16,41]. Furthermore, meticulous deoxygenation of the reaction system is critical, as dissolved oxygen can effectively quench free radicals and impede polymer growth [11]. Some of the initiators used are shown in Fig. 3.

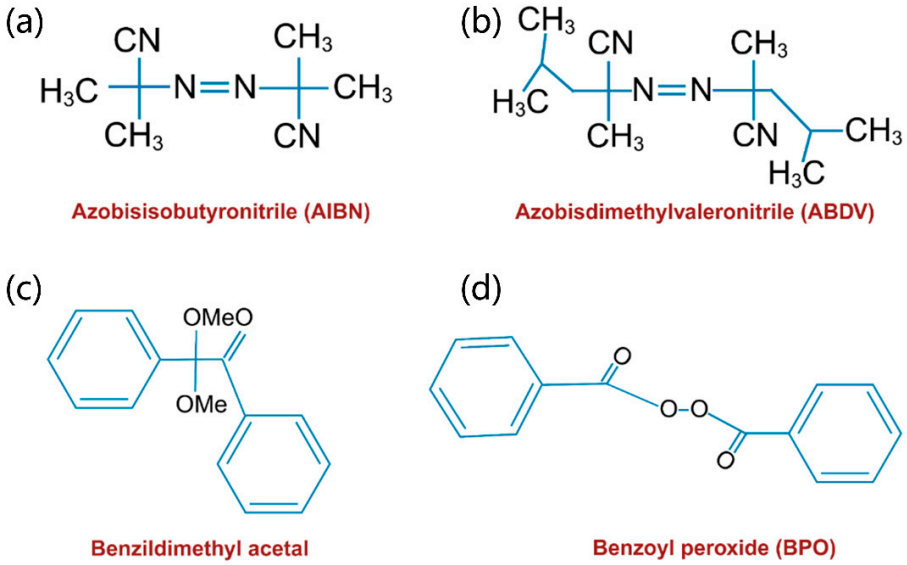


**Figure 3:** Commonly used polymerization initiators include: (**a**) azobisisobutyronitrile (AIBN), (**b**) azobisdimethylvaleronitrile (ABDV), (**c**) benzylidine dimethyl acetal, and (**d**) benzoyl peroxide (BPO).

## Porogens

Porogens act in a dual role as solvents and agents for pore formation, significantly impacting the morphology of polymers and the efficiency of imprinting processes [42]. The physicochemical characteristics of the porogen, such as polarity, dielectric constant, hydrogen-bonding capacity, and solubility parameters, dictate the intensity of pre-polymerization interactions between the template ion and functional monomers. Aprotic, low-polarity organic solvents, including toluene, acetonitrile, dichloromethane, and chloroform, are commonly preferred in non-covalent imprinting systems due to their ability to enhance stable template-monomer complexation and support the development of well-defined mesoporous structures [43]. Conversely, highly polar solvents can diminish these interactions, resulting in poorly formed recognition sites. Furthermore, the porogen volume fraction directly affects the distribution of pore sizes and surface area, which subsequently influences the adsorption kinetics and mass transfer behavior [44].

### *2.3 Fabrication Strategies for Ion-Imprinted Polymers*

There are two primary preparation methods for IIPs: the sol–gel method [45], which utilizes a progressive polymerization mechanism, and the free radical polymerization method, which involves chain polymerization techniques such as bulk, suspension, emulsion, and solution polymerization. To address the limitations of conventional imprinting materials, various advanced technologies have attracted significant interest, including surface imprinting [37], stimuli-responsive imprinting [37], dual- or multiple-component imprinting strategies [46], click chemistry [47], and microwave-assisted heating [48]. Surface imprinting, stimuli-responsive imprinting, and dual- or multiple-component imprinting strategies are widely used owing to their benefits.

#### *2.3.1 Surface Impriting*

Conventional IIP synthesis suffers from deeply embedded binding sites, difficult template elution, poor regeneration and low adsorption capacity. Surface imprinting polymerization directly addresses these issues by grafting imprinted sites onto high-surface-area carriers. This strategy minimizes inaccessible sites, significantly improving mass transfer, site accessibility and overall adsorption efficiency. The selection of suitable carrier materials is essential for effective surface imprinting polymerization [16]. The synthesis of surface-imprinted polymers (SIPs) typically comprises three stages (Fig. 4a). The template interacts with functional monomers to form a preorganized complex via covalent, noncovalent, or semicovalent interactions. Polymerization occurs on the surface of a solid substrate in the presence of initiators and crosslinkers, forming an imprinting layer that contains the template. The template is ultimately eliminated through physical or chemical methods, resulting in surface-exposed three-dimensional cavities. The cavities facilitate specific recognition and selective rebinding of the template from complex samples, thereby enabling efficient separation and detection.

Optimal carriers must demonstrate chemical stability, substantial specific surface areas, and cost-effectiveness. In recent years, numerous surface-imprinted ion-imprinted polymers (IIPs) have been developed utilizing various carriers, including carbon materials [49], silicon materials [50], metal–organic frameworks (MOFs) [50], magnetic materials [51], and clay minerals [52].

Our research group [52] described a surface ion-imprinting approach for synthesizing lithium-ion-imprinted polymers (LIPs). This method utilized dibenzo-14-crown-4 (DB14C4) as the chelating agent, $\alpha$-methacrylic acid as the functional monomer, and multi-walled carbon nanotubes as the carrier. The prepared IIPs exhibited favorable adsorption performance for $Li^+$ in aqueous solution and demonstrated high selectivity. A lithium-imprinted polymer, characterized by low cost and high efficiency, was effectively synthesized on the surface of vermiculite after using $HNO_3$ vapor and ultrasonic pretreatment. The isothermal adsorption curves indicate that the maximum adsorption capacity of the prepared IIPs reached 19.80 mg $g^{-1}$. Selectivity studies indicated that the selective separation coefficients of the IIPs for $Li^+$ were 9.2, 10.7, and 3.9 when compared to $Na^+$, $K^+$, and $Mg^{2+}$, respectively. Although surface imprinting markedly enhances site accessibility and adsorption performance, the dynamic regulation of binding and release processes remains constrained, leading to growing interest in stimuli-responsive imprinting methodologies.

Although surface imprinting improves kinetics, it often compromises mechanical stability and introduces carrier-dependent non-specific adsorption. In high-salinity seawater, thin imprinted layers may delaminate or foul rapidly, as evidenced by limited long-term marine exposure data.

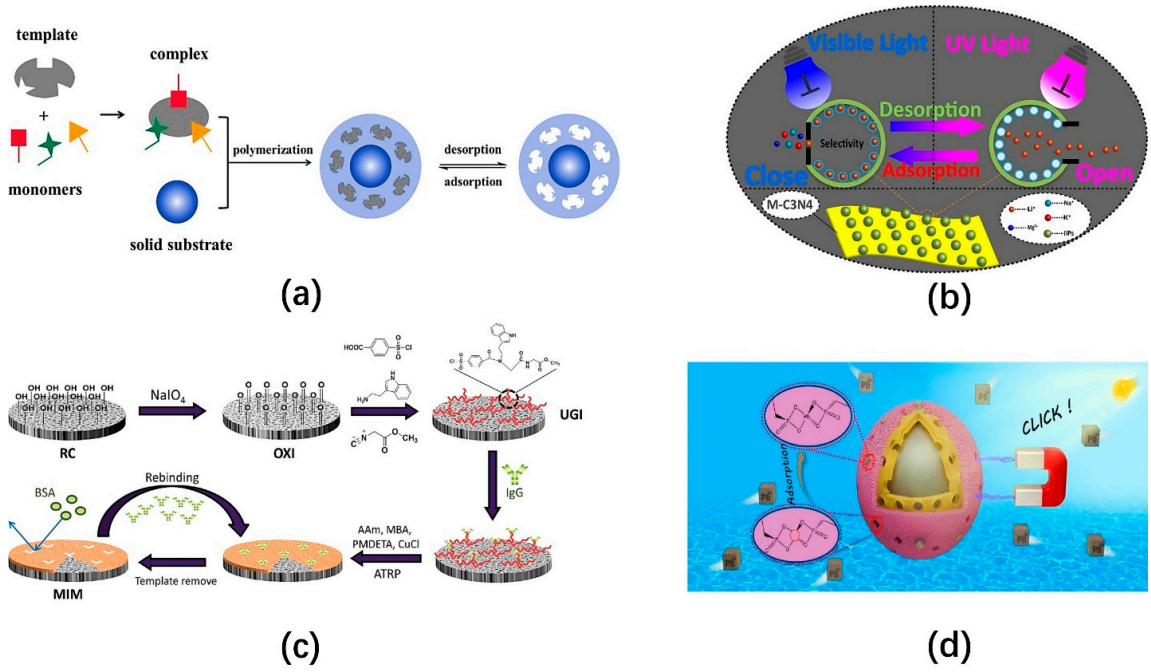


**Figure 4:** (**a**) Schematic representation of the preparation and recognition mechanism of SIPs. Reprinted with permission from reference [53]. Copyright 2021, Elsevier. (**b**) Schematic representation of the photocontrolled $Li^+$ adsorption behavior of the P-IIP system. Reprinted with permission from reference [54]. Copyright 2019, Elsevier. (**c**) Schematic illustration of a multi-component imprinting strategy for cooperative recognition in ion-imprinted polymers. Reprinted with permission from reference [55]. Copyright 2022, Elsevier. (**d**) Schematic illustration of click-chemistry-constructed recognition motifs for selective $Pb^{2+}$ adsorption. Reprinted with permission from reference [56]. Copyright 2024, Elsevier.

### *2.3.2 Stimuli-Responsive Imprinting*

Stimuli-responsive polymers, referred to as smart polymers and classified as functional polymers, demonstrate specific and reversible responses to external environmental stimuli, including temperature [57], pH [58], magnetic fields [59], light [60], and chirality [61]. The incorporation of stimuli-responsive elements into imprinted polymer systems enables external modulation of adsorption and desorption, thereby enhancing selectivity, regeneration efficiency, and operational control. Thermo-responsive imprinting has been extensively studied within the realm of stimuli-responsive strategies. Mizoguchi et al. [62] utilized N-isopropyl acrylamide (NIPAM) as a thermo-responsive component and acrylic acid (AA) as an interactive element to synthesize a linear thermo-responsive adsorbent for the recovery of Cu(II). The poly (NIPAM-co-AA) demonstrated an adsorption capacity roughly an order of magnitude greater than previously documented crosslinked thermo-responsive adsorbents, which was attributed to the enhanced incorporation of interactive functional groups. Temperature-sensitive imprinted polymer hydrogels have been developed using metal coordination interactions. Qin and colleagues [63] developed thermo-responsive imprinted hydrogels for the recognition of lysozyme, utilizing N-(4-vinyl)benzyliminodiacetic acid (VBIDA) to coordinate with Cu(II) and create a complex with the surface-exposed histidine residues of the template. At 28°C, the imprinting cavities were swollen, allowing the Cu(II)-chelated monomers to be readily accessible to the protein, resulting in the highest adsorption capacity. As the temperature rose to 43°C, the cavities collapsed, reducing Cu(II) accessibility and leading to a notable reduction in protein adsorption.

Photoresponsive imprinting has been used on ion-imprinted systems. In our previous studies [54], dibenzo-14-crown-4 (DB14C4) and 2,5-dicarboxyl-4-hydroxy azobenzene, a photoresponsive compound, served as functional monomers for forming a photoresponsive lithium-ion-imprinted polymer (P-IIP) on the surface of mesoporous $C_3N_4$ (M–$C_3N_4$). These findings indicated that ultraviolet–visible (UV–Vis) light irradiation effectively influenced the adsorption and desorption behavior of $Li^+$ ions, as shown in Fig. 4b. The P-IIP demonstrated improved adsorption performance and selectivity for $Li^+$, even amid competing $Na^+$, $K^+$, and $Mg^{2+}$ ions. Additionally, $Li^+$ ions adsorbed in the P-IIP can be effectively released upon UV irradiation, demonstrating strong regeneration capability [64]. The progress in dual- and multi-responsive molecularly imprinted polymers suggests that the development of stimuli-responsive ion-imprinted polymers will be a promising area of research.

Stimuli-responsive systems offer elegant control, yet repeated swelling-shrinking cycles frequently degrade imprinting fidelity and mechanical integrity. Moreover, external stimuli (light, temperature) may be energetically impractical for large-scale ocean deployment.

### *2.3.3 Dual/Multiple Components Imprinting Strategies*

Ion-imprinted polymers (IIPs) demonstrate efficacy in metal-ion separation; however, enhancements in selectivity and recognition efficiency remain necessary, particularly in complex aqueous environments. The development of novel functional monomers, along with dual and multiple functional monomers and dual and multiple template ion-imprinting strategies, has garnered significant attention due to their capacity for cooperative interactions and ability to expand the range of ion recognition [16].

Functional monomers such as methacrylic acid (MAA) and vinylpyridine (VP) serve as coordination sites for various metal ions, as evidenced in Cu(II)- [65] and Pb(II)-imprinted systems [66]. The concurrent application of multiple functional monomers can yield synergistic coordination effects, leading to enhanced adsorption kinetics and increased binding capacity. Simultaneously, dual-template imprinting facilitates the concurrent extraction of multiple target ions, as demonstrated by Cu(II)/Cd(II) and Cd(II)/Pb(II) dual-template imprinted polymers, both of which displayed superior imprinting efficacy [67]. Zhu et al. [68] synthesized a mixed As(V)–Cr(III) dual-template ion-imprinted polymer using two functional monomers, resulting in an effective material for addressing coexisting metal contamination in water.

Strategies involving dual or multiple components have been effectively utilized for the separation of alkali metals. Xu and colleagues conducted a series of studies on the simultaneous extraction of Li(I) and Rb(I) using dual-template, dual-functional-monomer ion-imprinting strategies, developing hierarchical mesoporous silica- and $Fe_3O_4$@$SiO_2$-based ion-imprinted polymers incorporating 12-crown-4 and 18-crown-6 that demonstrated effective separation performance in simulated salt-lake system [46].

Recent advancements have introduced multi-component imprinting concepts to improve cooperative recognition. Guo et al. [55] introduced a multicomponent-imprinted material (MIM) strategy that integrates multiple functional elements within a confined surface imprinting layer, facilitating synergistic interactions and enhancing site accessibility, as shown in (Fig. 4c). This strategy, initially demonstrated for molecular imprinting, offers a significant conceptual framework for ion-imprinted systems. The integration of multiple ligands, polymer matrices, and surface architectures can markedly improve selectivity and binding efficiency. Comprehensively, dual/multi-component imprinting methods—including multifunctional monomers, multi-templates and multi-component architectures—are a viable pathway of enhancing the work of IIPs and have specific potential in tricky multi-ion separation configurations.

### *2.3.4 Click Chemistry*

Click chemistry refers to a set of efficient, selective, and reliable reactions that enable rapid assembly of functional materials via robust heteroatom-linked bonds (C–X–C) [69]. Click chemistry, introduced by Sharpless in 2001, has found extensive applications in drug discovery [70], organic synthesis, and polymer chemistry [71], attributed to its high yields, mild reaction conditions, and modular design [72].

The use of click chemistry in imprinting systems, especially ion-imprinted polymers (IIPs), is comparatively severely limited. Recent studies indicate that click reactions serve as an effective synthetic platform for the construction of well-defined ion-recognition architectures. Li et al. [73] reported the synthesis of azo-chromophore-containing hyperbranched polymers through Cu(I)-catalyzed click reactions. In contrast, Naeimi et al. [47] developed Cu(II)-imprinted mesoporous organosilica nanocomposites utilizing click-derived 1,2,3-triazole ligands, emphasizing the structural stability and recyclability afforded by this method. Recently, structures supported by click chemistry have been applied to create highly selective systems for metal-ion adsorption. The use of click reactions to develop robust covalently linked recognition motifs that selectively capture $Pb^{2+}$ ions via well-defined coordination interactions (Fig. 4d). This strategy illustrates the ability of click chemistry to precisely control ligand positioning, binding-site geometry, and framework stability, which are essential for successful ion imprinting [56].

### *2.3.5 Microwave-Assisted Heating*

Microwave-assisted heating is widely used in synthesis, sintering, sterilization, and related areas due to its rapid heating rate, selective energy transfer, and high energy efficiency [74]. Microwave irradiation facilitates volumetric and uniform heating by directly interacting with polar molecules and ions, thereby significantly enhancing reaction kinetics, in contrast to traditional conductive or convective heating methods [48]. Microwave-assisted methods have been effectively utilized across nearly all significant polymerization pathways, encompassing bulk, emulsion, suspension, solution polymerization, and sol–gel synthesis [75]. Microwave-assisted polymerization in molecular imprinting exhibits distinct advantages. Magnetic molecularly imprinted polymer (MIP) beads produced through microwave-assisted suspension polymerization demonstrated narrow particle-size distributions, uniform morphology, high selectivity for target analytes, and improved imprinting efficiency, underscoring the significant potential of microwave-assisted imprinting techniques [76,77].

In a recent study, Yu et al. [78] reported an applicable example of microwave-assisted ion-imprinting, synthesizing a three-dimensional superhydrophilic Cu(II)-ion-imprinted polymer (Cu(II)-IIP) via surface ion imprinting and microwave-initiated polymerization, using a POSS/SBA-15 composite as the structured support. In this system, 4-vinylpyridine (4-VP) acted as the coordinating functional monomer to complex Cu(II) ions, which were subsequently crosslinked with ethylene glycol dimethacrylate (EGDMA) under AIBN initiation in a microwave reactor. Following acid elution, the Cu(II) templates were removed, yielding surface-accessible, well-defined recognition sites. Microwave irradiation significantly decreased the polymerization time to around 60 min, in contrast to the approximately 360 min needed with conventional water-bath heating, while maintaining robust imprinting performance and rapid adsorption kinetics (Fig. 5). This improvement is due to the uniform and efficient energy transfer linked to microwave heating, which facilitates homogeneous network formation and enhances site accessibility.

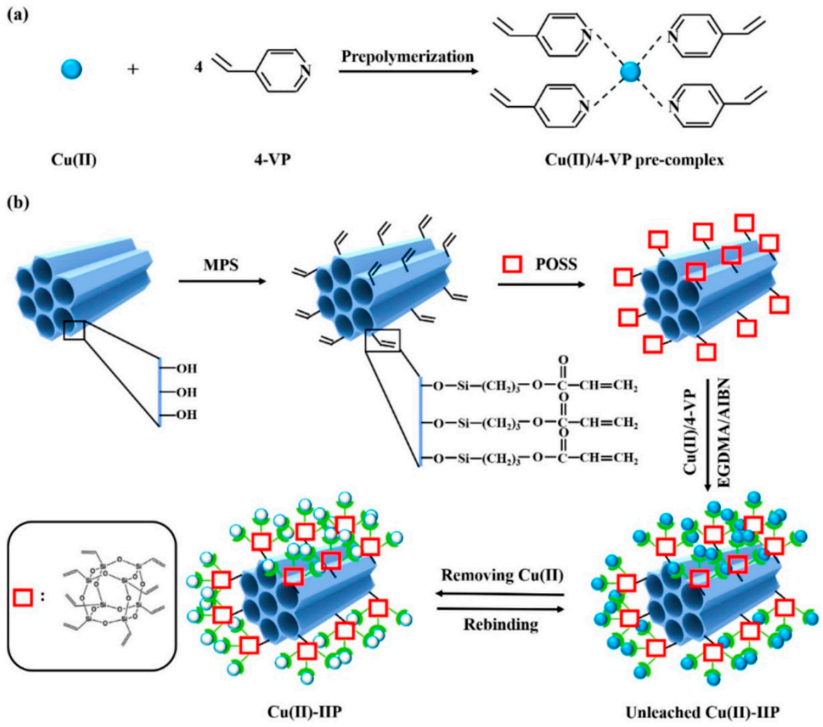


**Figure 5:** Schematic illustration of microwave-assisted surface ion imprinting for Cu(II)-IIP synthesis. Reprinted with permission from reference [78]. Copyright 2025, Elsevier.

Table 1 provides a systematic comparison of the advanced fabrication strategies outlined above, summarizing their core principles, the primary limitations they aim to address, and their respective advantages and ongoing challenges. This comparative overview elucidates how various imprinting methodologies address specific bottlenecks in traditional IIP fabrication, including restricted site accessibility, inadequate selectivity in multi-ion systems, suboptimal regeneration, and inefficient synthesis. It offers guidance on selecting suitable strategies tailored to specific separation needs and application contexts.

In addition to traditional surface imprinting and sol-gel methods, Zhao et al. developed an anhydrous interfacial polymerization (AIP) approach to fabricate polyamide membranes with sub-1 Å ionic sieving precision. By sublimating the amine monomer onto a porous substrate and reacting it with acyl chloride in alkane solution at a solid-liquid interface, water-induced side reactions are eliminated, resulting in a highly ordered and dense PA layer. The resulting AIP-PA membrane exhibited exceptional $Mg^{2+}/Li^{+}$ selectivity of 78.3 and a water permeance of 13.6 L $m^{-2}$ $h^{-1}$ $bar^{-1}$. Zhang et al. proposed that utilizing the cavity size of crown ethers to form host-guest complexes with specific alkali metal ions can also achieve efficient selective binding and transport. These preparation method also provides valuable insights for the synthesis of imprinting polymers.

**Table 1:** A comparative analysis of the advanced fabrication strategy of IIP strategies.

| Strategy | Primary Problem Addressed | Key Advantages | Key Limitations |
|---|---|---|---|
| **Surface imprinting** | Concealed binding sites and gradual mass transfer | Enhanced site accessibility; rapid kinetics; straightforward elution/regeneration; increased adsorption efficiency | Demands appropriate carriers; regulation of coating uniformity; complexity in synthesis |

**Table 1:** *Cont.*

| Strategy | Primary Problem Addressed | Key Advantages | Key Limitations |
|---|---|---|---|
| **Stimuli-responsive imprinting** | Ineffective adsorption and desorption, along with inadequate regeneration | Switchable binding and release mechanisms; enhanced regeneration capabilities; external control via temperature, light, pH, and magnetic fields | Intricate design; stability under recurrent stimuli; constrained ion-responsive systems |
| **Dual/multiple components imprinting** | Reduced selectivity in competitive or multi-ion systems | Coordinated synergy; increased capacity; multi-ion recognition ability | Complex optimization involves potential non-specific binding and selectivity trade-offs |
| **Click-chemistry-assisted imprinting** | Inadequate structural stability and inaccurate binding sites | Accurate ligand arrangement; durable covalent structures; elevated chemical resilience | Rarely applied in IIPs; higher cost; catalyst/purification concerns |
| **Microwave-assisted heating** | Extended synthesis duration and ineffective polymerization | long synthesis duration and suboptimal polymerization | Specialized equipment; scale-up and reproducibility still under study |

### *2.4 Fundamental of Hydrogels*

Hydrogels are three-dimensional crosslinked polymer networks that can absorb and retain significant quantities of water or aqueous solutions while maintaining their structural integrity. Key characteristics encompass elevated water content, a networked porous structure, a soft mechanical quality, and adjustable physicochemical properties. Due to these properties, hydrogels have been extensively investigated for applications in adsorption, separation, sensing, catalysis, drug delivery, and environmental remediation. The hydrated microenvironment of hydrogels in ion-recognition systems enhances the diffusion of dissolved ions and increases the accessibility of functional binding sites within the polymer matrix. This feature is crucial for selective ion capture from aqueous media, as the target species must compete with numerous coexisting ions and diffuse effectively through the network to reach recognition sites [79–81].

The introduction of ion imprinting into a hydrogel matrix results in a material that integrates the selective recognition properties of ion-imprinted polymers with the transport benefits of a water-swollen gel. In a standard ion-imprinting process, the target ion initially engages with functional monomers, ligands, or coordinating groups via mechanisms such as chelation, electrostatic attraction, host–guest binding, or supramolecular assembly [82]. Polymerization or gelation subsequently stabilizes these interactions within a crosslinked network. Following the removal of the template ion, complementary cavities or coordination environments persist within the hydrogel, facilitating the selective rebinding of the target ion in subsequent adsorption or sensing processes [83]. Ion-imprinted hydrogels provide a flexible and hydrated framework, in contrast to dense or rigid imprinted materials. This characteristic enhances mass transfer, facilitates template removal, and enables faster rebinding of the target ion [84].

The swelling behavior of hydrogels is a fundamental property that results from the interplay between polymer-water affinity and the elastic retractive force of the crosslinked network [79]. Hydrophilic groups, including hydroxyl, amino, carboxyl, amide, ether, and sulfonic groups, facilitate water absorption via hydrogen bonding and ion–dipole interactions. As swelling increases, the internal free volume of the hydrogel enhances pore accessibility and facilitates ion diffusion [85]. Excessive swelling can compromise mechanical strength and diminish the structural precision of imprinted sites, while insufficient swelling may restrict ion transport and hinder adsorption kinetics. An effective ion-imprinted hydrogel necessitates an optimized balance among water uptake, crosslink density, structural stability, and accessibility of recognition

cavities. The balance is essential, as the recognition event in many imprinted hydrogels is influenced not only by the chemical affinity of the functional groups but also by the efficiency of target-ion migration through the swollen network to the imprinted binding domains [85].

Another essential aspect of hydrogels is the nature of the polymer matrix itself. Natural polymer-based hydrogels, particularly chitosan systems, are attractive because of their biodegradability, biocompatibility, abundance, and intrinsic metal-binding amino and hydroxyl groups. These characteristics make chitosan a versatile matrix for ion imprinting, as demonstrated in $Ag^{+}$ imprinted chitosan hydrogels and $Nd^{3+}$ imprinted chitosan-based polymeric hydrogels. In contrast, synthetic hydrogels provide greater control over network architecture, functional-group density, and responsiveness. For example, P(NIPAM)-based systems offer thermo-responsive behavior, PEI-containing hydrogels provide abundant amine groups for metal chelation, and guanosine-functionalized hydrogels introduce supramolecular recognition through ion-stabilized G-quartet structures. Thus, the choice of hydrogel matrix strongly influences adsorption capacity, selectivity, regeneration performance, and environmental stability [86].

Ion-imprinted hydrogels are also distinguished by their ability to convert microscopic ion-recognition events into macroscopic material responses. In some systems, rebinding of the target ion induces contraction or swelling of the network, enabling direct signal transduction. For example, potassium-ion-imprinted P(NIPAM-co-B15C5Am) hydrogels show rapid $K^{+}$ induced shrinking because preorganized crown ether units can quickly reform host–guest complexes with the target ion [80]. Similarly, $Sr^{2+}$ imprinted P(NIPAM-co-APG) hydrogels respond to $Sr^{2+}$ through reformation of G-quartet-based complexes, causing hydrogel shrinkage that can be further converted into measurable optical signals in hydrogel grating systems. These examples show that ion-imprinted hydrogels are not merely adsorbents; they can also function as responsive platforms for sensing and signal amplification [86].

From an application perspective, the main advantages of ion-imprinted hydrogels include high water compatibility, improved ion diffusion, accessible recognition sites, relatively easy regeneration, and the possibility of integrating adsorption and sensing functions into a single material. Nevertheless, several challenges remain [87]. Hydrogel networks may suffer from limited mechanical strength, structural deformation during repeated swelling–deswelling cycles, pH sensitivity, or gradual loss of imprinting fidelity under harsh operating conditions. Recent studies have therefore increasingly focused on strengthening hydrogel matrices through improved crosslinking chemistry, alternative solvent-processing routes, and hybrid structural design, or refer to the preparation strategy described by Guan et al. [88]: combining the conductive component with ion imprinting technology not only significantly enhances the mechanical strength and conductivity of the hydrogel but also provides abundant active sites. These efforts indicate that the future development of ion-imprinted hydrogels will depend not only on maximizing selectivity but also on achieving sufficient robustness, reusability, and process stability for practical applications in complex aqueous environments [89].

### *2.5 Fabrication Strategies of Ion-Imprinted Hydrogels*

Ion-imprinted hydrogels can be fabricated through several distinct yet conceptually related strategies, depending on the nature of the polymer matrix, the ion-recognition motif, and the intended application. Despite these differences, the underlying principle remains the same: the target ion is first associated with functional ligands or polymer chains, the hydrogel network is then fixed through polymerization or crosslinking, and finally the template ion is removed to generate recognition sites capable of selective rebinding. As illustrated by representative studies, these strategies range from synthetic thermo-responsive

hydrogels and biopolymer-based adsorbents to supramolecularly engineered and sensing-oriented hydrogel platforms.

Fig. 6 reported by Wu et al. [80] provides one of the clearest illustrations of a template-preorganized free-radical polymerization strategy for responsive ion-imprinted hydrogels. Their scheme shows that $K^+$ is first complexed with benzo-15-crown-5-based functional units before polymerization, so that during gel formation the crown ether moieties are fixed in paired arrangements within the P(NIPAM-co-B15C5Am) network. After removal of $K^+$, these preorganized sites remain as size- and geometry-matched cavities that can rapidly rebind potassium ions. Importantly, the comparison between the non-imprinted and ion-imprinted hydrogels shown in Fig. 6 highlights the fundamental advantage of imprinting in soft polymer networks: the preorganized binding configuration minimizes the conformational rearrangement required for rebinding, thereby accelerating ion-recognition kinetics and improving response efficiency.

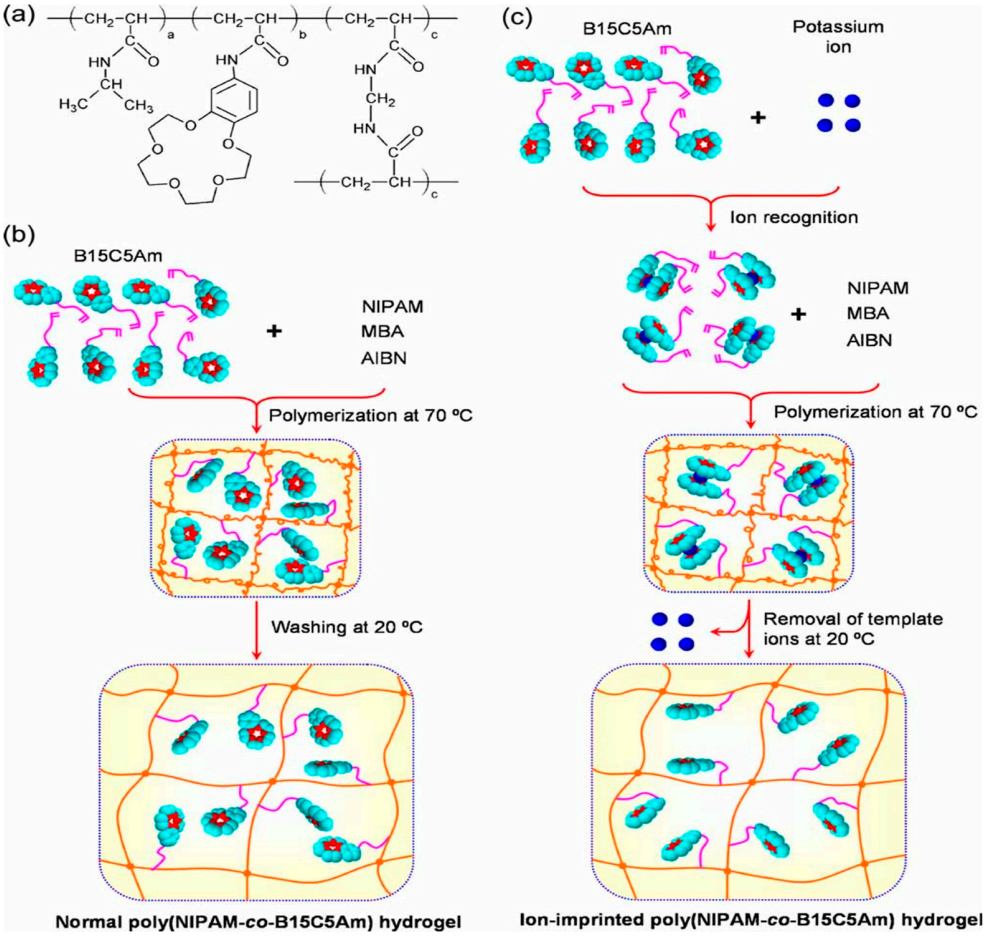


**Figure 6:** Schematic illustration of the synthesis strategy of ion-imprinted P(NIPAM-co-B15C5Am) hydrogel: (**a**) chemical structure of P(NIPAM-co-B15C5Am), (**b**) fabrication of the non-imprinted hydrogel, and (**c**) preparation of the ion-imprinted hydrogel. Reprinted with permission from reference [80]. Copyright 2011, Wiley.

In contrast, Song et al. [82] present a biopolymer-based phase inversion and chemical crosslinking route using chitosan hydrogels for $Ag^+$ imprinting, as shown in Fig. 7a. Their schematic shows that silver ions are introduced into chitosan solution before gel bead formation, followed by phase inversion in alkaline medium, chemical crosslinking, and subsequent acid elution to remove the template. This is important because

it highlights a fabrication pathway that is very different from synthetic vinyl monomer polymerization: here, the hydrogel is formed from a naturally derived polysaccharide matrix whose amino and hydroxyl groups already possess intrinsic metal-binding ability. The imprinting step therefore, enhances selectivity by generating $Ag^{+}$ compatible cavities within an already chelating biopolymer framework. Thus, this study can be discussed as a representative example of how ion-imprinted hydrogels based on natural polymers combine sustainability, facile preparation, and selective adsorption.

The study by Wang et al. [79] extends the fabrication concept by introducing radiation-assisted hydrogel synthesis, followed by post-synthetic ion imprinting and stabilization. As shown in Fig. 7b, the parent p(PEI/HEA) hydrogel is first synthesized through $^{60}Co$ gamma-radiation-induced copolymerization of polyethyleneimine and hydroxyethyl acrylate. This figure is important because it illustrates the formation of the functional hydrogel matrix itself, which contains abundant amine-rich chelating sites derived from PEI. In the subsequent steps described in the study, $Cu^{2+}$ is loaded into the hydrogel via chelation, the structure is stabilized by glutaraldehyde crosslinking, and the template ion is finally removed by EDTA treatment, generating selective binding sites. This route demonstrates that ion imprinting in hydrogels does not necessarily require simultaneous network formation; rather, a preformed functional hydrogel can be post-loaded with the target ion and chemically fixed to create selective recognition environments. Such a strategy is particularly attractive for multi-amine hydrogel systems designed for heavy-metal removal.

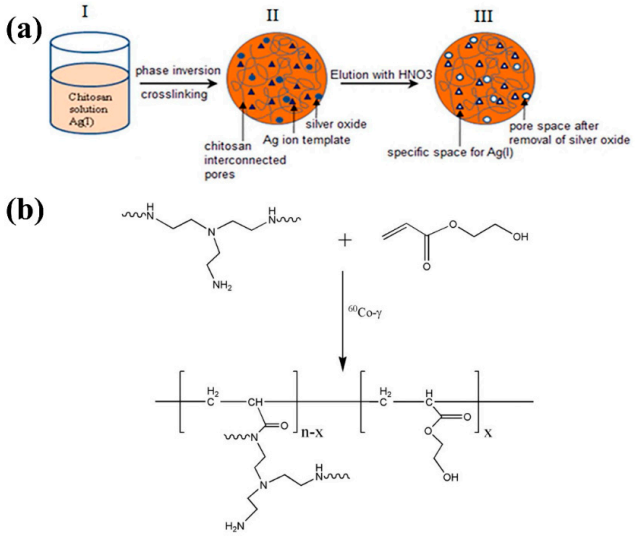


**Figure 7:** (**a**) Schematic illustration of the fabrication process of $Ag^{+}$-imprinted chitosan hydrogels. Reprinted with permission from reference [82]. Copyright 2012, ACS. (**b**) Schematic representation of the synthesis route of p(PEI/HEA) hydrogel. Reprinted with permission from reference [79]. Copyright 2015, Elsevier.

A more advanced, mechanistically sophisticated strategy is illustrated in Fig. 8 by Liu et al. [86] where $Sr^{2+}$-imprinted hydrogels are fabricated via ion-induced supramolecular self-assembly of guanosine-derived units. Their schematic shows that $Sr^{2+}$ first directs the assembly of APG (5′-O-acryloyl-2′,3′-O-isopropylidene guanosin) monomers into G-quartet structures, and these supramolecular complexes are then locked into a P(NIPAM-co-APG) hydrogel via thermally initiated polymerization. After template removal, the relaxed G-quartet-based cavities can selectively bind $Sr^{2+}$, leading to hydrogel shrinkage and enabling ion-responsive sensing. This is highly essential because it moves beyond conventional chelation-based imprinting and shows that hydrogel imprinting can also be built on reversible supramolecular motifs. Moreover, it links fabrication directly with function. The same imprinted structure that enables selective

rebinding also converts the recognition event into a measurable macroscopic volume response, which is later exploited in hydrogel grating-based chemosensors.

IIPs and IIHs represent two complementary yet structurally distinct classes of materials for selective lithium and uranium recovery from seawater. Although both utilize template-directed imprinting to create specific recognition cavities, their matrix characteristics, namely rigid cross-linked networks versus highly hydrated and stimuli-responsive gels, result in notable differences in fabrication, performance, and applicability (Table 2).

**Table 2:** Comparative analysis of IIPs and IIHs for seawater lithium and uranium recovery.

| | IIPs | IIHs | Trade-Offs |
|---|---|---|---|
| **Advantages** | High mechanical strength and structural stability; Strong selectivity; Good cycling stability; Easier scale-up and recovery | Fast mass transfer kinetics; High adsorption rate; Mild regeneration; Good hydrophilicity and high capacity potential | IIPs: stability and selectivity; IIHs: kinetics and operational convenience |
| **Limitations** | High mass transfer resistance, slower adsorption rate; Harsh regeneration, risk of cavity damage; Surface prone to biofouling and NOM fouling | Low mechanical strength, prone to shrinkage/collapse in high-salinity seawater; Selectivity easily affected by swelling; More sensitive to biofouling and NOM; Shorter cycling lifetime | Rigidity vs. flexibility; stability vs. kinetics |
| **Adsorption Capacity** | Moderate to high in lab conditions; utilization limited by mass transfer in real seawater | Moderate to high in lab conditions; utilization limited by mass transfer in real seawater | IIHs superior in lab; IIPs more reliable in real seawater |
| **Selectivity** | Higher and more stable, especially for $Li^+/Mg^{2+}$ and U(VI)/V | Good but susceptible to interference from swelling and complex matrices | IIPs offer more stable selectivity |
| **Adaptability to Real Seawater** | Better | Poorer | IIPs more suitable for marine engineering |
| **Regeneration Performance** | More cycles (typically 5–20); harsher conditions | Mild regeneration (temperature/pH/light responsive); fewer cycles | IPs: longer lifetime but higher operational cost; IIHs: easier to regenerate but less durable |

Collectively, these representative studies confirm that fabrication strategies for ion-imprinted hydrogels have evolved from simple template-directed cavity formation toward multifunctional material platforms integrating selective recognition, structural responsiveness, and application-specific performance. Despite the diverse architectural design strategies established thus far, several intrinsic bottlenecks of ion-imprinting technologies remain unresolved for practical marine extractions. Crucially, site heterogeneity represents a severe limitation because imprinted matrices inherently possess an uneven distribution of high- and low-affinity binding pockets [17]. Under ultra-dilute marine conditions where lithium and uranium concentrations drop to approximately 0.17 mg/L and 3.3 μg/L, only the minority of high-affinity sites contribute effectively to target capture. Consequently, evaluating adsorption capacities at artificially high concentration scales overestimates real-world performance by orders of magnitude. This challenge is further compounded by a fundamental conflict between structural rigidity and mass-transfer kinetics. Although high cross-linking densities are indispensable for stabilizing the spatial geometry of imprinted cavities, they impose severe steric hindrance and restrict diffusion, a limitation amplified for bulky uranyl

carbonate complexes. Parallel to these transport limitations, a thermodynamic dilemma arises between the high chelation affinity required for selective recognition in hypersaline matrices and the necessity for mild regeneration. Robust coordination bonds resist efficient elution, leading to incomplete regeneration and site degradation over extended cycling, whereas weak interactions fail to overcome the overwhelming competitive interference from background ions. These pervasive trade-offs underscore that standalone ion-imprinted materials are insufficient to meet the stringent demands of continuous seawater mining, necessitating their integration into multi-stage, complementary hybrid separation systems.

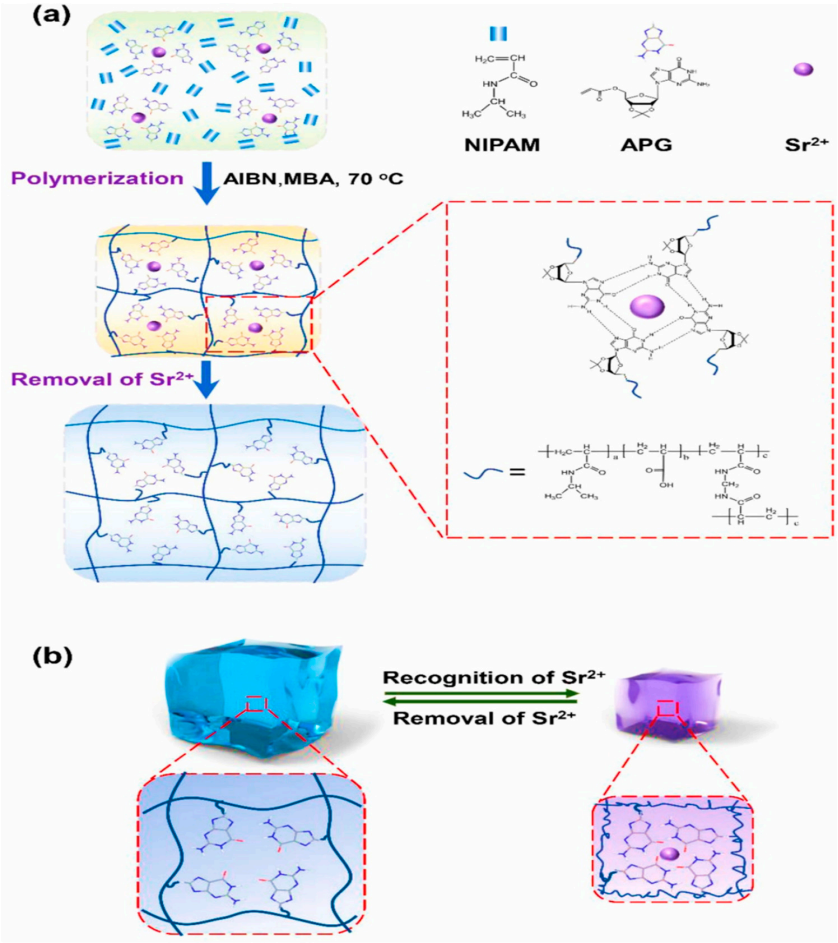


**Figure 8:** Schematic illustration of the fabrication process and ion-recognition behavior of $Sr^{2+}$-imprinted hydrogels: (**a**) incorporation of $Sr^{2+}$-induced G-quartets into the hydrogel network through thermally initiated polymerization, followed by removal of the $Sr^{2+}$ templates by repeated washing with deionized water; and (**b**) reversible $Sr^{2+}$-responsive behavior of the imprinted hydrogels. Reprinted with permission from reference [86]. Copyright 2022, Elsevier.

## 3 Lithium-Selective Ion-Imprinted Materials and Their Performance in Seawater Systems

Lithium concentration in seawater is extremely low, typically ranging from 0.1 to 0.2 ppm [90]. Meanwhile, seawater contains a large abundance of competing cations, including $Na^+$, $K^+$, $Mg^{2+}$, and $Ca^{2+}$, making it difficult for conventional adsorbent materials to achieve efficient and highly selective lithium extraction (Table 3). In contrast, lithium ions hosted in salt lake brines account for more than 60% of global lithium reserves, and most research efforts have focused on Salt Lake systems. Consequently, studies focusing on lithium recovery and adsorption from seawater remain relatively scarce.

**Table 3:** Representative overview of ion-imprinted polymer performance in lithium ion absorption.

| Material System | Adsorption Capacity (mg/g) | Selectivity Coefficient ($\alpha$) | Equilibrium Time (min) | Ref. |
|---|---|---|---|---|
| Li-I-IP (Calixarene/AA) | 28.52 | $Li^+/Na^+$: 2.476 | 25 | [18] |
| Li-I-IP (DB14C4/MWCNTs) | 19.80 | $Li^+/Na^+$: 9.2; $Li^+/K^+$: 10.7; $Li^+/Mg^{2+}$: 3.9 | — | [91] |
| Li-I-IP (magnetic GO) | 31.24 | $Li^+/Na^+$: 14.31; $Li^+/K^+$: 12.05; $Li^+/Mg^{2+}$: 10.9 | — | [92] |
| Li-I-IP (B15C5/MAA) | 30.53 | $Li^+/Na^+$: 2.04; $Li^+/K^+$: 2.67; $Li^+/Mg^{2+}$: 2.17; $Li^+/Ca^{2+}$: 2.43 | — | [93] |
| Li-I-IP (phthalocyanine) | 3.2 | $Li^+/Na^+$: 2.6–3.6; $Li^+/K^+$: 2.4–3.4; $Li^+/Ca^{2+}$: 1.85 | 60 | [94] |
| Li-I-IP (12-crown-4/$TiO_2$/PVDF) | — | $Li^+/Mg^{2+}$: 6.8; $Li^+/K^+$: 17.0; $Li^+/Ca^{2+}$: 21.3; $Li^+/Na^+$: 24.6 | — | [95] |
| Li-I-IP (2AM12C4/$Fe_3O_4$@$SiO_2$) | — | $Li^+/Na^+$: >50 | 10 | [96] |
| Li-I-IP (C4/ester) | 50.87 | $Li^+/Na^+$: 1.71; $Li^+/K^+$: 4.56; $Li^+/Rb^+$: 3.80 | 90 | [97] |
| Li-I-IP (POSS-crown ether, gamma) | 3.52–3.58 | $Li^+/K^+$: 23.21; $Li^+/Mg^{2+}$: >4.07 | — | [98] |
| Li-I-IP ($Fe_3O_4$@C, thermo) | 5.19 (35°C) | — | 60 | [99] |

### *3.1 Ion-Imprinted Polymer*

Functional polymeric materials fabricated via ion-imprinting technology are defined as ion-imprinted polymers (IIPs). Generally, target ions are employed as template ions to accomplish pre-assembly through coordination, electrostatic, and other interactions between template ions and functional monomers. Subsequent polymerization initiated by cross-linkers forms a three-dimensional polymer network, from which template ions are finally removed by elution. This process constructs specific recognition sites within the polymer backbone that are size-matched, charge-complementary, and possess an identical coordination environment to the target ions, enabling highly selective recognition and adsorption of target ions. As core materials in the field of lithium-ion separation and enrichment, ion-imprinted polymers integrate the structural stability and easy modifiability of polymeric materials with the specific recognition superiority of imprinted materials. Lithium-selective ion-imprinted materials are functional materials with tailor-made recognition sites, synthesized via ion-imprinting technology with lithium ions as templates. Among them, ion-imprinted polymers (IIPs) and ion-imprinted hydrogels (IIHs) serve as two major categories of core supports. IIPs are suitable for lithium separation in harsh environments owing to their high selectivity and stability, while IIHs exhibit prominent advantages in mild systems due to their high swelling capacity and environmental responsiveness. Both types of materials hold significant application prospects in lithium extraction from salt lakes and seawater, as well as lithium resource recovery.

### *3.1.1 Relationship between Fabrication Conditions and Performance*

Due to the low lithium concentration and high salinity of seawater, preparation conditions including template type, functional monomers, cross-linkers, polymerization method, elution and regeneration all significantly affect material performance [16].

#### The Types of Template Ions

Template ions are the core prerequisite for achieving the specific recognition properties of ion-imprinted materials and represent the essential difference from traditional adsorbent materials. In complex environments containing various interfering ions such as $Na^+$, $K^+$, $Cu^{2+}$, and $Zn^{2+}$, the absence of template ions directly leads to a significant decline in adsorption performance.

Most studies employ non-imprinted materials (NIPs) as the control group; the synthesis processes of NIPs and IIPs differ only in the presence of template ions, which avoids performance deviations caused by other factors. Zhao et al. [92] confirmed this using a magnetic graphene oxide-based $Li^+$-IIP. As shown in Fig. 9a,b, the IIP showed a maximum adsorption capacity of 31.24 mg/g, which was 2.08 times that of the non-imprinted control. Selectivity coefficients for $Li^+/Na^+$, $Li^+/K^+$ and $Li^+/Mg^{2+}$ were 14.31, 12.05 and 10.9, respectively, with a separation factor of 0.0315. In contrast, the non-imprinted material showed no obvious selectivity. These results demonstrate that template-induced cavities provide high capacity and high selectivity, distinguishing IIPs from conventional adsorbents.

#### Functional Monomers and Ligands

In the synthesis of IIPs, $Li^+$ serves as the template ion, and its small ionic radius (approximately 76 pm) and high charge density require functional monomers to provide a suitable coordination environment. Functional monomers are the core units that form coordination bonds with $Li^+$, their type of coordination sites, steric hindrance, and hydrophilic-hydrophobic properties determine the binding strength, selectivity, and seawater resistance of IIPs to $Li^+$, making them the most basic regulatory factor in preparation conditions. The most commonly used functional monomers include methacrylic acid (MAA) [93], acrylic acid (AA) [18], and calixarenes [100]. MAA and AA are two types of carboxyl-containing functional monomers that coordinate with $Li^+$ through carboxyl oxygen atoms. Cao et al. [18] compared a calixarene-containing $Li^+$-IIP with a conventional acrylic acid-based IIP. As shown in Fig. 9c,d, the calixarene-based material achieved a $Li^+/Na^+$ selectivity coefficient of 2.476, which is 2.4 times higher than that of the AA-only IIP. Its maximum adsorption capacity reached 28.52 mg/g, a 44.7% increase, while equilibrium time shortened from 38 to 25 min. These improvements arise from the synergistic effect of calixarene and carboxyl groups, demonstrating that single functional monomers are insufficient for efficient $Li^+$ recovery.

To break through the bottlenecks of insufficient selectivity and poor stability of traditional functional monomers in low-lithium systems, Jamoussi et al. [94] adopted a novel phthalocyanine-based acrylate (TMAPc) as the functional monomer and prepared Li-IIP via precipitation polymerization to meet the demand for lithium resource recovery from reverse osmosis wastewater of seawater desalination plants. Compared with traditional macrocyclic compounds such as crown ethers and calixarenes, or small-molecule monomers such as methacrylic acid (MAA), phthalocyanine-based monomers possess a rigid conjugated macrocyclic skeleton, a higher number of coordination sites, and stronger synergistic effects, leading to more stable structures. In a simulated wastewater system containing high concentrations of $Na^+$, $K^+$, $Ca^{2+}$, and $Mg^{2+}$, the selectivity factors of Li-IIP for $Li^+/Na^+$, $Li^+/K^+$, and $Li^+/Ca^{2+}$ were 2.6–3.6, 2.4–3.4, and 1.85, respectively. After 8 adsorption-desorption cycles, the $Li^+$ recovery rate of Li-IIP for low-concentration brine (Brine I) remained at 89%. Compared with other mentioned studies, the selectivity factor of this

material is not very prominent, but the unique chelating properties of phthalocyanine-based functional monomers solve the pain point of insufficient selectivity of traditional imprinted materials in high-salinity and low-lithium systems. Combined with SPE technology to achieve efficient separation, it provides an economical and environmentally friendly technical solution for lithium resource recovery from seawater desalination wastewater, with both large-scale application potential and environmental benefits.

Regardless of the type of functional monomer used, the selectivity of ion-imprinted materials prepared with independent functional monomers is limited. To further improve performance, composite functional systems integrating macrocyclic ligands have gradually entered the research scope. Compared with functional monomers that provide basic binding sites, ligands directly determine the specific recognition properties of ion-imprinting technology. In practical material design, ligands are preferentially determined according to the size and coordination characteristics of target ions, and then functional monomers compatible with ligands and capable of constructing stable skeletons are selected [101]. For $Li^+$ in seawater, crown ether ligands are preferred [100].

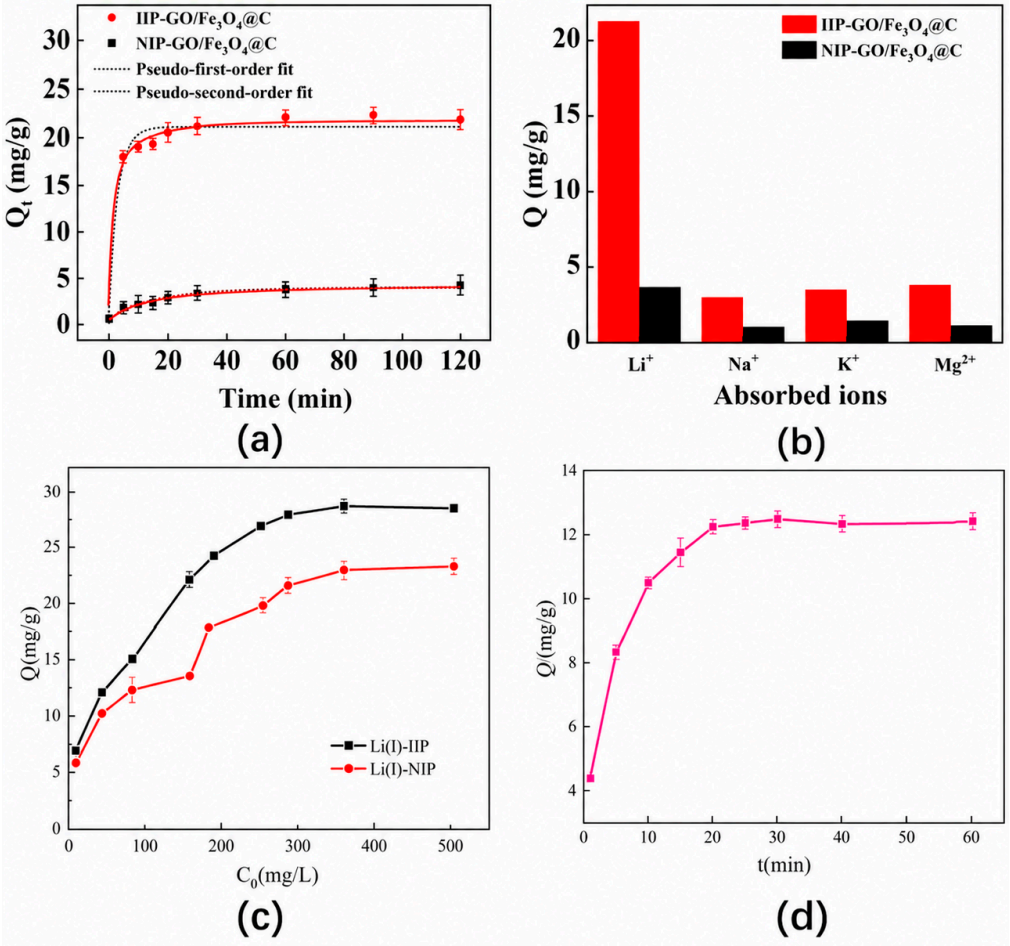


**Figure 9:** (**a**) Isothermal adsorption curves of IIP-GO/$Fe_3O_4$@C and NIP-GO/$Fe_3O_4$@C. (**b**) Adsorption selectivity of IIP-GO/$Fe_3O_4$@C and NIP-GO/$Fe_3O_4$@C. Reprinted with permission from reference [92]. Copyright 2025, Elsevier. (**c**) Effect of the initial $Li^+$ concentration on the adsorption amounts of Li(I)-IIPs and Li(I)-NIPs. Run conditions: pH = 10, and adsorption time = 25 min. (**d**) Adsorption time on the adsorption amount of Li(I)-IIPs. Run conditions: $C_0$ ($Li^+$) = 50 mg/L Reprinted with permission from reference [18]. Copyright 2024, ACS.

As shown in Fig. 10, Yang et al. [95] prepared an ion-imprinted membrane with specific recognition for $Li^+$ using 12-crown-4 as the specific ligand, which is a basic crown ether for lithium ions. The cavity size of 12-crown-4 is geometrically compatible with the size of bare lithium ions, thereby promoting its coordination with ether oxygen atoms, enabling the formation of stable host-guest coordination complexes and providing specific recognition sites for LIIMs, which fundamentally ensures the selectivity for $Li^+$. Different from common functional monomers such as carboxylic acid-based and amino-based monomers, the oxygen atoms on the crown ether ring can provide lone pairs of electrons to form stable coordination bonds with $Li^+$. XPS verification showed that the chemical state of O atoms changed after adsorption, confirming the specific role of this coordination. Meanwhile, in simulated multi-ion competition experiments, the separation factors of $Li^+/Mg^{2+}$, $Li^+/K^+$, $Li^+/Ca^{2+}$, and $Li^+/Na^+$ were 6.80, 17.00, 21.30, and 24.60, respectively, indicating that the selectivity of this material is significantly superior to that of existing similar imprinted materials. It was also proved that 12-crown-4 can bind to APTES through hydrogen bonds and form a stable cross-linked network via TEOS hydrolysis and polymerization, which is firmly loaded on the surface of the $TiO_2$/PVDF base membrane and is not easy to fall off. After 6 adsorption-desorption cycles, the retention rate of the adsorption capacity reached 97%, showing high structural stability. Although this material was used to treat waste lithium-ion batteries, the ion competition is highly similar to the actual seawater environment, thus possessing a high reference value.

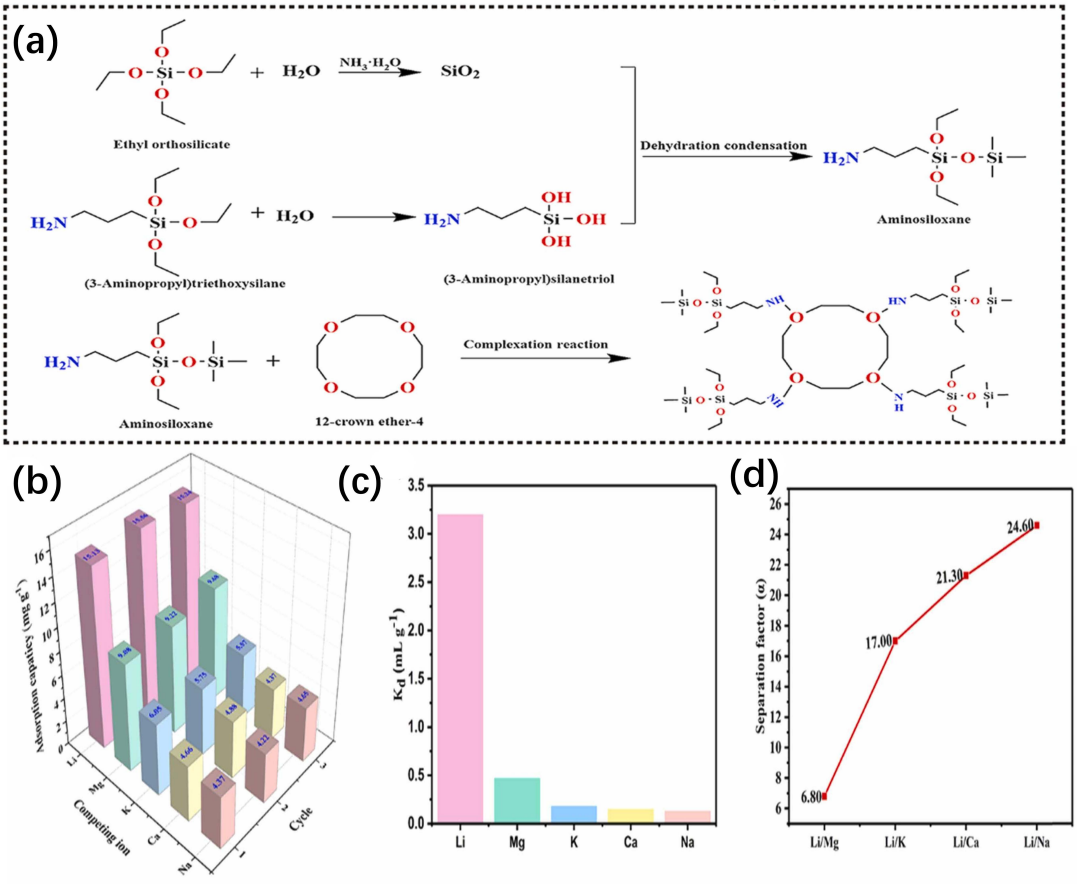


**Figure 10:** (**a**) Schematic diagram of the synthesis of LIIMs; (**b**) Selective adsorption of LIIMs toward lithium ions; (**c**) Ion distribution coefficient, and (**d**) Separation factor of four mixture solution systems (40 mg $L^{-1}$ $Li^+/Mg^{2+}$, $Li^+/K^+$, $Li^+/Na^+$, $Li^+/Ca^{2+}$). Reprinted with permission from reference [95]. Copyright 2022, Elsevier.

Similarly, Qi et al. [93] used benzo-15-crown-5 (B15C5) with a macrocyclic structure as the ligand, which is highly consistent with the hydrated ionic radius of $Li^+$ (approximately 3.87 Å). DFT calculations confirmed that the selectivity of B15C5 for $Li^+$ is higher than that of other crown ether derivatives such as B12C4 and B9C3, making it one of the crown ether ligands with the best-known selectivity for $Li^+$. Compared with a single functional monomer, the introduction of B15C5 increased the adsorption capacity of Li-IIP to 30.53 mg/g, which is much higher than the adsorption capacity of non-imprinted polymer (317.81 mg/g), with an imprinting factor of 1.71. In contrast, the hydrated radii of interfering ions such as $Na^+$ and $K^+$ do not match the cavity size, making it difficult for them to enter the ring to form stable coordination. In binary mixed systems containing $Na^+$, $K^+$, $Ca^{2+}$, and $Mg^{2+}$, the selectivity coefficients of Li-IIP for $Li^+$ were 2.04, 2.67, 2.43, and 2.17, respectively. After 8 adsorption-desorption cycles, the retention rate of Li-IIP adsorption capacity reached 89.20%, only decreasing by 10.80%, and it exhibited good stability below 200°C.

To enhance stability and performance, Luo et al. [96] developed a novel functional ligand 2AM12C4, which acts as both a crown ether for $Li^+$ recognition and a monomer for polymerization. Its allyl double bonds allow covalent incorporation into the polymer skeleton via surface imprinting on a magnetic $Fe_3O_4$@$SiO_2$ carrier, avoiding the instability of non-covalent entrapment (Fig. 11). The resulting material exhibits rapid equilibrium within 10 min, exceptionally high selectivity with $Li^+/Na^+$ separation factor above 50, and good reusability with 92.4% capacity retention after five cycles.

In addition to crown ether ligands, inspired by biology, Yu et al. [97] adopted a mussel-inspired modification strategy and used calixarene C4 as the ligand to prepare ester-functionalized lithium ion-imprinted composite membranes. Like other macrocyclic compounds, C4 also has a macrocyclic cavity size that matches the radius of $Li^+$ precisely. The electron-rich groups on its ring can form stable coordination with $Li^+$ through cation-π interactions. In a mixed system containing $Na^+$, $K^+$, and $Rb^+$, the relative selectivity coefficients of Li-IIMs for $Li^+$ were 1.71 ($Li^+/Na^+$), 4.56 ($Li^+/K^+$), and 3.80 ($Li^+/Rb^+$), respectively. As a macrocyclic aromatic compound, it has stable chemical properties, high temperature resistance, and acid-base resistance; its structure remains undamaged under pH 2–14 and temperature fluctuation environments, making it suitable for application conditions in complex water bodies such as seawater. The introduction of C4 avoids the detachment problem of traditional ligands caused by relying on hydrogen bonds and ionic bonds. Compared with the 4-tert-butyl modified membrane used in the control group, the adsorption capacity increased significantly from 19.10 mg/g to 50.87 mg/g, confirming the performance optimization space brought by its structural tunability. Li-IIMs adopt a delayed permeation mechanism, and the C4 ligands fixed by ester bonds form specific cavities matching $Li^+$ to specifically intercept $Li^+$, while interfering ions permeate unimpeded to achieve efficient separation. After 4 adsorption-desorption cycles, there was no significant attenuation in the adsorption capacity of Li-IIMs. However, C4 itself has the disadvantages of complex synthesis and strong hydrophobicity; it requires modification or strong polar solvents to maintain uniform dispersion, which increases certain costs and makes large-scale production difficult. Meanwhile, in lithium-based imprinting polymers using crown ether or cuparinated aromatic derivatives as functional monomers, the macromolecular size of NOMs (Natural Organic Matters) readily coats micropore entrances or mesoporous channels [94], hindering $Li^+$ entry into the imprint cavities. Moreover, ion competition under high salinity conditions is inherently challenging; the presence of NOMs further exacerbates mass transfer limitations, resulting in actual adsorption kinetics significantly lower than theoretical expectations [102]. Recent studies indicate that surface imprinting technology more effectively exposes recognition sites on material surfaces compared to conventional bulk polymerization, thereby reducing the risk of internal pore blockage by NOMs [5].

Crucially, the long-term operational viability of these advanced macrocyclic frameworks is significantly compromised by progressive chemical leaching and hydrolytic degradation under continuous marine exposure [4,39]. This structural degradation is further exacerbated at the solid-liquid interface due to complex microscopic thermodynamic interactions. Specifically, while the highly localized electron cloud density on the coordinating oxygen atoms of crown ethers or cuparinated aromatics is designed to capture lithium ions, it simultaneously creates a strong local electrostatic field that attracts ubiquitous background ions. Given the absolute concentration advantage of sodium and magnesium ions in seawater [12,43,103], this intense kinetic collision frequency substantially lowers the activation energy barrier for non-specific ion binding, enabling competing species to forcibly occupy the designed cavities despite insufficient spatial compatibility-induced steric hindrance [46]. Such microscopic competitive interference escalates into a profound techno-economic paradox when applied industrially. Under extremely dilute marine conditions with lithium concentrations of 0.1–0.2 mg/L, the marginal benefits from sporadic lithium capture are insufficient to offset the substantial upfront capital costs required for multi-step ligand synthesis. Consequently, rapid adsorption performance degradation caused by ligand loss and competitive fouling forces material replacement rates to unsustainable levels, creating a fundamental disconnect between actual service life and industrial return on investment.

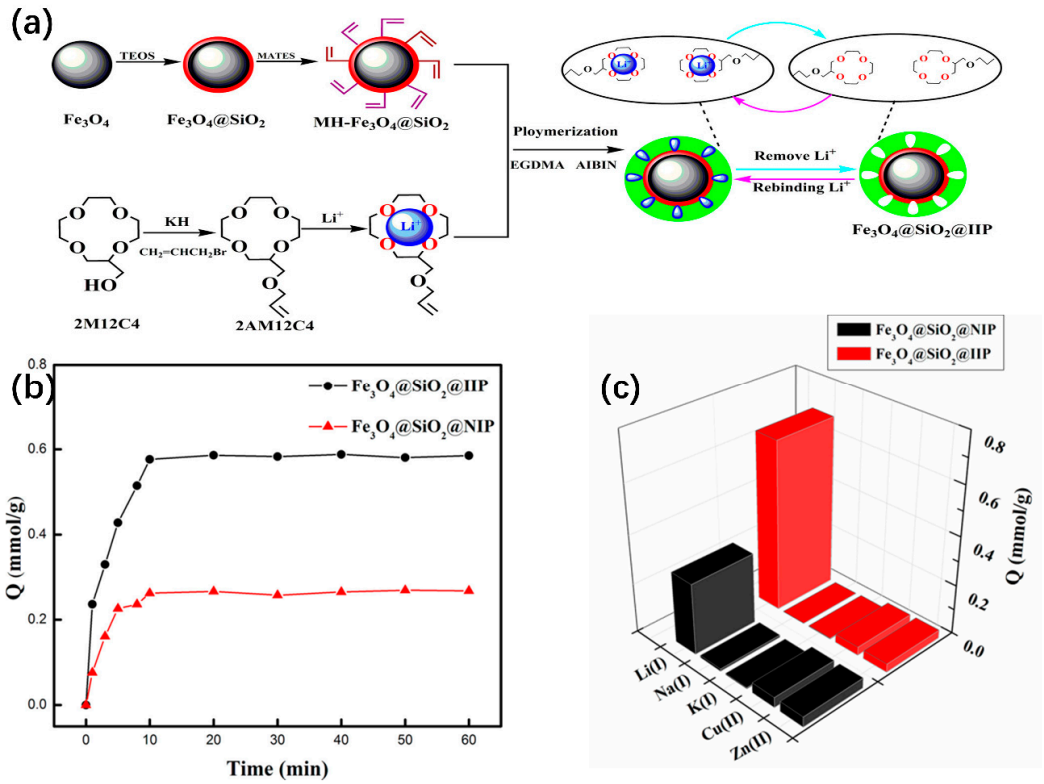


**Figure 11:** (**a**) Synthesis route for $Fe_3O_4$@$SiO_2$@IIP; (**b**) Adsorption kinetics for $Li^+$ ion adsorption on $Fe_3O_4$@$SiO_2$@IIP and $Fe_3O_4$@$SiO_2$@NIP. Conditions: 100 mg of sorbent, 200 mL of Li(I), concentration of 10 mmol/L, and temperature of 25°C; (**c**) Selective binding analysis of $Li^+$ ion by $Fe_3O_4$@$SiO_2$@IIP and $Fe_3O_4$@$SiO_2$@NIP. Conditions: 50 mg of sorbent, 50 mL of Li(I), concentration of 10 mmol/L, and temperature of 25°C. Reprinted with permission from reference [96]. Copyright 2015, ACS.

### Types of Crosslinking Agents

The cross-linker of ion-imprinted polymers is the core component for constructing a three-dimensional rigid imprinted skeleton, which determines the pore structure, mechanical strength, swelling performance of the polymer, and the stability of ion recognition sites. The selection of its type needs to match the coordination characteristics of template ions. Commonly used cross-linkers include ethylene glycol dimethacrylate (EGDMA) [43] and divinylbenzene (DVB), etc. Their dosage is usually much higher than that of functional monomers to form a rigid three-dimensional network, thereby effectively retaining the cavity structure after eluting the template ions and preventing their collapse. The increase in cross-linking degree can improve the mechanical and chemical stability of the material, which is conducive to multiple cycles of use. However, excessively high cross-linking degree may lead to a decrease in porosity and an increase in mass transfer resistance, thereby reducing the adsorption kinetic rate. Considering the actual characteristics of lithium ion recovery from seawater, cross-linkers need to meet the requirements of aqueous compatibility, low cross-linking density to adapt to the weak coordination characteristics of $Li^+$, and swelling resistance in the high-salinity environment of seawater. Therefore, acrylates are the main type, and composite systems are often used to balance performance; non-polar diene compounds such as DVB are rarely used [43].

In published papers related to $Li^+$ adsorption [97,100,104,105], almost all ion-imprinted polymers are prepared using EGDMA as the cross-linker. As a cross-linker, EGDMA contains two polymerizable methacryloyl groups, which are highly matched with the free radical polymerization activity of functional monomers (2AM12C4, MAA). It can form a uniform cross-linked network on the surface of the PVDF/GR-$TiO_2$ composite membrane, avoiding uneven polymerization caused by poor compatibility, which is an important prerequisite for the uniform distribution of $Li^+$ imprinted sites. Secondly, EGDMA contains weakly polar ether chains (-O-), which not only avoids the hydrophobicity of the membrane caused by non-polar cross-linkers but also prevents excessive swelling in the high-salinity seawater environment caused by highly polar cross-linkers such as MBA. As shown in Fig. 12, LiI-NcMs still maintain a stable pore structure with a narrow pore size in simulated seawater with a $Mg^{2+}$ concentration of 200 mg/L, which is conducive to the interaction between $Li^+$ and imprinted sites, proving the salt swelling resistance of the EGDMA cross-linked skeleton. Finally, the moderate cross-linking density of EGDMA can not only fix the spatial structure of coordination complexes and avoid the deformation of imprinted sites during polymerization but also prevent site embedding caused by excessive cross-linking.

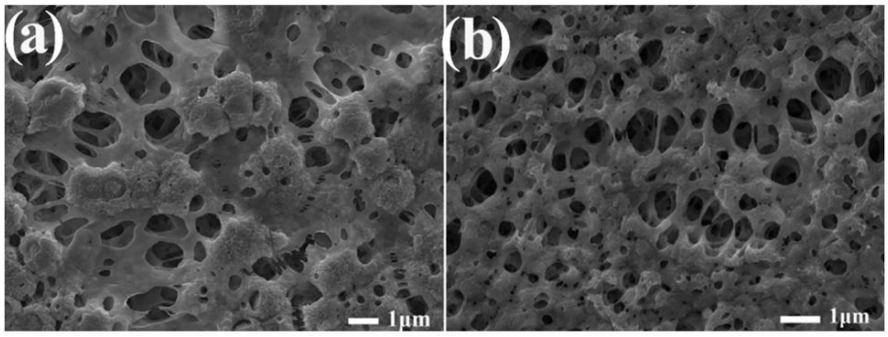


**Figure 12:** SEM images of (**a**) PVDF membrane and (**b**) LiI-NcM. Reprinted with permission from reference [105]. Copyright 2022, Springer.

## Polymerization Methods

The polymerization method of ion-imprinted polymers directly participates in shaping the macro morphology, micro pore structure, effective specific surface area, and spatial distribution of recognition sites of the material, profoundly affecting its separation efficiency in complex seawater environments. The independent polymerization methods for preparing ion-imprinted polymers to adsorb metal ions include the following three: As shown in Fig. 13a, bulk polymerization [106,107] consists only of monomers, template ions, cross-linkers, and initiators, without additional solvents or porogens. The polymerization reaction proceeds in the monomer phase itself, and the polymerized product needs to be ground and sieved to obtain granular IIPs. The bulk polymerization system is simple, and the coordination between template ions and functional monomers is not interfered by solvents, resulting in high density of imprinted sites and strong selectivity. It is the earliest and most basic preparation method for IIPs. Suspension polymerization [103,108] is a classic free radical polymerization technology. By dispersing the organic phase containing template ions, functional monomers, cross-linkers, and initiators in an aqueous continuous medium, polymers, as shown in Fig. 13b, are formed under the action of stabilizers. As shown in Fig. 13c, the sol-gel method [109,110] is based on the hydrolysis and condensation reactions of silane or metal alkoxide precursors, constructing inorganic or organic-inorganic hybrid networks with Si-O-Si or M-O-M as the main chain under mild conditions. This method can precisely control the pore structure, endowing the material with a high specific surface area and abundant surface functional groups.

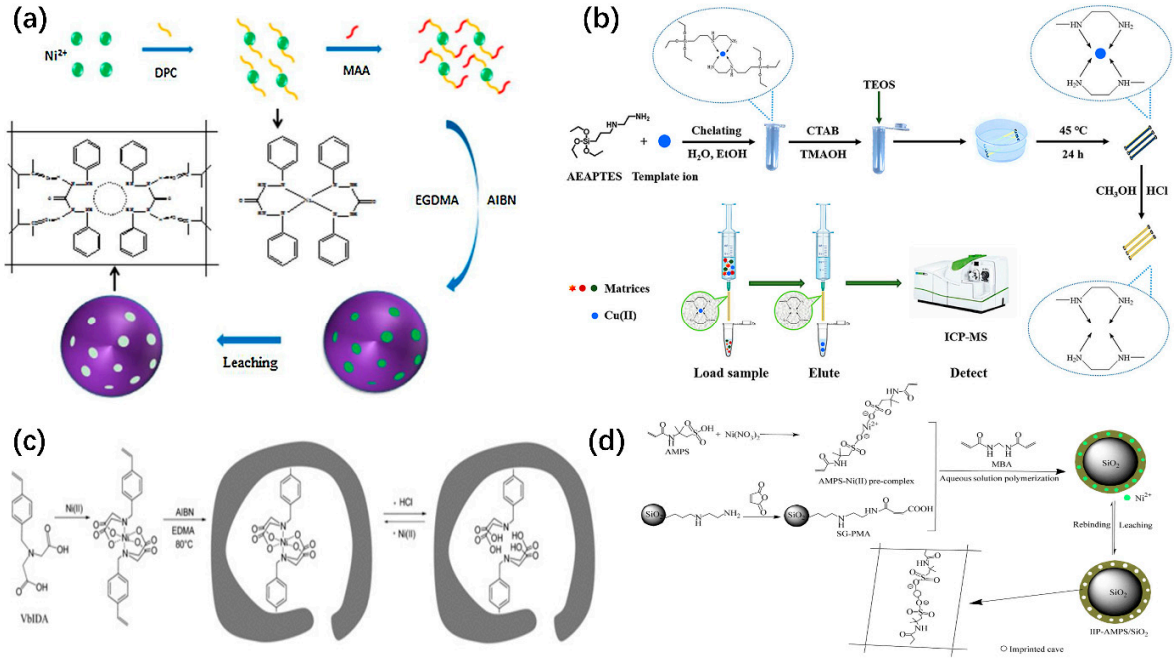


**Figure 13:** (**a**) Ni (II)-impacted polymer was prepared by bulk polymerization. Reprinted with permission from reference [107]. Copyright 2018, Elsevier; (**b**) Preparation of copper (II) ion-imprinted hybrid monolithic column by sol gel method. Reprinted with permission from reference [109]. Copyright 2021, Elsevier; (**c**) Synthesis of IIP polymer beads prepared by reverse suspension polymerization. Reprinted with permission from reference [103]. Copyright 2012, Wiley; (**d**) The preparation of IIP-AMPS/$SiO_2$. Reprinted with permission from reference [111]. Copyright 2018, Springer.

To overcome the problems of large mass transfer resistance and difficult template elution in traditional bulk imprinting, the synthesis method of IIPs has developed from a single traditional polymerization to a multi-strategy integrated system. The integrated system is mainly composed of surface imprinting technology combined with the sol-gel method, graft polymerization, or layer-by-layer self-assembly, which fully exposes and concentrates the imprinted sites on the carrier surface. At the same time, the carrier provides a rigid skeleton such as $SiO_2$, which combines high selectivity and stability. As shown in Fig. 13d, He et al. [111] successfully prepared a Ni (II) ion-imprinted silica polymer (IIP-AMPS/$SiO_2$) by combining surface imprinting technology with aqueous solution polymerization. The ion-imprinted material prepared by the composite system can reach adsorption equilibrium within 10 min, with a maximum adsorption capacity of 66.22 mg/g, which is 1.5 times that of the non-imprinted material. By comparing with surface imprinted materials such as imprinted materials using 3-aminopropyltrimethoxysilane and chitosan as monomers, the performance advantages of the composite system of surface imprinting and aqueous solution were verified. With the in-depth research, novel composite systems such as inorganic-organic hybrid composites [26], grafting-surface imprinting [27], and surface imprinting-reversible addition-fragmentation chain transfer [28] have emerged.

For lithium recovery from seawater, factors including high salinity, low lithium ion concentration, and the requirement for balanced hydrophilicity and selectivity must be taken into account. Jamoussi et al. [94] adopted precipitation polymerization, a method characterized by simple operation, excellent product dispersibility, and compatibility with the coordination requirements between phthalocyanine-based functional monomers and lithium ions. As illustrated in Fig. 14a, highly selective and stable lithium ion-imprinted polymer particles were prepared through a sequential process involving template coordination with monomers, free-radical polymerization in solution, product precipitation, and template removal. Porous structures were obtained solely by solvent selection and control over polymerization conditions, with no additional porogens or stabilizers needed. Precipitation polymerization directly yields granular products without complex forming steps, and the uniform particle size eliminates the need for grinding. The particles feature a specific surface area of 106.03 $m^2/g$ and a pore volume of 0.387 $cm^3/g$, providing ample adsorption sites for lithium ions and reaching near-complete adsorption equilibrium within 60 min. These particles are also suitable for packing into solid-phase extraction columns, enabling their application in dynamic adsorption scenarios. As shown in Fig. 14b, Yu et al. [97] employed surface graft polymerization to realize surface imprinting technology. Imprinted polymer layers were constructed on the surfaces of polydimethylsiloxane membranes via surface chemical modification and graft polymerization. Unlike bulk polymerization and precipitation polymerization, the polymerization reaction occurs exclusively on the surface of the membrane support, concentrating imprinted sites within the surface layer and avoiding internal entrapment. This structure delivers high lithium ion mass transfer efficiency, allowing adsorption equilibrium to be reached within 90 min. Moreover, the imprinted layers are firmly bound to the support through covalent bonds, preventing detachment. No significant decline in adsorption capacity is detected after four adsorption–desorption cycles, indicating excellent cyclic stability. The polydimethylsiloxane-polydopamine layer fabricated via surface graft polymerization significantly improves membrane hydrophilicity, reducing the contact angle from 128° to 47.1° (Fig. 14c). The ester-based ligands introduced by surface grafting exhibit stronger coordination interactions with lithium ions, enabling the material to retain a high selectivity coefficient of 4.56 in aqueous systems including seawater, as presented in Fig. 14d.

Surface imprinted polymerization has emerged as a pivotal strategy developed in recent years to overcome the limitations of bulk polymerization, and it is particularly applicable to lithium recovery from

seawater. This approach constructs the imprinted layer on the surface of supports with high specific surface area and favorable mechanical performance, such as silica gel, magnetic nanoparticles and graphene. Such a structural design not only shortens the ion diffusion pathway and improves adsorption kinetics but also facilitates the separation and recycling of the materials. Urbanová et al. [112] adopted surface imprinted polymerization, which involves support activation, surface grafting and precise imprinting. Biochar activated by $K_2CO_3$ provides sufficient active sites for polymerization, enabling the WC-900-1-KL material prepared under activation at 900°C with a mass ratio of 1:1 to achieve a maximum adsorption capacity of 0.569 mg/g, representing an increase of 65.9% compared with materials supported on unactivated carriers. During polymerization, the imprinted layer is uniformly grafted onto the biochar surface, with recognition sites fully exposed and structurally regular. Adsorption equilibrium data conform to the Langmuir isotherm model with goodness of fit values $R^2$ all greater than 0.88, indicating homogeneous monolayer adsorption and a substantial improvement in the utilization efficiency of recognition sites. The imprinted cavities exposed on the surface shorten the lithium ion diffusion pathway, allowing all materials to reach adsorption equilibrium within 60 min. The adsorption capacity of WC-900-1-KL reaches more than 80% of its equilibrium value within the initial 20 min, which is far faster than the 2–4 h required for conventional bulk imprinted materials, thus significantly accelerating the adsorption kinetic rate.

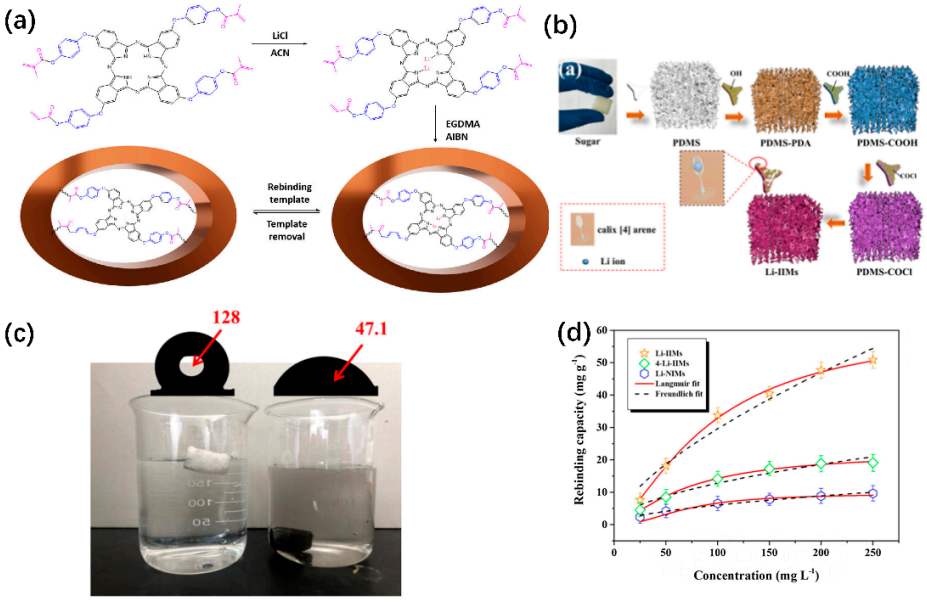


**Figure 14:** (**a**) Schematic illustration of Li-IIP synthesis steps and Li removal from IIP binding sites. Reprinted with permission from reference [94]. Copyright 2023, MDPI; (**b**) Schematic diagram of the Li-IIMs preparation process; (**c**) The water contact angle images of PDMS (white) and PDMS-PDA (black); (**d**) Adsorption isotherm curves of Li-IIMs toward $Li^+$. Reprinted with permission from reference [97]. Copyright 2020, Elsevier.

Electrochemical polymerization and radiation-initiated polymerization are two advanced polymerization techniques with unique advantages in the synthesis of functional polymeric materials, and they show remarkable potential especially in the preparation of ion-imprinted polymers for the selective recovery of lithium ions. These two methods enable precise control over the polymerization process and allow the construction of functional materials with high integrity of recognition sites and excellent structural stability under mild conditions, which is of great importance for addressing the complex separation challenges arising from extremely low lithium concentrations and the coexistence of numerous competing ions

in seawater. Inspired by the aforementioned polymerization techniques, Prigyai et al. [98] successfully fabricated two functional materials, P-POSS_Methyl$D_4$_2H12C4 and P-POSS_Vinyl$D_4$_2H12C4, through gamma radiation-induced graft polymerization followed by post-functionalization, as shown in Fig. 15a. The radiation dose directly determines the grafting yield. A higher grafting yield leads to a greater subsequent loading of 2H12C4 and a denser distribution of lithium ion adsorption sites. Both materials exhibit a $Li^+/Mg^{2+}$ separation factor higher than 4.07, and the $Li^+/K^+$ separation factor of P-POSS_Vinyl$D_4$_2H12C4 reaches 23.21, which is far superior to that of lithium ion-imprinted polymers prepared via conventional polymerization methods. Following functionalization, the adsorption capacity of the materials in real seawater increases to 3.52–3.58 mg/g, representing a more than fourfold enhancement compared with un-functionalized P-POSS which ranges from 0.44 to 0.78 mg/g, as illustrated in Fig. 15b. In systems containing coexisting sodium, potassium, magnesium and calcium ions, the lithium ion adsorption capacity ranges from 3.17 to 3.28 mg/g, which is considerably higher than the adsorption capacity of 0.33–1.55 mg/g for other ions. The distribution coefficient $K_d$ of lithium ions ranges from 1.65 to 1.80 L/g, which is 3 to 26 times that of other competing ions as depicted in Fig. 15c. After five adsorption–desorption cycles, the adsorption capacity decreases by only 15–20%, confirming the favorable structural stability of the materials. Radiation polymerization shows strong adaptability to high-salinity environments with low lithium ion concentrations. It involves no chemical initiators or residual catalysts and proceeds under mild conditions, making it compatible with the marine ecosystem. However, this method requires radiation sources or electron accelerators, leading to high initial capital equipment investment. The reaction duration exceeds 72 h, resulting in relatively low efficiency compared with conventional methods.

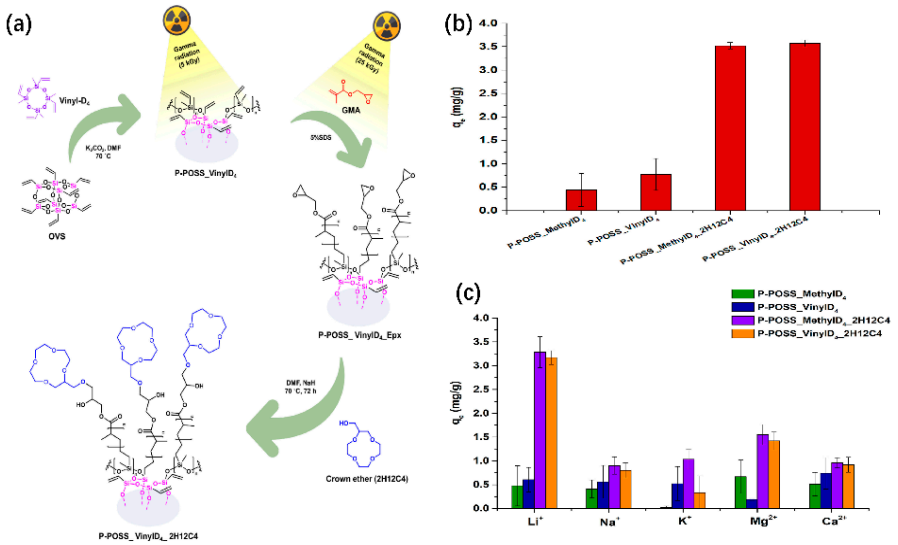


**Figure 15:** (**a**) Synthetic route for P-POSS_VinylD4_2H12C4 materials; (**b**) Lithium-ion adsorption capacity of different materials; (**c**) Adsorption selectivity of different materials. Reprinted with permission from reference [98]. Copyright 2025, Elsevier.

## Elution Conditions and Regeneration Capability

The practical application performance of ion-imprinted polymers depends not only on their adsorption properties but also crucially on the mildness of elution conditions and the durability of regeneration capability, which directly determines the economic efficiency and sustainability of the overall process. Elution conditions should be selected by balancing elution efficiency, namely lithium ion desorption rate,

the protection of imprinted sites and process economic efficiency. For lithium recovery from seawater, the extremely low-concentration of lithium ions imposes higher requirements on the selectivity of eluents to prevent the co-elution of other competing ions. Lithium recovery places greater emphasis on elution rate and concentration effect, and a higher lithium ion concentration in the eluent reduces the cost of subsequent lithium extraction processes. The most widely used eluents are strong acids. Acidic reagents can effectively protonate the coordinating groups on functional monomers and break the coordination bonds between lithium ions and the polymer network. Inorganic acids are prone to volatilization and leave no residues, which avoids secondary pollution to seawater caused by organic eluents and meets the demand for ecological friendliness in marine environments. The regeneration capability of ion-imprinted materials is affected by multiple factors rather than a single variable. The stability of the skeletal structure, the binding strength and distribution of imprinted sites, the pore structure, hydrophilicity and hydrophobicity, as well as the cross-linking degree collectively determine the upper limit of regeneration performance. However, no relevant studies have directly clarified the specific contribution of each factor to regeneration performance.

Jamoussi et al. [94] immersed lithium ion-imprinted polymers with saturated adsorption in 1 mol/L nitric acid and performed ultrasonic-assisted elution. The elution process was repeated until no lithium ions were detected in the eluent by inductively coupled plasma optical emission spectrometry, followed by washing with distilled water until neutral. The eluted materials were vacuum-dried at 60°C for 24 h for subsequent adsorption-desorption tests. 1 mol/L nitric acid achieved an elution efficiency of 95%, which effectively disrupted the coordination between lithium ions and nitrogen atoms in the phthalocyanine ring, completely removed template ions and regenerated imprinted cavities. Compared with 0.5 mol/L hydrochloric acid and sulfuric acid, nitric acid leaves no residual impurities and prevents secondary pollution to seawater in subsequent applications. After eight adsorption-desorption cycles, the lithium ion adsorption capacity decreased from an initial 3.2 mg/g to 2.57 mg/g, corresponding to a reduction of only 19.7%. This result indicates that elution with nitric acid does not damage the Si-O-Si cross-linked skeleton and phthalocyanine functional groups of the ion-imprinted polymer, demonstrating excellent structural stability of the material. Shao et al. [104] placed CQD@$SiO_2$@IIP after lithium-ion adsorption into 0.1 mol/L nitric acid and performed oscillatory elution at room temperature for 12 h. The elution endpoint was determined by the recovery of fluorescence intensity, and the material was finally washed with distilled water until the pH value reached 7. Regeneration was completed via vacuum drying at 50°C for 12 h after elution. After five cycles, the $Li^+$ adsorption capacity decreased from an initial 4.53 mg/g to 3.89 mg/g, with a reduction of 14.1%. Sun et al. [105] immersed saturated adsorbed LiI-NcMs in 0.5 mol/L hydrochloric acid and conducted stirring elution at room temperature for 1 h. The concentration of lithium ions in the eluent was monitored by inductively coupled plasma optical emission spectrometry, and elution was stopped when the concentration stabilized. The membrane surface was rinsed with distilled water until neutral. After 20 cycles, the lithium ion to magnesium ion separation factor decreased from an initial 8.58 to 7.62, representing a reduction of only 11.2%. Mild elution with 0.5 mol/L hydrochloric acid does not damage the nanocomposite structure of graphene oxide/titanium dioxide and the crown ether cavities of 2M12C4, and the size matching and coordination specificity of the ion-imprinted polymer toward lithium ions remain intact.

In addition to traditional acid elution, several innovative strategies have been developed to achieve milder and smarter regeneration. The elution strategy proposed by Liang et al. [99] is based on nitric acid and utilizes the superparamagnetism of the $Fe_3O_4$@C support to realize rapid solid-liquid separation between lithium ion-imprinted polymers and the eluent under an external magnetic field. This approach avoids the cumbersome operations of conventional centrifugation and filtration and reduces material loss.

Meanwhile, the thermosensitive monomer N-isopropylacrylamide incorporated in the material possesses a lower critical solution temperature. When the temperature exceeds the lower critical solution temperature, the polymer chains collapse, disrupting the structure of imprinted cavities and weakening the interaction between lithium ions and binding sites to promote lithium ion desorption. When the temperature falls below the lower critical solution temperature, the polymer chains swell and the imprinted cavities recover, facilitating re-adsorption. Temperature regulation can assist acid elution to improve elution efficiency and simplify operational procedures. The adsorption capacity retains 91.47% of its initial value after five cycles.

*3.1.2 Dependence of Performance on Operation Conditions*

In addition to the regulatory effects of preparation conditions on the performance of ion-imprinted polymers in lithium recovery from seawater as elucidated in the preceding sections, the application conditions of the materials also exert direct influences on their performance. The regulatory roles of factors including pH, temperature and interfering ions will be discussed in detail in the following context [11].

pH

pH serves as a core operational parameter governing the selective adsorption of $Li^+$ by lithium ion-imprinted polymers from seawater. The pH of natural seawater remains stable within the range of 7.5 to 8.5 [113]. This parameter regulates the adsorption process through both direct and indirect mechanisms. On one hand, it modifies the ionization state of functional groups and the surface charge characteristics of lithium ion-imprinted polymers, which directly determines the complexation efficiency between imprinted recognition sites and $Li^+$. On the other hand, it indirectly influences the selective adsorption performance toward $Li^+$ by regulating the existing forms of major competing ions such as $Mg^{2+}$ and $Ca^{2+}$ in seawater. Notably, the solubility product constant of lithium hydroxide is sufficiently large to prevent hydrolytic precipitation of $Li^+$ in seawater matrices. As a result, the regulatory effect of pH on $Li^+$ adsorption is confined exclusively to the material phase of lithium ion-imprinted polymers. Under acidic conditions with pH below 6, functional groups including carboxyl and phosphonic acid groups become protonated and lose their ability to form complexes or electrostatic interactions with $Li^+$. Imprinted sites are occupied by hydrogen ions, leading to a sharp decline in the adsorption capacity of lithium ion-imprinted polymers [114]. The competitive effect between hydrogen ions and $Li^+$ also significantly slows down the adsorption kinetic rate [115,116].

At pH values above 9, although further ionization of functional groups can be promoted, high concentrations of $Mg^{2+}$ and $Ca^{2+}$ in seawater undergo hydrolysis to form hydroxide precipitates. These precipitates physically block the imprinted sites and pore channels of the polymers and deposit on the material surface to form mass transfer barriers [117], which prevents $Li^+$ from accessing internal binding sites. Both adsorption capacity and kinetic rate decrease substantially, and the precipitates are difficult to desorb, causing irreversible contamination of the materials.

Within the pH range of 6 to 9, functional groups undergo partial or complete ionization, rendering the material surface negatively charged. This enables dual binding mechanisms involving electrostatic attraction and coordination complexation with $Li^+$. The accessibility and activity of imprinted sites reach an optimal level, with adsorption capacity approaching the theoretical maximum of the material [104] and the fastest kinetic rate. This range matches well with the natural pH of seawater [118] and represents the primary optimized pH window for most existing lithium ion-imprinted polymers. The above mechanisms are supported by the findings of Cao et al. [18]. The zeta potential of lithium ion-imprinted polymers remains negative across the pH range of 4 to 10 and decreases gradually with increasing pH. As illustrated in

Fig. 16a, the adsorption capacity of the polymers for $Li^+$ increases continuously with rising pH from 4 to 10 and reaches a maximum at pH 10. A further increase beyond pH 10 leads to a slight reduction in adsorption, confirming the mechanism by which enhanced surface negative charge promotes electrostatic adsorption of $Li^+$. Qi et al. [93] reported similar trends. At pH below 5, adsorption capacity is extremely low because oxygen atoms in benzo-15-crown-5 undergo extensive protonation and exhibit reduced electronegativity, thus repelling $Li^+$. From pH 5 to 8.5, adsorption capacity increases continuously due to the reduced concentration of hydrogen ions and weakened protonation of oxygen atoms, which strengthens binding toward $Li^+$. The maximum adsorption capacity is achieved at pH 8.5. A decline in adsorption was observed above pH 8.5, although its underlying mechanism was not conclusively established, resulting in decreased adsorption capacity as shown in Fig. 16b.

Conversely, Alshuiael and Al-Ghouti reported minimal pH dependence for a $Li^+$-imprinted polymer synthesized using LiCl as the template ion, dicyclohexano-18-crown-6 as the ionophore, and tert-butyl acrylate as the functional monomer. As shown in Fig. 16c, the $Li^+$ removal efficiency remained between 98.6% and 99.0% over the pH range of 2–10, corresponding to a variation of only 0.4 percentage points [114]. Although dicyclohexano-18-crown-6 is not conventionally regarded as size-matched to $Li^+$, its use in the $Li^+$-imprinted polymer was explicitly reported in the original study. The same $Li^+$-imprinted polymer, rather than a separately prepared $Sr^{2+}$-imprinted polymer, was subsequently evaluated for $Sr^{2+}$ adsorption. However, the mechanistic origin of the observed pH-independent $Li^+$ removal was not conclusively established.

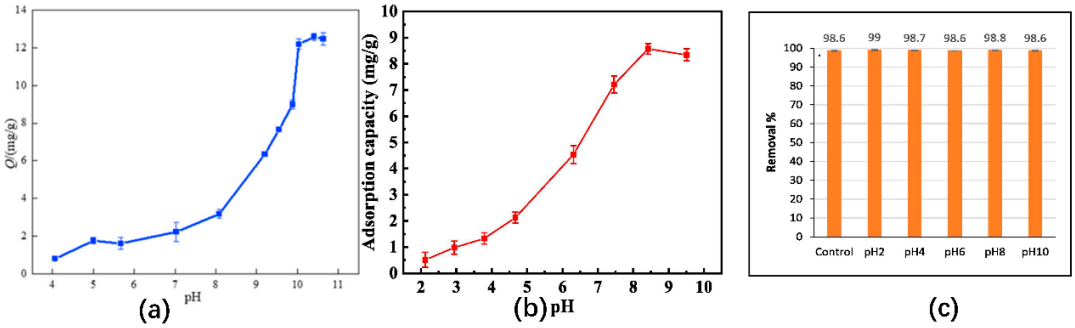


**Figure 16:** (**a**) Effect of pH on the adsorption amount of Li(I)-IIPs. Reprinted with permission from reference [18]. Copyright 2024, ACS; (**b**) Effects of ph. Reprinted with permission from reference [93]. Copyright 2024, Elsevier; (**c**) Effect of pH on the IIP adsorption removal % toward Lithium. Reprinted with permission from reference [98]. Copyright 2022, Elsevier.

## Temperature

Temperature exerts a pronounced influence on adsorption performance. By regulating the diffusion rate of lithium ions and the thermodynamic properties of the adsorption process, it governs the adsorption kinetics and equilibrium capacity of lithium ion-imprinted polymers (Li-IIPs). Concurrently, temperature moderately modulates the swelling behavior of the polymer backbone, indirectly altering the accessibility of imprinted sites. Moderate heating markedly accelerates the diffusion of lithium ions within bulk seawater, the liquid film on material surfaces, and internal pore channels, while reducing the thickness of the mass transfer boundary layer. This promotes faster contact between lithium ions and imprinted sites, shortens the adsorption equilibrium time, and significantly elevates the rate constant k2 of the pseudo-second-order kinetic model. Conversely, cooling impedes ion diffusion, slowing kinetic rates and prolonging adsorption equilibrium, yet does not fully inhibit the adsorption process.

Liang et al. [99] reported that the temperature-dependent performance of $Li^+$-IIP materials is primarily governed by modulating the swelling or shrinkage of thermosensitive polymers and the efficiency of ion mass transfer. This mechanism is jointly supported by the data presented in Fig. 17a,b. The optimal adsorption temperature for this material is 35°C. The hydrodynamic diameter of $Li^+$-IIPs decreases from 450 nm to 345 nm as the temperature rises from 20°C to 55°C. Differential calculations yield a critical solution temperature of 37.89°C for the polymer, which is higher than the 32°C value of pristine N-isopropylacrylamide (NIPAM) monomer. This shift arises from the intricate chain architecture and conformation within $Li^+$-IIPs, which impart greater structural rigidity and hydrophobicity. In terms of adsorption capacity, tested under an initial lithium ion concentration of 10 mg/L, pH 7.0, and an adsorption duration of 60 min, $Li^+$-IIPs exhibit an adsorption capacity of 5.19 mg/g at 35°C, significantly exceeding the 4.25 mg/g measured at 25°C. Adsorption capacity declines at 45°C, while the corresponding capacity of non-imprinted polymers ($Li^+$-NIPs) is only 2.20 mg/g at 35°C. The underlying mechanism is as follows. At temperatures below the critical solution temperature, polymer swelling distorts imprinted sites and increases the separation distance between lithium ions and binding domains, resulting in lower adsorption capacity. When the ambient temperature exceeds the critical solution temperature, $Li^+$-IIPs undergo a volume phase transition, where the outer polymer layer converts from hydrophilic to hydrophobic. This transition disrupts the imprinted structure, reduces the population of specific active sites, and causes a sharp decrease in adsorption capacity. These results clearly demonstrate the significant regulatory effect of temperature on the structural stability and adsorption performance of $Li^+$-IIPs.

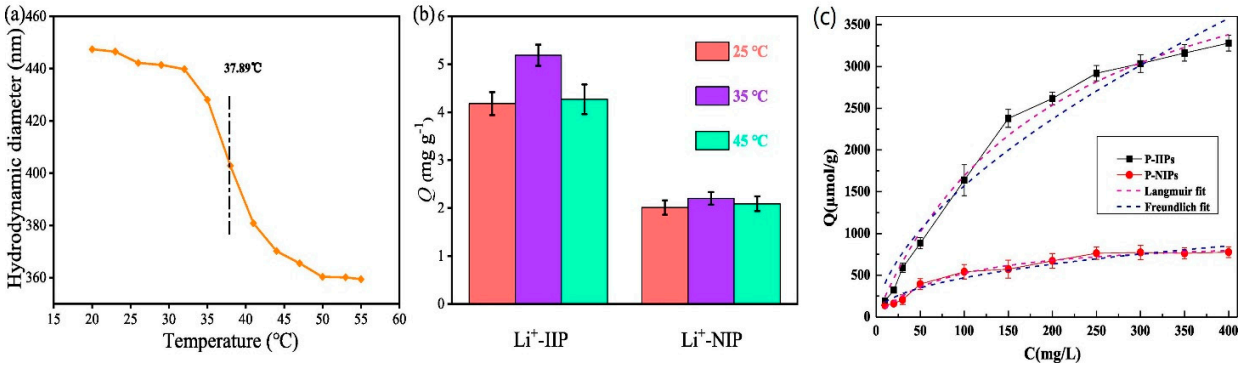


**Figure 17:** (**a**) Hydrodynamic diameters and (**b**) Adsorption capacities of $Li^+$-IIP at various temperatures. Reprinted with permission from reference [99]. Copyright 2023, Elsevier. (**c**) Adsorption isotherms and fitting curves of P-IIPs and P-NIPs. Reprinted with permission from reference [54]. Copyright 2019, Elsevier.

### Initial Ion Concentration

With increasing initial $Li^+$ concentration, the adsorption isotherms generally follow the Langmuir model, indicating that adsorption takes place on finite, energetically uniform specific sites. The equilibrium adsorption capacity rises accordingly and eventually approaches the theoretical maximum adsorption capacity. However, such ideal single-component adsorption behavior is severely disrupted in real seawater or high-salinity brine environments. High concentrations of $Mg^{2+}$ and $Ca^{2+}$ not only weaken the Coulombic attraction between $Li^+$ and imprinted sites via electrostatic shielding, but also alter the swelling behavior and microenvironmental polarity of the IIP matrix through their strong hydration effects, thereby indirectly influencing the mass transfer rate and binding strength of $Li^+$ [35]. Furthermore, although $Na^+$ carries the same charge as $Li^+$, its larger ionic radius and lower hydration energy still allow non-specific occupation of partial active sites, reducing the actual selectivity of IIPs as background salt concentration increases.

Huang et al. [54] have verified the impact of initial concentration on adsorption performance. As illustrated in Fig. 17c, initial $Li^+$ concentration exerts a pronounced regulatory effect on the $Li^+$ uptake of P-IIPs. Under visible-light irradiation, pH 7.0 and an adsorption time of 1 h, the adsorption capacities of both materials increase monotonically as the initial $Li^+$ concentration rises from 0 to 400 mg/L, with the maximum adsorption capacity of P-IIPs reaching 3280.5 μmol/g. Fitting of experimental data reveals that the adsorption processes of both materials agree well with the Langmuir isotherm model, with correlation coefficients of 0.99 for P-IIPs and 0.98 for P-NIPs. These results confirm uniformly distributed binding sites on both surfaces and a monolayer chemisorption mechanism. Higher initial $Li^+$ concentrations enhance the collision frequency between $Li^+$ and surface sites, which in turn elevates the overall adsorption capacity.

Interfering Ions

Beyond the factors discussed above, the complex chemical matrix of seawater contains a wide range of competing ions that impair the lithium adsorption performance of ion-imprinted polymers. With a concentration typically several thousand times higher than that of $Li^+$, $Na^+$ generates a strong mass effect and competes for partial imprinted sites, reducing the effective adsorption capacity for $Li^+$. In particular, $Mg^{2+}$ and $Na^+$, with ionic and hydration radii similar to $Li^+$, give rise to more intense competitive adsorption, further lowering both the uptake and selectivity for $Li^+$ [119]. A Li(I)-imprinted polymer based on calixarene ligands developed by Cao et al. [18] exhibits an exceptionally high $Li^+/Na^+$ selectivity coefficient $\alpha$(Li/Na) of 12.5 when exposed to high concentrations of $Na^+$, $K^+$, $Mg^{2+}$ and $Ca^{2+}$. The Li-imprinted polymer synthesized by Qi et al. [93] also displays excellent $Li^+/Mg^{2+}$ selectivity, with $\alpha$(Li/Mg) values well above unity, confirming its ability to overcome separation challenges associated with brines featuring high Mg/Li ratios. Detailed mechanistic studies have further clarified the microscopic pathways by which interfering ions affect adsorption performance. Analyses using X-ray photoelectron spectroscopy and Fourier-transform infrared spectroscopy show that interfering ions including $Mg^{2+}$ can form stable complexes with carboxyl groups on functional monomers or oxygen atoms in crown ether structures. Such interactions reshape the electron cloud distribution and chemical microenvironment around imprinted cavities, weakening the binding affinity toward $Li^+$. Research demonstrates that rationally designed ligands maximize the binding energy for $Li^+$ while minimizing interactions with larger or highly charged ions, which constitutes the molecular basis for achieving high selectivity [54,99].

### *3.2 Ion-Imprinted Hydrogel*

To date, no research has documented the recovery of lithium ions from seawater via ion-imprinted hydrogels. The highly complex matrix of seawater presents a fundamental challenge, with the lithium ion concentration at merely 0.17 ppm, while the mass concentrations of competing ions, including $Na^+$, $Mg^{2+}$, and $Ca^{2+}$, are approximately $6.4 \times 10^4$, $7.6 \times 10^3$, and $2.4 \times 10^3$ times higher than that of $Li^+$, respectively. Current imprinted hydrogels synthesized from functional monomers such as acrylic acid and methacrylic acid fail to preserve their recognition capacity in authentic seawater. Their selectivity coefficients drop drastically under high ionic strength, leaving these materials unable to differentiate lithium ions from other alkali and alkaline earth metal ions effectively. In addition, the physicochemical stability of hydrogel materials is severely challenged in seawater. High-salinity triggers the shrinkage and even collapses of hydrogel networks, impeding lithium ion mass transfer kinetics. Biofouling clogs imprinted sites, and pH fluctuations undermine the coordination interaction between functional groups and lithium ions. The combination of antifouling and ion-imprinting technologies is still at the proof-of-concept stage. Moreover, most existing studies on ion-imprinted polymers concentrate on salt lake brine systems, where lithium ion

concentrations are substantially higher than in seawater and total ionic levels are relatively controllable. Material design strategies targeting the distinct challenges of seawater remain seriously insufficient.

## 4 Uranium-Selective Ion-Imprinted Materials and Their Performance in Seawater Systems

Seawater uranium resources exceed 4.5 billion tons, more than a thousand times the reserves of terrestrial uranium ores. As the core raw material for the nuclear power industry [120], its efficient extraction possesses irreplaceable value for safeguarding the strategic security of nuclear energy and has become a research hotspot in the field of marine scattered resource extraction. Compared with seawater lithium extraction, seawater uranium extraction faces more stringent challenges due to fundamental differences in the intrinsic characteristics of target ions. Uranium exists at an ultra-trace level of 3.3 ppb in seawater, far lower than the trace concentration of 0.17 mg/L for lithium [121,122]. Moreover, under the naturally weakly alkaline conditions of seawater, uranium does not exist in the form of free ions but forms a stable anionic complex $UO_2(CO_3)_3^{4-}$ with carbonate ions [123], which is in stark contrast to the free $Li^+$ cation form of lithium. Their core interference mechanisms are also starkly different. The main obstacles to seawater uranium extraction stem from the complexation of high-concentration carbonate ions and non-specific adsorption contamination by seawater organic matter, rather than the cationic competition between $Li^+$ and $Mg^{2+}$ caused by similar hydration radii and coordination properties in seawater lithium extraction. With its specific recognition capability for target ions, ion-imprinted materials provide an ideal material solution for the ultra-trace enrichment and anti-interference separation in seawater uranium extraction [124].

### *4.1 Ion-Imprinted Polymer*

Although the applications of ion-imprinted polymers in seawater uranium and lithium extraction seemingly fall into the category of ion-selective adsorption, they exhibit systematic and fundamental differences in molecular recognition mechanisms, material design logic, environmental response behaviors, and engineering failure modes. These differences are not minor adjustments of technical details but an underlying paradigm divergence determined by the distinctly different physicochemical intrinsic properties of target ions in seawater medium. Below, the preparation conditions for adsorbing uranium from seawater using ion-imprinted polymers are discussed in detail (Table 4).

**Table 4:** Representative overview of ion-imprinted polymer performance in uranium absorption.

| Material System | Adsorption Capacity (mg/g) | Selectivity Coefficient ($\alpha$) | Equilibrium Time (min) | Ref. |
|---|---|---|---|---|
| IIP-$UO_2(CO_3)_3^{4-}$/VI/4-VBC | 5.2 (real seawater) | U/V: 12.8 | — | [124] |
| IIP-bis-salicylaldoxime | 5.79 (real seawater, 56 d) | U/V: >100 | — | [125] |
| IIP-IIZMS-G (guanidine/zeolite) | 85.82 | U/$Zn^{2+}$: 11.23, U/$Mg^{2+}$: 8.40, U/$Ca^{2+}$: 6.94 | — | [126] |
| IIP-Schiff base/DVB microspheres | 147.8 | U/V: 14.22, U/Co: 19.66, U/Ni: 21.75 | — | [127] |
| MIPAF-11c | 37.28 | U/$Fe^{3+}$: 746 | — | [128] |
| IIP-$Fe_3O_4$@m$SiO_2$@FIIP | — | U/$Eu^{3+}$: ~8% capacity loss | — | [129] |
| IIH-SPUIT (thermosensitive, ε-PL) | 125.57 | U/$Cd^{2+}$: 14.78 | — | [130] |
| IIH-SPUIT (thermosensitive) | 109.37 | U/$K^+$: 15.76 | — | [130] |
| IIH-UITAC (NIPAM/chitosan) | 81.2 | U/$V^{3+}$: 1.4–10.3 | — | [131] |

#### *4.1.1 Relationship between Fabrication Conditions and Performance*

Template Ions

Fundamental differences in template ions directly determine the structural design logic of imprinted cavities. For IIPs used in seawater lithium extraction, the template is typically $Li^+$, which has a hydration radius of approximately 3.8 Å, low charge density, simple coordination configuration, and exists as free hydrated $Li^+$ cations in seawater at pH 8.1. Therefore, the core of imprinted cavity design lies in constructing a flexible pocket with a matching size and weak Lewis basicity (such as crown ether oxygen and amide nitrogen), achieving recognition through dipole-ion interactions and hydration shell displacement. Template selection for ion-imprinted materials intended for uranium extraction from seawater should account for the actual aqueous speciation of U(VI), rather than assuming free $UO_2^{2+}$ as the sole target. At the typical seawater pH of approximately 8.2, U(VI) occurs predominantly as ternary alkaline-earth-metal–uranyl–carbonate complexes, particularly neutral $Ca_2UO_2(CO_3)_3$(aq), with $CaUO_2(CO_3)_3^{2-}$ and $MgUO_2(CO_3)_3^{2-}$ also contributing substantially, whereas $UO_2(CO_3)_3^{4-}$ represents only a minor fraction. This complex exhibits a bulky structural feature with a molecular diameter exceeding 10 Å, highly concentrated charge carrying four negative charges, and a rigid geometric configuration, with axial uranyl double bonds and equatorial plane coordinated with tridentate carbonate groups. The imprinted recognition cavity constructed for this complex must simultaneously meet three constraints: first, to build a positive charge-enriched region that can provide strong electrostatittraction, such as protonated amino groups and metal Lewis acid centers, to counteract the high-salinity matrix background of seawater; second, to preset a precisely arranged array of hydrogen bond acceptors and donors to achieve specific anchoring of uranyl oxygen atoms and carbonate bridging oxygen atoms; third, to have sufficient spatial volume and appropriate geometric flexibility, which can not only accommodate the large-volume anionic complex but also allow slight conformational adjustments.

Early attempts using the simple $UO_2^{2+}$ ion as a template proved ineffective in carbonate-rich seawater simulants, as the material failed to recognize the dominant $UO_2(CO_3)_3^{4-}$ complex, leading to over 40% loss in capacity and poor vanadium selectivity [132]. Subsequent efforts using a $UO_2^{2+}$-vinylpyridine binary complex template improved performance in low-salinity water but still suffered from severe cavity

mismatch in the presence of carbonate ions, with capacity dropping from 89.6 to 23.1 mg/g [129]. These studies highlighted the critical need to use the $UO_2(CO_3)_3^{4-}$ complex directly as the template for seawater applications. To address issues such as improving adsorption capacity, subsequent studies revealed that uranium mainly exists as $Mg(UO_2)(CO_3)_3^{2-}$ and $Ca_2UO_2(CO_3)_3(aq)$ ternary complexes rather than free $UO_2^{2+}$ when seawater pH is approximately 8.2, providing a key theoretical basis for subsequent template innovation [133]. Zhang et al. [124] first prepared surface-imprinted materials through the copolymerization of 1-vinylimidazole and 4-vinylbenzyl chloride on the surface of polypropylene nonwoven fabrics using $UO_2(CO_3)_3^{4-}$ as the template. Experiments confirmed that due to the complete matching between the cavities and the steric configuration of $UO_2(CO_3)_3^{4-}$, the material exhibited a uranium adsorption capacity of 5.2 mg/g in real seawater and a U(VI)/V selectivity ratio of 12.8. With the deepening of research, a bis-salicylaldoxime-$UO_2(CO_3)_3^{4-}$ complex was proposed as the template to construct molecular coordination imprinted cavities in porous aromatic frameworks. The material achieved a distribution coefficient of $1.4 \times 10^7$ mL/g for uranium in simulated seawater, a U/V selectivity ratio of no less than 100, and an adsorption capacity of 5.79 mg/g in real seawater after 56 days, providing a design reference for template innovation [125].

### Functional Monomers and Ligands

Fundamental differences between uranium and lithium ions in aqueous seawater systems lead to distinct criteria for the selection of functional monomers and ligands. Whereas most lithium ion-imprinted polymers (IIPs) rely on size-matched ligands such as crown ethers and calixarenes, combined with neutral or weakly polar functional monomers to achieve pore-size sieving and weak electrostatic adsorption, uranium-targeted IIPs prioritize strong chelation, charge compatibility, and spatial configuration matching between functional monomers, ligands, and uranyl ions. Stable chelates are formed through multidentate coordination, while tuning the local charge and donor environment enhances affinity for uranium-bearing species, improves discrimination against V(V), and mitigates matrix effects associated with $Ca^{2+}$, $Mg^{2+}$, and carbonate in seawater, as well as interference from $PO_4^{3-}$, $Eu^{3+}$, $Zn^{2+}$, and $Cu^{2+}$ in nuclear wastewater, thereby facilitating the selective capture of uranium at trace concentrations.

To accommodate the cationic and acidic character of $UO_2^{2+}$, chelating monomers are employed to synthesize ion-imprinted polymers for uranium adsorption. Salicylaldoxime (SA) is used as a functional monomer [125], bearing both hydroxyl and oxime groups that provide dual-site synergistic binding to $UO_2^{2+}$, forming U–O and U–N coordination bonds. In simulated seawater, the selectivity coefficient for $UO_2^{2+}$ is 113 times that for vanadium ions, with selectivity values over 100-fold for 13 other coexisting cations, and a maximum adsorption capacity of 253 mg/g. The acidic monomer methacrylic acid (MAA) coordinates with $UO_2^{2+}$ through oxygen atoms, generating binary $UO_2^{2+}$–ligand–monomer complex templates and establishing basic coordination sites. However, low site density and limited selectivity result in a uranium uptake efficiency of only 29.3% [134]. Vinylphosphonic acid (VPA), another acidic functional monomer, forms stable chelates with $UO_2^{2+}$. Phosphonic acid groups exhibit higher specificity for uranium than for common seawater cations such as $Ca^{2+}$ and $Mg^{2+}$, and the relative selectivity coefficient of IIZMS-G for U(VI)/Zn(II) reaches 11.23 [126], far exceeding values for conventional monomer systems. Cationic functional monomers include (3-methacrylamidopropyl) trimethylammonium chloride (MAPTAC) and vinylpyridine (VP). Nitrogen atoms in 4-vinylpyridine (4-VP) act as strong coordination sites for $UO_2^{2+}$, supporting the construction of ternary $UO_2^{2+}$–SALO–4-VP–MAA complex templates with multidentate synergistic sites. This architecture yields a $UO_2^{2+}$ adsorption capacity of 37.28 mg/g and a $UO_2^{2+}/Fe^{3+}$ selectivity coefficient of 746, markedly outperforming binary systems. Zhang et al. [124] blended three

functional monomers—1-vinylimidazole (VI), 4-vinylbenzyl chloride (4-VBC), and MAPTAC solution—to investigate how monomer molar ratios influence adsorption performance, providing guidance for designing composite functional monomer systems.

The performance of IIPs in the selective capture of $UO_2^{2+}$ from seawater depends strongly on the chemical structure, coordination ability, and environmental stability of functional moieties, as well as their compatibility with complex marine matrices. Amidoxime (AO) has been widely validated as the most suitable ligand for seawater environments [135,136]. From a coordination-chemistry perspective, amidoxime groups can bind U(VI) in neutral or deprotonated forms through their O- and N-donor atoms, occupying equatorial coordination sites around the approximately linear O=U=O unit. Depending on the protonation state and ligand architecture, amidoxime-derived ligands may adopt $\eta^2$(N, O), O, N-chelating, monodentate, or bridging coordination modes; five-membered chelate rings have been reported for certain O, N-binding configurations, whereas six-membered chelation generally requires additional, appropriately positioned donor groups. Amidoxime-based IIPs achieve distribution coefficients $K_d > 10^4$ mL/g and uranium adsorption capacities of 3–8 mg U/g in natural seawater, while maintaining structural stability over several weeks—performance far superior to non-imprinted control materials [137]. Nevertheless, the oxygen-containing functional groups in natural organic matter (NOM) can form strongly stable complexes with uranyl ions, altering the coordination environment of uranium in aqueous solutions and rendering the imprinted cavities originally designed for free uranyl ions ineffective at recognizing target species [138]. To address this challenge, introducing phosphate groups together with amidoxime groups to generate synergistic binding effects has emerged as a promising strategy for enhancing uranium selectivity [46]. Such multi-ligand designs can improve uranium-specific coordination while reducing interference from competing ions to a certain extent. However, ligand optimization alone is often insufficient to overcome pore blockage, surface fouling, and active-site masking induced by natural organic matter (NOM). Therefore, complementary surface-engineering strategies are frequently required to further improve anti-fouling performance and maintain adsorption efficiency.

### Types of Crosslinking Agents

Irrespective of the target metal ion present in seawater, crosslinking agents serve a consistent core function in the preparation of ion-imprinted polymers (IIPs). They construct a three-dimensional network framework with superior thermodynamic and kinetic stability, thereby guaranteeing the geometric fidelity of recognition cavities following template elution. Crosslinking agents also regulate the crosslinking density of polymers, enabling precise control over pore size distribution and specific surface area. Furthermore, they provide a chemically inert supporting matrix to avoid non-specific adsorption interference toward target ions arising from intrinsic functional groups. To date, ethylene glycol dimethacrylate (EGDMA) has demonstrated favorable adsorption performance as a cross-linker for the majority of metal ion systems [139]. In addition, divinylbenzene (DVB), a rigid crosslinking agent, has been utilized to synthesize $UO_2^{2+}$-chelated microspheres employing salicylaldehyde-p-aminostyrene Schiff base as the chelating ligand. The core strategy relies on the construction of a stable polymer backbone through free radical polymerization, which immobilizes specific recognition cavities for $UO_2^{2+}$. This material exhibits high adsorption capacity and excellent selectivity for uranium in uranium capture processes [127]. The selectivity coefficients of this material for $UO_2^{2+}$ are 14.22 relative to vanadium, 19.66 relative to cobalt, and 21.75 relative to nickel, all of which are substantially greater than unity. The uranium adsorption capacity reaches 147.8 mg/g, which is significantly higher than that of materials prepared using non-imprinted polymers or crosslinking agents with weak rigidity.

## Polymerization Methods

The polymerization methods for ion-imprinted polymers (IIPs) targeting uranium and lithium are essentially identical, including bulk polymerization, surface imprinting, and sol-gel methods, which are consistent with the polymerization strategies for lithium-adsorbing materials. In practical applications, composite strategies are often adopted to simultaneously achieve high adsorption capacity, rapid kinetics, excellent selectivity, and easy recoverability. Su et al. [140] developed a composite system combining carrier surface free radical polymerization with ion imprinting technology, integrating surface imprinting technology and the synergistic effect of dual functional monomers to realize highly selective uranium adsorption under low template loading (Fig. 18a). Polymerization occurs exclusively on the surface of BSG carriers, forming a thin polymer layer that avoids the problems of buried recognition sites and mass transfer limitation caused by bulk polymerization, with adsorption equilibrium achieved in only 90 min. The thin polymer layer ensures the accessibility of recognition sites, resulting in a template elution efficiency of 98% without template leakage; after 5 adsorption-desorption cycles, the adsorption capacity remains above 90%. Meanwhile, there is also a composite strategy of thermal-initiated polymerization and ion imprinting (Fig. 18b) [141], which achieves precise surface grafting through vinyl functionalization of the carrier surface, forming highly selective recognition sites. Surface graft polymerization exposes the recognition sites on the carrier surface, with a uranium adsorption rate of over 99% within 5 min; the polymer layer formed by free radical polymerization is covalently bonded to the carrier, enhancing the thermal stability and mechanical strength of the material. After 5 adsorption-desorption cycles, the adsorption efficiency still remains above 99%.

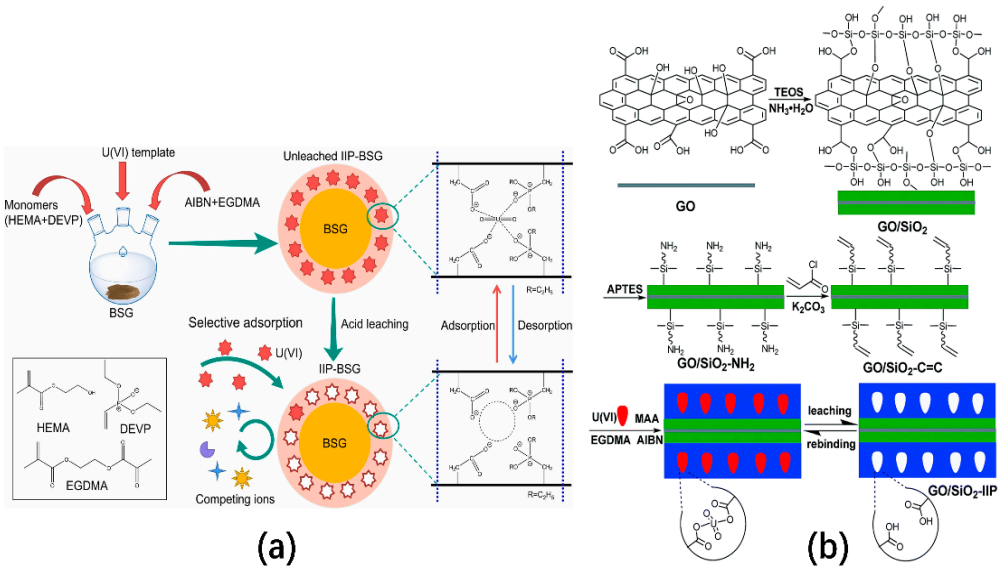


**Figure 18:** (**a**) Preparation of IIP-BSG with selective adsorption sites. Reprinted with permission from reference [140]. Copyright 2022, Elsevier; (**b**) The preparation route for GO/$SiO_2$-IIP. Reprinted with permission from reference [141]. Copyright 2015, RSC.

## Elution Conditions and Regeneration Capability

The coordination number of uranyl ions ($UO_2^{2+}$) is typically 6–8. Within the recognition cavities of ion-imprinted polymers (IIPs), uranyl ions form stable coordination structures with ligands, where the spatial arrangement of ligands precisely matches the linear configuration (O=U=O) of $UO_2^{2+}$ to further

enhance binding stability. Once this structure is formed, eluents at ordinary concentrations cannot break the coordination bonds, and strong eluents are required for disruption; in contrast, lithium ions only involve weak interactions and can be desorbed under mild conditions. In terms of regeneration capacity, $Li^+$-IIPs exhibit superior cycle stability and simpler operation due to their mild elution conditions. Su et al. [140] reported that the optimal eluent for the IIP-BSG material was 0.5 M HCl, with 98% elution efficiency of uranyl ions achieved by shaking at room temperature for 2 h, which was significantly superior to the mixed solution of 0.1 M hydrochloric acid and 0.1 M EDTA (elution efficiency of only 73%). The former could efficiently protonate the carboxyl and phosphonyl groups in the material through high-concentration protons, completely disrupting the electrostatic interactions and coordination bonds between uranyl ions and ligands. In contrast, EDTA in the mixed solution failed to break the strong multidentate coordination between uranyl ions and ligands, and the protonation efficiency of low-concentration protons was also insufficient; the ineffective synergistic effect of the two even reduced the elution performance. Compared with other eluents in similar studies, 0.5 M hydrochloric acid had mild corrosiveness and did not damage the glycosidic bonds of the brewer's spent grain (BSG) carrier or the polymer backbone. After 5 cycles, there was no significant change in the phosphorus content corresponding to the phosphonyl groups in the material, the adsorption capacity remained 90%, and the selectivity coefficient maintained above 92%. Meng et al. [141] used 3 M high-concentration HCl and required repeated washing until no uranyl ions were detected in the filtrate. The strong protonation of carboxyl groups disrupted the strong coordination bonds between template ions and ligands, ensuring no template residue affected the subsequent adsorption selectivity. Although 3 M HCl was used for the initial removal of the U(VI) template after polymerization, Meng et al. employed 1 M HCl as the eluent during cyclic regeneration of GO/$SiO_2$-IIP. After five consecutive adsorption–desorption cycles, the material maintained its U(VI) adsorption performance with only a limited decline, demonstrating good reusability.

#### *4.1.2 Dependence of Performance on Operation Conditions*

In the process of extracting uranyl ions ($UO_2^{2+}$) from seawater using ion-imprinted polymers (IIPs), operating conditions have a significant impact on adsorption performance. These conditions include pH value, temperature, contact time, and interfering ion concentration, which collectively determine the efficiency, selectivity, and stability of the adsorbent. The extremely low uranium concentration in seawater, coupled with the presence of a large number of competitive ions, makes the design of adsorption materials and the optimization of their operating conditions particularly critical [142].

pH

Both the existing form of $UO_2^{2+}$ in aqueous solutions and the protonation state of functional groups on the adsorbent are regulated by pH value. Under acidic conditions, uranyl ions typically exist in the form of $UO_2^{2+}$. In carbonate-free aqueous systems, increasing pH promotes the hydrolysis of $UO_2^{2+}$, producing mononuclear and polynuclear hydroxo species such as $UO_2OH^+$ and $(UO_2)_3(OH)_5^+$. This hydrolysis-driven speciation should not be extrapolated directly to seawater. Under typical seawater conditions, carbonate and the abundant $Ca^{2+}$ and $Mg^{2+}$ ions suppress the accumulation of uranyl hydroxo species by stabilizing soluble ternary uranyl–carbonate complexes, particularly $Ca_2UO_2(CO_3)_3(aq)$, $CaUO_2(CO_3)_3^{2-}$, and $MgUO_2(CO_3)_3^{2-}$. Specifically, it exists as a monomeric pentagonal bipyramidal structure when pH < 5, a $[(UO_2)_3O(OH)_3]$ trimer when 5 < pH < 7, and a $[(UO_2)(OH)_2]_n$ chain structure when 7 < pH < 8 [128].

Most studies have shown that the optimal adsorption pH value of IIPs for uranyl ions is usually in the neutral or weakly alkaline range. As shown in Fig. 19a,b, Wang et al. [143] found that the adsorption

efficiency of AFNH gradually increased with increasing pH, reaching a maximum of 99.2% at pH 8.0, with a corresponding adsorption capacity of 945.2 mg/g, and maintained high stability in the alkaline range, which was significantly superior to NH. This difference can be attributed partly to their distinct PZC values. At pH 8.0, AFNH (PZC = 8.4) has a slightly positive or nearly neutral surface, whereas NH (PZC = 4.4) is negatively charged. This difference may enhance the interaction of AFNH with anionic U(VI) carbonate species and reduce electrostatic repulsion, although coordination chemistry and high-ionic-strength screening also contribute to the overall adsorption behavior. At pH 8.0, the surface of AFNH is negatively charged, enabling efficient capture of positively charged uranyl ions through electrostatic attraction, whereas the surface of NH is positively charged, resulting in repulsion with uranyl ions. Meanwhile, the introduction of amidoxime groups enhances the complexation ability of AFNH with uranyl ions under alkaline conditions, making up for the insufficient alkaline affinity of hydroxyapatite itself. This study clarified that the optimal adsorption pH of AFNH is 8.0, which perfectly matches the weakly alkaline environment of seawater, providing a key pH regulation basis for its practical application in seawater uranium extraction. Similarly, the research results of Anirudhan et al. [144] showed (Fig. 19c) that the U(VI) adsorption rate increased continuously and significantly as the pH increased from 2.0 to 7.0; when the pH increased from 7.0 to 9.0, the adsorption rate remained basically stable with no obvious increase. It was determined that pH = 7.0 is the optimal condition for the material to adsorb U(VI), at which the adsorption efficiency is the highest.

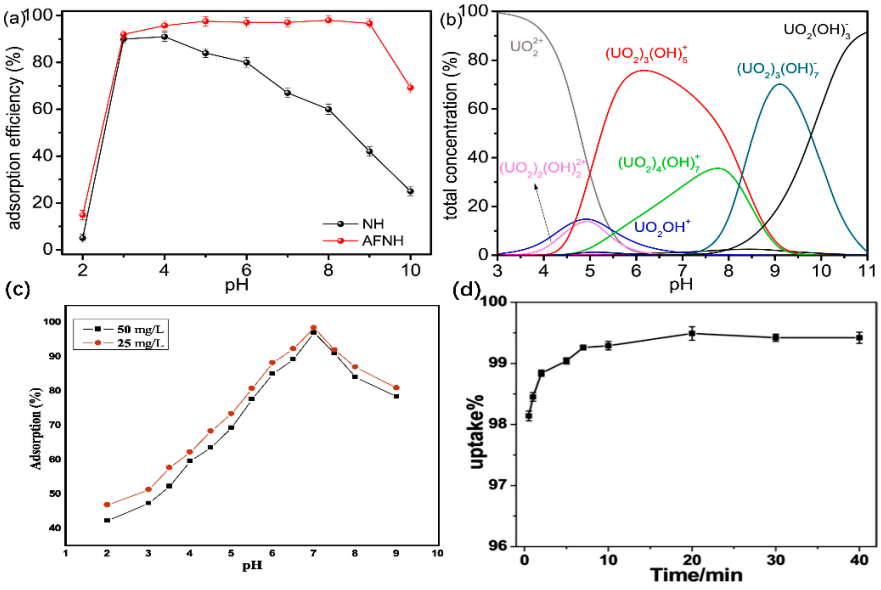


**Figure 19:** (**a**) Effects of pH on the adsorption efficiency of NH and AFNH for uranium ($C_0$ = 10 mg $g^{-1}$, t = 6 h, m/V = 0.1 g $L^{-1}$ and T = 298 K); (**b**) The uranium species distribution under diffeent Ph. Reprinted with permission from reference [143]. Copyright 2023, Elsevier; (**c**) Effect of pH on U(VI) adsorption by U(VI)-IIP. Reprinted with permission from reference [144]. Copyright 2015, Elsevier; (**d**) Effect of contact time on the uptake of U(VI) on GO/SiO2-IIP ($C_0$ = 5 mg $L^{-1}$, pH = 4.0, W = 50 mg, V = 10 mL, and T = 298.15 K). Reprinted with permission from reference [141]. Copyright 2015, RSC.

## Temperature

Temperature is an important parameter affecting thermodynamics and kinetics. Moderate temperature elevation is usually beneficial to the adsorption of uranyl ions, which is reflected by the increase in adsorption capacity. Meng et al. [141] set a temperature gradient of 15–35°C, detected uranium concentration by ICP-

AES, and derived thermodynamic parameters combined with the Van't Hoff equation. As the temperature increased from 15°C to 35°C, the adsorption capacity of the material for uranium increased continuously. Thermodynamic analysis showed that the enthalpy change ΔH = 23.40 kJ/mol was positive, indicating that the adsorption process was endothermic; the Gibbs free energy change ΔG = −3.40 kJ/mol (298.15 K) was negative, proving that the adsorption was spontaneous and the spontaneity became stronger with increasing temperature; the entropy change ΔS = 89.90 $J \cdot mol^{-1} \cdot K^{-1}$ was positive, indicating an increase in molecular randomness at the solid-liquid interface. Temperature regulates material performance by increasing the diffusion rate of uranyl ions and enhancing their coordination with carboxyl groups of methacrylic acid. This adsorption process belongs to endothermic, spontaneous, and entropy-increasing chemical adsorption; high temperature can reduce the reaction energy barrier and enhance adsorption spontaneity. Gan et al. [145] set three temperature gradients: 288K, 298K, and 308K. As the temperature increased from 288K to 308K, the uranium adsorption capacity of the material continued to increase, reaching a maximum of 962.226 mg/g at 308K, 532.329 mg/g at 298K, and 427.089 mg/g at 288K (Fig. 20a,b). Adsorption at different temperatures conformed to the Langmuir model (Fig. 20c), showing the characteristics of monolayer chemical adsorption. Thermodynamic analysis showed that the positive enthalpy changes ΔH indicated an endothermic adsorption process; the positive entropy changes ΔS reflected an increase in molecular randomness at the solid-liquid interface; the negative Gibbs free energy change ΔG, which became more negative with increasing temperature, proved that the adsorption proceeded spontaneously and the spontaneity was stronger at high temperatures.

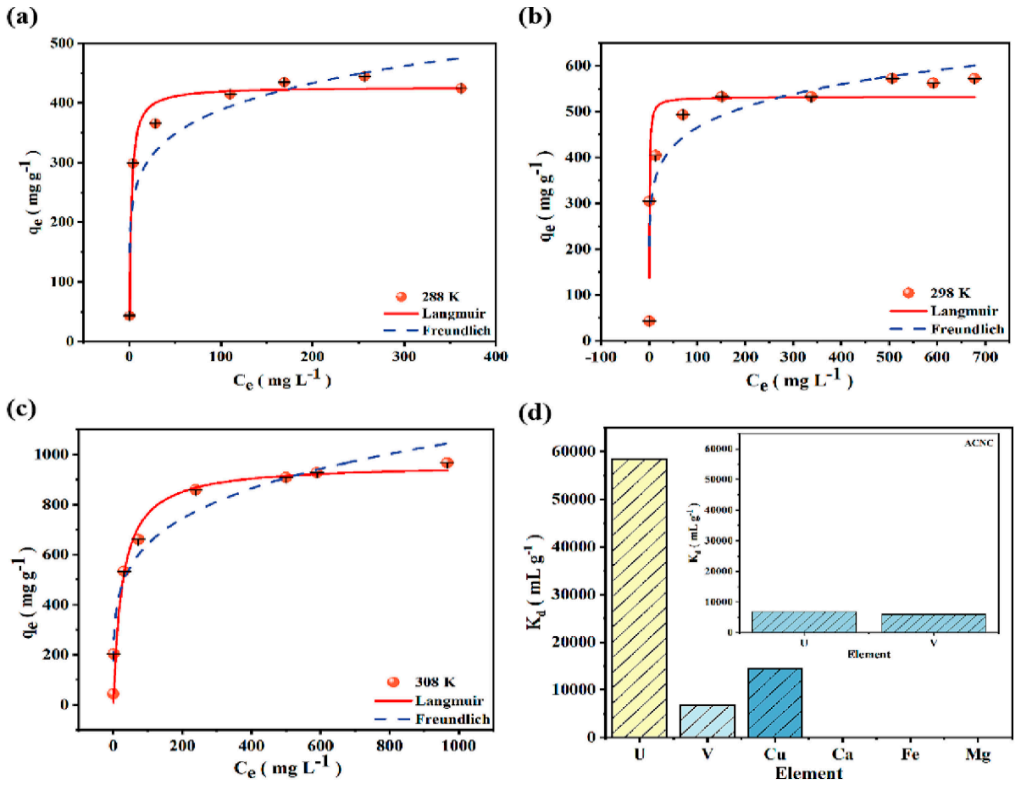


**Figure 20:** Adsorption isotherms of PACNC for U(VI) at (**a**) 288 K, (**b**) 298 K, and (**c**) 308 K (the initial uranium concentration was 10–900 $mg \cdot L^{-1}$, and the initial solution pH was 7). In the experiment, 90 mL of uranium solution with a pH of 7 was used, and the PACNC dosage was 20 mg. (**d**) Distribution coefficient of competitive ions and $K_d$ comparison with PANCN and ACNC. Reprinted with permission from reference [145]. Copyright 2023, Elsevier.

### Contact Time

Contact time is a key parameter in adsorption kinetics research, directly affecting the rate of the adsorption process and the establishment of adsorption equilibrium. Adsorption is usually a dynamic process; as contact time increases, the adsorption capacity gradually increases until adsorption equilibrium is achieved. Most adsorption processes conform to the pseudo-second-order kinetic model, indicating that chemical adsorption is the main adsorption mechanism. Meng et al. [141] designed a contact time range of 0.5–40 min in their experiments, determining the uranium concentration in the solution at different time points by ICP-AES and calculating the adsorption rate. The process of uranium adsorption by the material showed obvious two-stage characteristics: 0–5 min was the rapid adsorption stage, where the uranium adsorption rate quickly climbed to more than 99% (Fig. 20d); 5–40 min was the adsorption equilibrium stage, where the adsorption rate showed no obvious change and the adsorption sites on the material surface were basically saturated. The fitting results of the kinetic model showed that the correlation coefficient of the pseudo-second-order kinetic model (0.9928) was much higher than that of the pseudo-first-order kinetic model (0.8928), indicating that the adsorption process was more consistent with the pseudo-second-order kinetic characteristics. Similarly, Zhu et al. [146] found that in the initial stage, due to the large concentration gradient between the solution and the adsorbent surface, uranium ions quickly occupied the surface adsorption sites, leading to a rapid increase in adsorption capacity. Subsequently, the surface sites were gradually saturated, and uranium ions needed to diffuse slowly into the interior of the material, resulting in a slowdown in the adsorption rate, and finally reaching adsorption equilibrium within 180 min. The fitting results of the kinetic model showed that the adsorption process of GOG-RE was more consistent with the pseudo-second-order kinetic model, with a correlation coefficient as high as 0.99, indicating that adsorption was dominated by chemical adsorption, and the equilibrium adsorption capacity calculated by the model was 171.82 mg/g.

### Interfering Ions

In seawater systems, $Mg^{2+}$ and $Ca^{2+}$ are the divalent cations with the highest concentrations, exerting strong interference effects on both uranium and lithium IIPs. Uranium IIPs are also subject to competitive interference from anions such as $PO_4^{3-}$ and $CO_3^{2-}$. Moreover, the imprinted sites of uranium IIPs are coordination-type, while those of lithium IIPs are spatial size-matched, leading to essential differences in their competitive interaction mechanisms.

As shown in Fig. 21a,b, during the adsorption of U(VI), the interfering ions mainly act through specific chelation competition of cations and physico-chemical synergistic interference of anions. In cation competition, $Eu^{3+}$ has the highest priority due to its chemical similarity to U(VI) and its ability to form stable chelates with phosphate groups (P-O). Ion competition experiments [129] showed that $Eu^{3+}$ can directly compete with U(VI) for P-O coordination sites on the surface of FIIP, occupying part of the active centers by forming Eu-O-P chelate bonds, resulting in a decrease of approximately 5%–8% in U(VI) adsorption capacity, making it the strongest competitive ion among all coexisting ions. Secondly, although divalent alkaline earth metal ions such as $Mg^{2+}$ and $Ca^{2+}$ have weaker coordination ability than $Eu^{3+}$, their extremely high concentrations in uranium-containing seawater still enable them to compete with U(VI) for sites through weak chelation. In terms of anion competition, $Cl^-$, $SO_4^{2-}$, $CO_3^{2-}$ and others mainly exert physical interference by thickening the liquid film and changing the ionic strength, but indirect competitive effects still exist at high concentrations. $CO_3^{2-}$ may form $UO_2(CO_3)_2^{2-}$ and $UO_2(CO_3)_3^{4-}$ complexes with U(VI), reducing the concentration of free U(VI) in the solution and indirectly decreasing its chance of binding to adsorption sites. However, the chelation between phosphate groups on the FIIP surface and U(VI) is

extremely strong, which can effectively break through the complexation limitation, compete free U(VI) from the complexes and bind to them. In contrast, $Cl^-$ and $SO_4^{2-}$ cannot form stable interactions with P-O groups and thus cannot replace the coordination binding of U(VI), so their competitive effects are negligible. When the guanidine-functionalized ion-imprinted adsorbent IIZMS-G adsorbs U(VI), the influence of interfering ions is centered on cation site competition [126]. Zn(II) is the ion with the strongest competitive ability; the relative selectivity coefficient of IIZMS-G for U(VI)/Zn(II) reaches 11.23, much higher than that of other interfering ions, but its adsorption capacity is only 3.30 mg/g, far lower than 85.82 mg/g of U(VI) (Fig. 21c,d). As high-concentration divalent alkaline earth metal ions in seawater, Mg(II) and Ca(II) have relative selectivity coefficients of 8.40 and 6.94, respectively, with adsorption capacities of only 0.16 mg/g and 1.69 mg/g, showing weaker competitiveness than Zn(II). Cu(II) has the weakest competitive ability, with a relative selectivity coefficient of 3.97 and an adsorption capacity of 8.91 mg/g. V(V), as a uranium-like ion, exhibits moderate competition with an adsorption capacity of 132.76 mg/g, which is still lower than 148.37 mg/g of U(VI). The relative selectivity coefficients of all interfering ions are greater than 3.0, confirming the significant adsorption selectivity of IIZMS-G for U(VI).

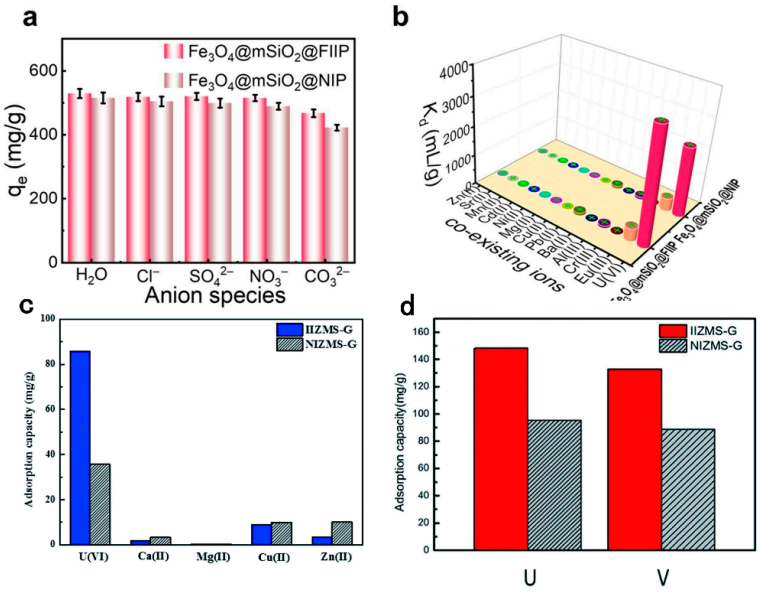


**Figure 21:** Effect of salinlty on the U(VI) sorption by (**a**) $Fe_3O_4$@$mSiO_2$@FIIP and (**b**) $Fe_3O_4$@$mSiO_2$@NIP. Reprinted with permission from reference [129]. Copyright 2024, Elsevier; Selective adsorption of U(VI) on (**c**) N/IIZMS-G and (**d**) N/IIZMS-G in the multicomponent system. Reprinted with permission from reference [126]. Copyright 2022, RSC.

### *4.2 Ion-Imprinted Hydrogel*

Ion-imprinted hydrogels combine the high swelling and environmental responsiveness of hydrogels with the specific recognition capability of ion imprinting. For seawater uranium extraction, IIHs offer not only the high selectivity of traditional IIPs but also new mechanisms and improved engineering adaptability derived from the hydrogel matrix.

#### *4.2.1 Relationship between Fabrication Conditions and Performance*

The selection of template ions, functional monomers, crosslinking agents, and ligands for both IIHs and IIPs is centered around the construction of specific imprinted sites, and the core goals of elution and regeneration are consistent. The core of the difference lies in the structural characteristics of the matrix:

the rigid or dense structure of IIPs enables them to be compatible with hydrophobic systems in terms of monomers, crosslinking agents, and polymerization methods, with more drastic elution conditions but better cyclic stability; the hydrophilicity and swelling network of IIHs require water-phase compatibility throughout the process, resulting in mild elution but easy deformation of sites and weaker regeneration capacity. The following mainly introduces the influence of various aspects on adsorption performance during the preparation of IIHs.

### Template Ions

The influences of template ions on the performance of ion-imprinted polymers (IIPs) and ion-imprinted hydrogels (IIHs) are homologous in basic principle. However, the sites induced by template ions in IIPs have high rigidity and structural stability in seawater environments. In contrast, during the aqueous-phase polymerization of IIHs, template ions induce the formation of imprinted sites in a swollen state; the structure of these sites depends on the support of the hydrophilic network and has a certain degree of flexibility, leading to slight shrinkage or deformation of the cavities induced by template ions and a decrease in the matching degree with the size and configuration of $UO_2^{2+}$.

When $UO_2^{2+}$ is used as the template ion, it forms coordination interactions with groups such as N-H, O-H, and C=O of the functional monomer NIPAM and the matrix sodium alginate during the polymerization process [130], inducing the formation of specific imprinted cavities complementary to its own size and linear bicoordinate configuration. FTIR (Fig. 22a) and XPS (Fig. 22b) characterizations confirmed that after adsorption, the N-H bending vibration peaks of SUIT-U/SPUIT-U shifted from 1550 $cm^{-1}$ to 1533–1534 $cm^{-1}$, the O-H/N-H stretching peaks weakened significantly, and the characteristic peak of O=U=O appeared at 927 $cm^{-1}$. These results prove that the sites induced by template ions form stable coordination bonds with $UO_2^{2+}$; meanwhile, these specific sites have exclusive recognition for $UO_2^{2+}$, significantly enhancing the anti-interference selectivity of adsorption. In a mixed system containing 7 common interfering ions in seawater such as $Pb^{2+}$, $Cu^{2+}$, $Mg^{2+}$, $Ca^{2+}$, and $Na^{+}$, the selectivity coefficients of SUIT for $UO_2^{2+}/M^{n+}$ range from 9.1 to 15.8, among which the $UO_2^{2+}/K^{+}$ selectivity coefficient is as high as 15.76; the selectivity coefficients of SPUIT range from 7.4 to 13.3, with the $UO_2^{2+}/Cd^{2+}$ selectivity coefficient reaching 14.78. The adsorption capacities of the two materials for $UO_2^{2+}$ are 109.37 mg/g and 125.57 mg/g, respectively, which are much higher than 10–30 mg/g for other interfering ions and significantly superior to the non-imprinted material NUIT. These findings fully confirm that the specific sites constructed by template ions can effectively repel the competition of interfering ions and greatly improve adsorption selectivity. Similarly, Yang et al. prepared materials using $UO_2^{2+}$ as the template ion. In a mixed system containing common seawater interfering ions such as $Ca^{2+}$, $Mg^{2+}$, $Zn^{2+}$, and $V^{3+}$, the selectivity coefficients of UITAC for $UO_2^{2+}/M^{n+}$ range from 1.4 to 10.3, which is significantly superior to the non-imprinted material UNTAC. Its adsorption capacity for $UO_2^{2+}$ reaches 12.2 mg/g, much higher than that for other interfering ions, and the maximum adsorption capacity of UITAC for $UO_2^{2+}$ in a single system can reach 81.2 mg/g. These results fully confirm that the sites induced by template ions can effectively repel the competition of interfering ions, highlighting excellent high selectivity advantages.

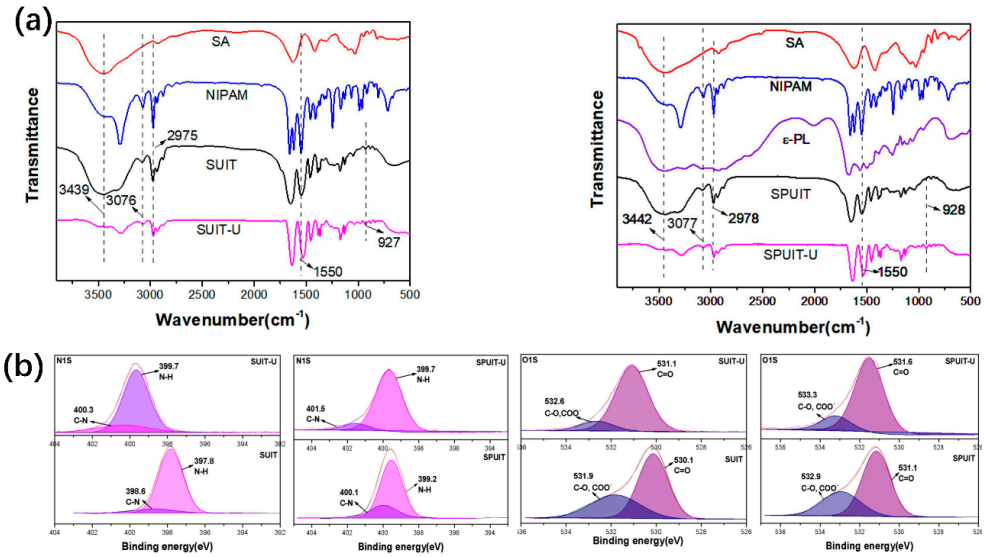


**Figure 22:** (**a**) FTIR spectra, TGA curves; (**b**) XPS spectra of SUIT, SUIT-U, and SPUIT, SPUIT-U. Reprinted with permission from reference [130]. Copyright 2021, Elsevier.

## Functional Monomers and Ligands

Ion-imprinted hybrid polymers (IIHs) impose stringent requirements on functional monomers, which must be either hydrophilic or zwitterionic hydrophilic monomers. This viewpoint was validated by the work of Yan et al. [147]. The material fabricated by Yan employed poly(amidoxime) (PAO) as the functional monomer. Owing to its intrinsic hydrophobicity, PAO forms a compact structure in aqueous solution that impedes the mass transfer of uranyl ions, thereby necessitating hydrophilic modification via $Zn^{2+}$ cross-linking. Such modification merely requires simple mixing of alkaline PAO aqueous solution with zinc chloride solution. The superhydrophilic $Zn^{2+}$, accounting for no more than 4 wt% of the dry gel, forms ionic cross-links with the amidoxime anions of PAO. This strategy retains a high PAO content of approximately 96 wt% while drastically enhancing hydrophilicity, lowering the water contact angle of $Zn^{2+}$-PAO dry gel to 11.7° within 4.00 s, which is far superior to pure PAO and PAO hydrogels containing extra hydrophilic networks. The modified material exhibits comprehensively optimized adsorption properties, delivering a saturated adsorption capacity of 1188 mg/g in 32 ppm uranium-spiked water. Among hydrophilic monomers, N-isopropylacrylamide (NIPAM) is the most mature and widely applied thermo-responsive monomer at present, and also the preferred candidate for thermo-responsive IIHs in uranium extraction from seawater. Its lower critical solution temperature (LCST) is around 32°C, which matches the actual temperature of seawater remarkably well, constituting the key advantage for its compatibility with marine systems. The uranyl ion-imprinted antibacterial hydrogel (UITAC) designed by Yang et al. [131] utilizes NIPAM to impart thermo-responsive behavior, regulating the swelling–shrinking dynamics of the hydrogel to meet the temperature-controlled requirements of adsorption and desorption. The PNIPAM network formed by NIPAM polymerization leads to endothermic peaks at 36.3–38.5°C and exothermic peaks at 30.5–34.1°C in the DSC curve of UITAC, corresponding to its volume phase transition temperature. The network contracts at elevated temperatures to strengthen $UO_2^{2+}$ adsorption and swells at low temperatures to facilitate desorption.

Ligand selection directly determines the intrinsic affinity and morphological adaptability of recognition sites toward $UO_2^{2+}$, acting as the fundamental constraint on the upper performance limit. $UO_2^{2+}$ possesses a

unique linear O=U=O configuration, a strong tendency toward hydrolysis, and pH-dependent transformation of complex species, which demand ligands to provide multiple synergistic recognition capabilities. 1-Hydroxy-2-(allyl)-9,10-anthraquinone (HAQ) developed by Fasihi et al. [148] serves as an excellent paradigm. 1-Hydroxy-9,10-anthraquinone contains a phenolic hydroxyl group adjacent to a quinone carbonyl group. Upon metal-assisted deprotonation of the hydroxyl group, the phenolate and carbonyl oxygen atoms can coordinate $UO_2^{2+}$ in a bidentate manner, forming a six-membered chelate ring. The hydroxyl and carbonyl groups in HAQ are weakly acidic coordination moieties, enabling the IIH to maintain stable adsorption within pH 4.0–7.0 and avoiding competitive occupation of coordination sites by $H^+$ at low pH, thus adapting well to aqueous environments. Furthermore, the strong coordination interaction between HAQ and $UO_2^{2+}$ shortens the ion binding process. Coupled with the large specific surface area endowed by the nanoscale dimension of the IIH, more than 95% of $UO_2^{2+}$ can be adsorbed within 5 min, which is significantly faster than conventional imprinted materials.

### Cross-Linking Agents

Both IIHs and IIPs commonly adopt rigid cross-linkers with high double-bond density and strong hydrophobicity to construct thermodynamically stable microporous frameworks. Ethylene glycol dimethacrylate (EDMA) is the most classic and widely used cross-linker. Although EDMA or divinylbenzene (DVB) can also be applied in IIHs, they are rarely used as the primary cross-linker in practical applications, as their strong hydrophobicity severely undermines the hydrophilic network of hydrogels, leading to a sharp decrease in swelling ratio (SR) and severe pore blockage. Findings from two studies by Wang et al. [149,150] demonstrate that triethylene glycol divinyl ether (DVE-3), when employed as the core cross-linker, contains long flexible ether linkages that endow the polymeric network with exceptional segmental mobility and sufficient hydration space. Experimental data reveal that increasing the DVE-3 dosage from 5 mol% to 15 mol% raises the SR of IIHs from 12.7 to 18.3, whereas EDMA reduces the SR to 8.9 under identical conditions. This result confirms the irreplaceable role of flexible and hydrophilic cross-linkers in preserving the macroscopic swelling performance of hydrogels.

### Polymerization Methods

The preparation of IIHs also relies on polymerization, sharing similar strategies with IIPs including precipitation polymerization and suspension polymerization. However, hydrogels require relatively milder techniques to maintain the structural integrity of hydrophilic networks. In addition, the emergence of thermo-responsive hydrogels has introduced approaches such as thermally initiated free radical polymerization and photoinitiated cationic polymerization [149]. For the monomer 2-(dimethylamino) ethyl methacrylate (DMAEMA), thermally initiated free radical polymerization is adopted, using a free radical initiator and heating at 50°C for 1 h to form a thermo-responsive PDMAEMA network. For bis(3,4-epoxycyclohexyl) adipate (BECA), photoinitiated cationic polymerization is employed, using a cationic photoinitiator and UV irradiation for 1 h to form a poly (BECA) network. The two polymerization reactions synergistically construct an interpenetrating polymer network (IPN), which not only retains the thermo-responsive properties of PDMAEMA but also enhances mechanical strength via BECA, while stably immobilizing the imprinted sites.

### Elution Conditions and Regeneration Performance

Functional groups form stable coordination bonds with $UO_2^{2+}$, and $UO_2^{2+}$ tends to precipitate as hydroxides under neutral or alkaline conditions. To avoid regeneration degradation caused by uranium

residue, both IIPs and IIHs require the use of acidic eluents. Under acidic conditions, $H^+$ protonates these functional groups and reduces their electron-donating ability, which directly breaks the coordination bonds and promotes the desorption of $UO_2^{2+}$. Typical acidic eluents include nitric acid ($HNO_3$) [130,131] and hydrochloric acid (HCl) [148,151]. IIHs containing thermosensitive components show reversible phase-transition behavior: the network swells dramatically at low temperatures (10°C for SUIT, 15°C for SPUIT), with increased pore size and weakened coordination interactions between $UO_2^{2+}$ and groups such as -NH and -OH in the material. During high-temperature adsorption, the network contracts, allowing imprinted sites to bind $UO_2^{2+}$ precisely. Benefiting from the reversibility of such thermosensitive response, cold water can expand the network directly via physical swelling, enabling $UO_2^{2+}$ to separate spontaneously from imprinted sites without breaking coordination bonds by chemical reagents. After 10 adsorption–desorption cycles, the thermosensitive material prepared by Tang et al. [130] maintained 82.42% of its initial adsorption capacity and 96.46% initial elution efficiency for SUIT, along with 84.99% adsorption capacity retention and 97.21% initial elution efficiency for SPUIT. Desorption by low-temperature water is green and environmentally friendly without secondary pollution, granting the material excellent cycling stability.

#### *4.2.2 Dependence of Performance on Operation Conditions*

When adsorbing uranium from seawater, the suitable pH range, the effects of temperature on adsorption capacity and adsorption rate, and the competition from interfering ions have roughly the same impacts on both IIPs and IIHs. Moreover, due to the relatively scarce current research on IIHs for uranium adsorption from seawater, the effects of various preparation conditions on the adsorption performance of IIPs will not be elaborated in detail here; see Section 4.1.1 for details.

## 5 Technical and Economic Feasibility and Commercial Prospects

Although significant progress has been made in the design and laboratory performance of IIP and IIH for seawater lithium and uranium recovery, their transition from academic research to practical application still requires critical evaluation of techno-economic feasibility, scalability, and market maturity. Based on the aforementioned discussions regarding material properties, preparation complexity, operational constraints, and reported performance data, this section assesses these dimensions and identifies major obstacles and potential pathways toward commercialization [4,11,17]. The economic feasibility of IIPs and IIHs for seawater mining is governed by four primary cost components: raw materials, synthesis and processing, adsorption–desorption operation, and material lifetime.

### *5.1 Cost Drivers and Economic Viability*

The economic feasibility of IIPs and IIHs for seawater mining is governed by four primary cost components: raw materials, synthesis and processing, adsorption–desorption operation, and material lifetime.

Functional monomers and ligands represent a substantial fraction of material cost, particularly for lithium-selective systems that rely on crown ethers or calixarene derivatives [96,100,102]. These macrocyclic compounds require multi-step organic synthesis, with current market prices exceeding $500–2000 per gram for high-purity grades, rendering them prohibitive for large-scale deployment. Uranium-selective amidoxime-based monomers are considerably cheaper, but advanced ligands such as phthalocyanine derivatives or bis-salicylaldoxime complexes remain expensive and synthetically demanding [98,130]. Cross-linkers and initiators are commodity chemicals with low cost while carriers vary widely from $0.5 per kg for biochar to >$1000 per kg for functionalized carbon nanotubes or MOFs [50,51,55,114]. The choice of carrier thus presents a critical trade-off between performance and economic viability.

The fabrication strategies discussed in Section 2 entail markedly different cost profiles. Bulk and precipitation polymerization are inherently low-cost and scalable, requiring only standard reactors and thermal initiation, but yield materials with deeply embedded sites and poor accessibility [98,107,108]. Surface imprinting improves site utilization but introduces additional steps—carrier functionalization, grafting, and purification—that increase processing time and cost by an estimated factor of 3–5 relative to bulk methods [17,54,55]. Microwave-assisted synthesis reduces reaction time from hours to minutes but demands specialized equipment with high capital cost and uncertain scale-up behavior [49,80]. Multi-component imprinting and click-chemistry approaches, while offering superior selectivity, involve multiple synthetic steps, catalysts, and rigorous purification, rendering them currently impractical for ton-scale production [47,69,70,75]. Radiation-induced graft polymerization produces high-quality materials but requires access to gamma or electron-beam facilities, severely limiting geographic and economic accessibility [115].

In seawater systems with target ion concentrations of 0.1–0.2 mg/L for $Li^+$ and 3.3 μg/L for U(VI), the energy and chemical inputs for pumping, pH adjustment (where required), and regeneration dominate operational expenditure. Most IIPs and IIHs require acidic elution to achieve >90% desorption efficiency [98,105,106,138]. For a hypothetical facility processing 1000 $m^3$ of seawater per day, acid consumption alone would reach 10–100 kg per day, generating equivalent volumes of acidic waste requiring neutralization and disposal. Thermo-responsive and photo-responsive systems offer the prospect of stimulus-driven desorption without chemical inputs, but the energy cost of heating or UV irradiation over large volumes remains nontrivial [61–63,94,147]. Moreover, the need to handle biofouling—through periodic cleaning or biocide addition—adds further operational complexity and cost [142].

The number of effective adsorptions–desorption cycles before capacity decay exceeds an acceptable threshold is the single most important determinant of long-term economic viability. Current reported cycle lives are modest: 5–8 cycles for most $Li^+$-IIPs [96,101,105], 8–10 cycles for U(VI)-IIPs [138,139], and up to 10–20 cycles for selected IIHs with mild regeneration [106,147]. Even at 10 cycles, a material must be replaced every 10–30 days of continuous operation. Such rapid turnover would render seawater mining economically non-competitive unless material costs are reduced by two orders of magnitude. Mechanical degradation of imprinted sites, ligand leaching, and irreversible fouling collectively limit cycle life, and no study has yet demonstrated stable operation beyond 50 cycles under realistic conditions.

### *5.2 Commercialization Landscape and Technology Readiness*

The technology readiness level (TRL) of IIPs and IIHs for seawater lithium and uranium recovery is uniformly low, ranging from TRL 2–3 to at most TRL 4. By comparison, non-imprinted amidoxime-based adsorbents for uranium extraction have reached TRL 6–7 through the Japanese JAEA marine field tests (2000–2010) and US Department of Energy programs, with braided amidoxime fibers deployed at >100 kg scale and ocean testing of ~1000 $m^2$ adsorbent modules [125,133,134]. For lithium, inorganic ion sieves have advanced to TRL 5–6, with pilot-scale electrochemical and adsorption systems tested in salt-lake brines [120,121]. Imprinted materials lag far behind these competing technologies in maturity, scale, and field validation.

The high market value of lithium ($10–20 per kg as $Li_2CO_3$, historically fluctuating up to $80 per kg) creates strong incentive for recovery from unconventional sources. However, the extremely low concentration in seawater 0.17 mg/L means that even a highly efficient IIP with 5 mg/g capacity would require processing ~200 t of seawater to recover 1 g of lithium. At a hypothetical processing rate of 10,000 $m^3$/day, annual lithium recovery would be ~600 kg, worth ~$10,000–50,000 at current prices—far below the capital and operating costs of any conceivable adsorption facility. Thus, IIPs for seawater lithium extraction are

economically unviable unless they simultaneously achieve >100 mg/g capacity in real seawater, >1000 cycle lifetime, and near-zero chemical input costs. None of these targets are imminent. A more realistic near-term application is lithium recovery from salt-lake brines (100–1000 mg/L $Li^+$) or desalination plant brines (10–50 mg/L $Li^+$), where higher concentrations improve economic metrics [97,98].

Uranium commands a lower price, but the strategic importance of nuclear fuel supply has driven government-funded extraction programs since the 1960s. The economic breakeven point for seawater uranium extraction is estimated at $200–400 per kg $U_3O_8$, requiring adsorbent capacities of 3–10 mg U/g, cycle lives of 50–100, and deployment scales of 10,000–100,000 kg of adsorbent per year [124,125]. Amidoxime-based non-imprinted adsorbents approach these targets (3–8 mg U/g in real seawater, 10–20 cycles), whereas imprinted materials offer higher selectivity but similar or lower capacity and poorer cycle life [127,135,138]. The premium for selectivity over vanadium—the most problematic interfering ion—may justify a higher cost for imprinted materials in niche applications such as uranium recovery from acidic mine waters or nuclear wastewater, but not for bulk seawater mining.

## 6 Present Research Disagreement in Process Rationale and Material Performance

In the field of lithium and uranium extraction from seawater, regarding IIPs and ion-imprinted hydrogels (IIHs), the core controversies, divergent viewpoints, and key issues without a unified conclusion in the research community—related to process principal design, material performance characterization, and application—are sorted out from four dimensions, combining the contradictory conclusions, differentiated design ideas, and evaluation deviations of existing studies. These four dimensions include fundamental divergences in process principles, divergences in performance index determination, controversies in stability evaluation, and divergences in application effects in real seawater systems.

### *6.1 Disagreements in Process Rationale Design of Ion-Imprinted Materials*

#### *6.1.1 Controversies on the Dominant Mechanism of Imprinting Site Formation*

For IIPs, the research community holds divergent views on the criterion for the thermodynamic stability of pre-polymerization complexes. Some researchers argue that only the formation of thermodynamically stable template–functional monomer complexes prior to polymerization can guarantee the specificity of imprinted cavities, thereby requiring rigorous screening of strongly coordinating monomers via quantum chemical calculations. Others propose that dynamic pre-polymerization complexes formed through weak coordination interactions can generate effective recognition sites during polymerization via the immobilization effect of cross-linkers, while also reducing the difficulty of elution. In contrast, strong coordination tends to cause severe template ion residue. No consensus has been reached regarding the stability requirement for such pre-polymerization complexes.

#### *6.1.2 Disputes on the Optimal Cross-Linking Strategy Design*

For IIHs, disputes exist over the dominant factor governing the formation of imprinted sites. Some studies maintain that the initial coordination interaction constitutes the core of imprinted site generation, with network swelling or shrinkage serving only as auxiliary regulation. Other investigations, however, demonstrate that the network formation kinetics of hydrogels and the subsequent segmental rearrangement during swelling–shrinking cycles exert a more profound influence on the number and accessibility of imprinted sites, and can even alter the binding mode of coordination interactions. The two perspectives contradict each other in identifying the key driving force underlying the imprinting mechanism of hydrogels.

#### *6.1.3 Differences in the Selection of Template Ion-Functional Monomer Matching Strategies*

Regarding ligand selection for lithium ion-imprinting, the research community is split by a core controversy between crown ether-based and calixarene-based ligands. Some studies verify that crown ethers such as benzo-12-crown-4 show optimal cavity matching toward $Li^+$, with selectivity coefficients considerably higher than those of other ligands, thus serving as the preferred functional monomers for lithium ion-imprinted polymers. Another line of research, however, suggests that modified calixarene derivatives are more stable in high-salt seawater environments and suffer less interference from competing ions during $Li^+$ coordination, giving them better selectivity in real seawater systems than crown ether ligands. Their comparative advantages remain controversial, with opposite conclusions reached under different testing conditions.

As for the dispute over coordination priority of functional monomers in uranyl ion-imprinting, one view holds that the amidoxime group is the optimal candidate, as it provides the highest coordination bond energy with $UO_2^{2+}$ and exceeds carboxyl and phosphate groups in both adsorption capacity and selectivity. The opposing view argues that phosphate groups possess stronger chemical stability in high-salt, low-pH seawater environments, while amidoxime groups are susceptible to hydrolysis and thus exhibit much poorer long-term durability in practical use. In addition, no unified conclusion has been formed regarding whether the synergistic effect of composite functional groups is superior to that of single functional groups.

### *6.2 Disagreements in the Characterization of Core Performance Indicators*

Current studies have not established unified specifications for the testing methods, calculation criteria and evaluation standards of the core performance indicators of ion-imprinted materials, resulting in numerous contradictory conclusions regarding the performance evaluation of IIPs and hydrogels. The divergences are mainly concentrated in the characterization and judgment of four core performance indicators: adsorption capacity, distribution coefficient/selectivity coefficient, imprinting factor and equilibrium adsorption time.

#### *6.2.1 Disputes on the Determination and Testing of Adsorption Capacity*

The first disagreement lies in the selection of testing systems. Some studies take the maximum theoretical adsorption capacity obtained from static simulated solution tests as the core evaluation indicator, holding that it can reflect the intrinsic adsorption capability of materials. Other studies, however, argue that static tests are drastically different from the dynamic mass transfer environment of real seawater, and the actual adsorption capacity measured via dynamic column tests or in real seawater is a more practically meaningful indicator. The difference between the two test results can reach 1–2 orders of magnitude [152,153], and no consensus has been reached on the core evaluation dimension of adsorption capacity.

The second divergence is the definition of effective adsorption capacity. Some researchers regard the saturated adsorption capacity of materials as the effective adsorption capacity. Others point out that the concentration of target ions in seawater is extremely low (3.3 μg/L for uranium and 0.17 mg/L for lithium), so the adsorption capacity of materials at low-concentrations is the actual effective capacity, while saturated adsorption capacity is only a theoretical reference in the laboratory. The different definitions of effective adsorption capacity directly led to deviations in performance evaluation.

#### *6.2.2 Differences in the Calculation and Evaluation of the Distribution Coefficient and Selectivity Coefficient*

The distribution coefficient ($K_d$) and selectivity coefficient are core indicators for evaluating material selectivity, yet notable divergences exist in their calculation standards across current studies. For the

calculation of $K_d$, some studies base it on the ratio between the adsorbed amount of target ions and the equilibrium concentration in solution, without subtracting the adsorption contribution of the blank carrier. By contrast, rigorous studies argue that the non-specific adsorption of the blank matrix should be excluded, and only the actual $K_d$ originating from imprinted sites should be quantified. The results obtained from these two approaches may therefore not be directly comparable. Disputes also exist regarding the ratio design of competing ions in selectivity coefficient measurements. Some studies employ equal concentrations of target ions and competing ions to simplify experimental conditions, which however deviates severely from the realistic ion proportions in seawater. Other studies adopt the authentic ionic composition of simulated seawater, yielding results closer to practical scenarios but with much lower selectivity coefficients. The outcomes from these two types of studies cannot be directly compared, leading to contradictory assessments of IIPs and IIHs.

#### *6.2.3 Controversies on the Validity of the Imprinting Factor (IF)*

The imprinting factor (IF) serves as a core indicator for evaluating the imprinting efficiency of materials. However, the rationality of blank control design for non-imprinted polymers (NIPs) remains controversial in the research community. Some researchers hold that NIPs can be used as a valid control as long as they are synthesized via the same protocol as IIPs, without the need for template ion removal. In contrast, other researchers argue that the synthesis of NIPs must completely eliminate the influence of template ions, while ensuring consistent pore structure and specific surface area with IIPs. Otherwise, discrepancies in pore structure will lead to distorted IF values, which fail to genuinely reflect the actual imprinting effect. Several studies have further verified that unreasonable NIPs design can give rise to artificially elevated IF values, making the indicator lose its practical evaluation significance.

#### *6.2.4 Disagreements on the Evaluation Dimension of Equilibrium Adsorption Time*

Equilibrium adsorption time characterizes the adsorption kinetic properties of materials, but divergent evaluation criteria prevail across relevant studies. Some researchers take a shorter equilibrium time as the primary optimization target, holding that rapid adsorption equilibrium is more compatible with the dynamic flow environment of seawater, thereby advocating hydrogels with superior mass transfer efficiency. Other studies argue that equilibrium adsorption time should be evaluated jointly with equilibrium adsorption capacity. Although certain IIPs require a longer period to reach equilibrium, they enable continuous enrichment of trace target ions during adsorption and deliver a higher cumulative adsorption capacity in natural seawater. Judging kinetic performance solely by the time to reach equilibrium is therefore considered unreasonable.

#### *6.2.5 Recommended Evaluation Criteria*

To address the lack of unified performance characterization standards, this paper proposes a standardized evaluation protocol for ion-imprinted materials (IIPs, IIHs) suitable for real seawater environments, as summarized in Table 5. The protocol mandates testing under natural or synthetic seawater conditions with salinity of approximately 35 g/L and pH 8.0–8.2, using target ion concentrations close to natural levels ($Li^+$: 0.1–0.2 mg/L; U(VI): 3–5 μg-U/L), while accounting for multi-ion competition, organic contaminants, and biofouling [11,16]. Specific criteria cover adsorption capacity [18,124], distribution and selectivity coefficients [124,130], imprinting factor (IF > 2.5 under seawater conditions), adsorption kinetics [3,6]. Cycle regeneration performance should involve at least 10 adsorption-desorption cycles, recording capacity retention and selectivity preservation rates, with material structural stability evaluated via FTIR, SEM,

and BET characterization using mild desorption conditions [98,130]. Additionally, resistance to biological fouling must be assessed through prolonged immersion in seawater containing microorganisms or simulated biofilms (≥14 days), comparing capacity decay rates and surface contamination levels [143].

**Table 5:** Standardized evaluation protocol for ion-imprinted materials in seawater environments.

| Evaluation Metric | Specific Requirements and Criteria | Test Conditions and Remarks |
|---|---|---|
| General test conditions | natural or artificial seawater with salinity of approximately 35 g/L and pH 8.0–8.2; target ion concentrations close to natural seawater levels: $Li^+$ 0.1–0.2 mg/L, U(VI) 3–5 μg-U/L | Must account for multi-ion competition, organic contaminants, and biofouling effects |
| Adsorption capacity | Primarily determine low-concentration equilibrium adsorption capacity qe (mg/g) and long-term cumulative adsorption capacity; report results from both static batch tests and dynamic column experiments | Contribution of blank carriers must be excluded |
| Distribution coefficient $K_d$ and selectivity coefficient α | Measure in a multi-ion competitive system with authentic seawater ion composition; pay special attention to $Li^+/Mg^{2+}$, $Li^+/Na^+$, and U/V selectivity | Strictly account for non-specific adsorption when calculating $K_d$ |
| Imprinting factor IF | NIP and imprinted material must share identical synthesis conditions and structural properties except for template ions. An IF above 2.5 under seawater conditions indicates effective imprinting. | — |
| Adsorption kinetics | Fit using a pseudo-second-order model; report rate constant $k_2$, half-life $t_{1/2}$, time to reach 95% equilibrium, and initial adsorption rate | — |

**Table 5:** *Cont.*

| Evaluation Metric | Specific Requirements and Criteria | Test Conditions and Remarks |
|---|---|---|
| Cyclic regeneration performance | Perform at least 10 adsorption-desorption cycles; record capacity retention and selectivity retention; use mild desorption conditions | Evaluate material structural stability via FTIR, SEM, and BET |
| Biofouling resistance | Prolonged immersion ≥14 days in seawater containing microorganisms or simulated biofilms | Compare capacity decay rates and surface contamination levels before and after exposure |

Note: "—" indicates none available.

## 7 Conclusions and Future Perspectives

Ion-imprinted materials (IIPs) are polymeric materials formed by the polymerization of functional monomers and cross-linkers induced by template ions, featuring specific recognition sites complementary in size and coordination geometry. This review provides a detailed summary of the preparation, design, and practical application of ion-imprinted materials for lithium and uranium recovery from seawater, analyzes the effects of various preparation conditions and application environments on adsorption performance, and offers new impetus for the development prospects of efficient utilization of seawater resources. Despite some progress, IIPs face several challenges in adsorbing uranium and lithium from seawater, including low mass transfer efficiency, secondary pollution easily caused by reliance on chemical elution, difficulty in process scaling, low lithium adsorption capacity, and insufficient selectivity. Their rigid skeletons lead to high diffusion resistance for target ions, high costs of precise preparation processes, great difficulty in

controlling $Li^+$ imprinted cavities, and high susceptibility to $Na^+$ competition. IIHs, on the other hand, suffer from shortcomings such as actual adsorption capacity in seawater far lower than laboratory data, poor anti-interference ability and stability, lagging research on lithium adsorption without a mature system, and easy attenuation of responsive performance. Their hydrophilic network structures are easily damaged by high-salt environments, natural matrices are prone to microbial degradation, and flexible structures struggle to stabilize $Li^+$ imprinted cavities. Both materials share common deficiencies: poor adaptability to seawater environments, lack of engineering transformation, inconsistent performance evaluation standards, inadequate in-depth research on basic mechanisms, disconnect between laboratory test conditions and practical applications, shortage of large-scale preparation technologies and unified evaluation systems, and insufficient interpretation of the interactions between target ions and imprinted sites in complex seawater.

Based on the systematic review of the research status of ion-imprinted polymers (IIPs) and ion-imprinted hydrogels (IIHs) in the field of uranium and lithium extraction from seawater, current research still has many key challenges and gaps from basic principles to practical applications. To promote the substantive breakthrough and industrialization of this technology, future research should focus on the following core directions.

## 1. Development of New Materials and Innovation in Structural Design

**High-Selectivity Functional Monomers:** The selectivity of currently widely used functional monomers for target ions still needs to be improved. In the future, quantum chemical calculations and molecular dynamics simulations should be employed to rationally design new functional monomers or complexing agents with higher affinity and specificity [154]. For uranyl ions ($UO_2^{2+}$), multi-dentate ligands containing oxygen and nitrogen with specific coordination geometries can be developed [155]; for $Li^+$, it is necessary to optimize the cavity size and coordination environment of crown ether or calixarene derivatives to effectively distinguish $Li^+$ from a large number of coexisting ions such as $Na^+$, $K^+$, and $Mg^{2+}$.

**Regulation of Hierarchical Pore Structure and Surface Imprinting Structure:** Traditional bulk polymerization tends to result in deeply embedded imprinted sites, which affects mass transfer and utilization efficiency. Emphasis should be placed on the development of surface imprinting technology, where recognition sites are constructed on the surface of carrier materials to significantly improve mass transfer rate and site accessibility [156]. Meanwhile, the construction of a hierarchical pore system with micro-meso-macropores via template-directed methods can optimize ion transport paths and match target ion sizes, thereby synergistically enhancing adsorption kinetics and capacity.

## 2. Multifunctional Integration and Intelligent Response Systems

**Multi-Stimulus-Responsive Intelligent Materials:** Endowing materials with responsiveness to external stimuli can realize precise and energy-saving control of the adsorption-desorption process. For example, the volume phase transition properties of thermosensitive hydrogels can be exploited for thermally driven desorption. The development of pH-responsive or photo-responsive materials can regulate adsorption selectivity and regeneration processes by changing solution pH or light conditions [157].

**Integration of Anti-Biofouling and Self-Cleaning Functions:** Marine biofouling is one of the key factors leading to the attenuation of adsorbent performance [158]. Future material design should proactively integrate antibacterial and anti-fouling functions, such as introducing quaternary ammonium salts, antimicrobial peptides (ε-polylysine) or natural antibacterial components (chitosan) into the polymer network, or constructing superhydrophobic/superhydrophilic surfaces to inhibit biofilm adhesion. This requires considering the balance between long-term antibacterial properties and structural stability from the material synthesis stage.

### 3. Improvement of Environmental Adaptability and Long-Term Stability

**Maintenance of Selectivity Under High-Salinity and Complex Ion Competition:** The presence of high concentrations of competing ions in seawater and seawater reverse osmosis concentrate poses a severe challenge to selectivity [155]. It is necessary to go beyond the single indicator of adsorption capacity and more systematically evaluate and report key selectivity parameters such as distribution coefficient ($K_d$) and separation factor (SF). Material design should focus on utilizing the subtle differences in size, charge, and coordination chemistry between target ions and competing ions to construct multiple recognition and sieving mechanisms.

**Long-Term Cyclic Stability and Mild Regeneration Strategies:** Many materials show a significant decrease in adsorption capacity after multiple cycles in the laboratory. Directions to improve stability include: Optimize the cross-linking strategy and density parameters, or employ post-processing enhancement techniques such as mechanical training to improve the mechanical strength of the network [159], developing milder and more efficient desorption methods to avoid damage to imprinted cavities during elution with strong acids and alkalis; and designing polymer networks with self-healing capabilities.

### 4. Integration of Interdisciplinary Disciplines and Application of Cutting-Edge Methods

**Artificial Intelligence and High-Throughput Computing-Assisted Design:** Using machine learning and artificial intelligence algorithms [154] for high-throughput virtual screening of a large number of combinations of monomers, templates, and cross-linkers, and predicting the structure-activity relationship between material structure and adsorption performance, can greatly accelerate the discovery and optimization of high-performance materials.

**Advanced *In-Situ* Characterization and In-Depth Mechanism Analysis:** Develop and apply *in-situ* and real-time characterization technologies (such as *in-situ* X-ray absorption spectroscopy and attenuated total reflection infrared spectroscopy) to dynamically observe the coordination and transport processes of ions in imprinted cavities at the molecular scale, providing direct experimental evidence for the rational design of materials.

**Acknowledgement:** Not applicable.

**Funding Statement:** This research was funded by the Ministry of Science and Technology, China, as Research Exchange Project of the China-Slovak Scientific & Technical Cooperation Committee (2024 No. 9-2).

**Author Contributions:** Writing—original draft preparation: Jianrui Wang, Mahshab Sheraz; Writing—review and editing: Jianrui Wang, Mahshab Sheraz, Rui Wang; Supervision: Rui Wang, Martin Pipíška, Vladimír Frišták; Project administration: Rui Wang; Funding acquisition: Rui Wang. All authors reviewed and approved the final version of the manuscript.

**Availability of Data and Materials:** Not applicable.

**Ethics Approval:** Not applicable.

**Conflicts of Interest:** Given his role as guest editor of this journal, Rui Wang had no involvement in the peer review of this article and had no access to information regarding its peer review. Full responsibility for the editorial process for this article was delegated to another journal editor. The authors declare no other conflicts of interest.

### References

1. Fatoki O, Mohammed H, Parupelli SK, Mathew A, Kaur M, Rehmat A, et al. Review of recent advances in lithium-ion batteries: Sources, extraction methods, and industrial uses. Batteries. 2025;11(12):433. [CrossRef].

2. Wang T, Tao B, Zuo B, Yan G, Liu S, Wang R, et al. Challenges and opportunities of uranium extraction from seawater: A systematic roadmap from laboratory to industry. Small Meth. 2025;9(3):2401598. [CrossRef].
3. Lynnyk PM. Potential impact of climate change on mineralization and main ions ratio in surface fresh waters (a review). Hydrob J. 2023;59(4):83–97. [CrossRef].
4. Rao TP, Kala R, Daniel S. Metal ion-imprinted polymers—Novel materials for selective recognition of inorganics. Anal Chim Acta. 2006;578(2):105–16. [CrossRef].
5. Ding C, Deng Y, Merchant A, Su J, Zeng G, Long X, et al. Insights into surface ion-imprinted materials for heavy metal ion treatment: Challenges and opportunities. Sep Purif Rev. 2023;52(2):123–34. [CrossRef].
6. Qiu X, Wang B, Zhao X, Zhou X, Wang R. Green and sustainable imprinting technology for removal of heavy metal ions from water via selective adsorption. Sustainability. 2024;16(1):339. [CrossRef].
7. Hande PE, Samui AB, Kulkarni PS. Highly selective monitoring of metals by using ion-imprinted polymers. Environ Sci Pollut Res Int. 2015;22(10):7375–404. [CrossRef].
8. Silva AT, Figueiredo R, Azenha M, Jorge PAS, Pereira CM, Ribeiro JA. Imprinted hydrogel nanoparticles for protein biosensing: A review. ACS Sens. 2023;8(8):2898–920. [CrossRef].
9. Tan Z, Chen C, Tang W. Advances in hydrogels research for ion detection and adsorption. Crit Rev Anal Chem. 2025;55(8):1667–89. [CrossRef].
10. Prasada Rao T, Daniel S, Mary Gladis J. Tailored materials for preconcentration or separation of metals by ion-imprinted polymers for solid-phase extraction (IIP-SPE). TrAC Trends Anal Chem. 2004;23(1):28–35. [CrossRef].
11. Zhou X, Wang B, Wang R. Insights into ion-imprinted materials for the recovery of metal ions: Preparation, evaluation and application. Sep Purif Technol. 2022;298:121469. [CrossRef].
12. Shakerian F, Kim KH, Kwon E, Szulejko JE, Kumar P, Dadfarnia S, et al. Advanced polymeric materials: Synthesis and analytical application of ion imprinted polymers as selective sorbents for solid phase extraction of metal ions. TrAC Trends Anal Chem. 2016;83:55–69. [CrossRef].
13. Du M, Xu Z, Xue Y, Li F, Bi J, Liu J, et al. Application prospect of ion-imprinted polymers in harmless treatment of heavy metal wastewater. Molecules. 2024;29(13):3160. [CrossRef].
14. Ni P, Earwood J, Deng B. Application of ion imprinted polymers (IIPs) for rare earth elements recovery from secondary aqueous sources—A data-based review. Crit Rev Environ Sci Technol. 2025;55(20):1559–77. [CrossRef].
15. Keçili R, Hussain CG, Ghorbani-Bidkorpeh F, Hussain CM. Environmentally-friendly ion imprinted polymers (IIPs) towards metal pollutants in environmental samples: Recent advances and future prospects. TrAC Trends Anal Chem. 2025;184:118132. [CrossRef].
16. Fu J, Chen L, Li J, Zhang Z. Current status and challenges of ion imprinting. J Mater Chem A. 2015;3(26):13598–627. [CrossRef].
17. Huang H, Dong Z, Ren X, Jia B, Li G, Zhou S, et al. High-strength hydrogels: Fabrication, reinforcement mechanisms, and applications. Nano Res. 2023;16(2):3475–515. [CrossRef].
18. Cao Z, Qi D, Liu X, Zhou Z, Du C, Ren Z. Selective recovery of lithium from salt lake brine by using ion-imprinted polymers. Ind Eng Chem Res. 2024;63(2):1100–8. [CrossRef].
19. Sharma G, Kandasubramanian B. Molecularly imprinted polymers for selective recognition and extraction of heavy metal ions and toxic dyes. J Chem Eng Data. 2020;65(2):396–418. [CrossRef].
20. Niu J, Du M, Wu W, Yang J, Chen Q. Advances in the selection of functional monomers for molecularly imprinted polymers: A review. J Sep Sci. 2024;47(16):e2400353. [CrossRef].
21. Urraca JL, Carbajo MC, Torralvo MJ, González-Vázquez J, Orellana G, Moreno-Bondi MC. Effect of the template and functional monomer on the textural properties of molecularly imprinted polymers. Biosens Bioelectron. 2008;24(1):155–61. [CrossRef].
22. Wang L, Li J, Wang J, Guo X, Wang X, Choo J, et al. Green multi-functional monomer based ion imprinted polymers for selective removal of copper ions from aqueous solution. J Colloid Interface Sci. 2019;541:376–86. [CrossRef].
23. Karlsson BC, O'Mahony J, Karlsson JG, Bengtsson H, Eriksson LA, Nicholls IA. Structure and dynamics of monomer-template complexation: An explanation for molecularly imprinted polymer recognition site heterogeneity. J Am Chem Soc. 2009;131(37):13297–304. [CrossRef].
24. Svenson J, Zheng N, Föhrman U, Nicholls IA. The role of functional monomer–template complexation on the performance of atrazine molecularly imprinted polymers. Anal Lett. 2005;38(1):57–69. [CrossRef].

25. Garg M, Pamme N. Strategies to remove templates from molecularly imprinted polymer (MIP) for biosensors. TrAC Trends Anal Chem. 2024;170:117437. [CrossRef].
26. Zahedi P, Ziaee M, Abdouss M, Farazin A, Mizaikoff B. Biomacromolecule template-based molecularly imprinted polymers with an emphasis on their synthesis strategies: A review: Biomacromolecule template-based MIP. Polym Adv Technol. 2016;27(9):1124–42. [CrossRef].
27. Koohpaei AR, Shahtaheri SJ, Ganjali MR, Forushani AR, Golbabaei F. Application of multivariate analysis to the screening of molecularly imprinted polymers (MIPs) for ametryn. Talanta. 2008;75(4):978–86. [CrossRef].
28. Zhang H, Song T, Zong F, Chen T, Pan C. Synthesis and characterization of molecularly imprinted polymers for phenoxyacetic acids. Int J Mol Sci. 2008;9(1):98–106. [CrossRef].
29. Xu S, Chen L, Li J, Guan Y, Lu H. Novel $Hg^{2+}$-imprinted polymers based on thymine-$Hg^{2+}$-thymine interaction for highly selective preconcentration of $Hg^{2+}$ in water samples. J Hazard Mater. 2012;237–238:347–54. [CrossRef].
30. Buica G, Bucher C, Moutet JC, Royal G, Saint-Aman E, Ungureanu E. Voltammetric sensing of mercury and copper cations at poly(EDTA-like) film modified electrode. Electroanalysis. 2009;21(1):77–86. [CrossRef].
31. Liu Y, Zai Y, Chang X, Guo Y, Meng S, Feng F. Highly selective determination of methylmercury with methylmercury-imprinted polymers. Anal Chim Acta. 2006;575(2):159–65. [CrossRef].
32. Zhai Y, Liu Y, Chang X, Chen S, Huang X. Selective solid-phase extraction of trace cadmium(II) with an ionic imprinted polymer prepared from a dual-ligand monomer. Anal Chim Acta. 2007;593(1):123–8. [CrossRef].
33. He Q, Chang X, Wu Q, Huang X, Hu Z, Zhai Y. Synthesis and applications of surface-grafted Th(IV)-imprinted polymers for selective solid-phase extraction of thorium(IV). Anal Chim Acta. 2007;605(2):192–7. [CrossRef].
34. Zhang H, Liang H, Chen Q, Shen X. Synthesis of a new ionic imprinted polymer for the extraction of uranium from seawater. J Radioanal Nucl Chem. 2013;298(3):1705–12. [CrossRef].
35. Karim K, Breton F, Rouillon R, Piletska EV, Guerreiro A, Chianella I, et al. How to find effective functional monomers for effective molecularly imprinted polymers? Adv Drug Deliv Rev. 2005;57(12):1795–808. [CrossRef].
36. Okay O. Macroporous copolymer networks. Prog Polym Sci. 2000;25(6):711–79. [CrossRef].
37. Dakova I, Yordanova T, Karadjova I. Non-chromatographic mercury speciation and determination in wine by new core-shell ion-imprinted sorbents. J Hazard Mater. 2012;231–232:49–56. [CrossRef].
38. Tarley CR, Andrade FN, de Oliveira FM, Corazza MZ, de Azevedo LF, Segatelli MG. Synthesis and application of imprinted polyvinylimidazole-silica hybrid copolymer for $Pb^{2+}$ determination by flow-injection thermospray flame furnace atomic absorption spectrometry. Anal Chim Acta. 2011;703(2):145–51. [CrossRef].
39. Branger C, Meouche W, Margaillan A. Recent advances on ion-imprinted polymers. React Funct Polym. 2013;73(6):859–75. [CrossRef].
40. Shamsipur M, Fasihi J, Ashtari K. Grafting of ion-imprinted polymers on the surface of silica gel particles through covalently surface-bound initiators: A selective sorbent for uranyl ion. Anal Chem. 2007;79(18):7116–23. [CrossRef].
41. Zepeda-Navarro A, Segoviano-Garfias JJN, Bivián-Castro EY. The multi-challenges of the multi-ion-imprinted polymer synthesis. Polymers. 2024;16(19):2804. [CrossRef].
42. Matsui J, Nicholls IA, Takeuchi T, Mosbach K, Karube I. Metal ion mediated recognition in molecularly imprinted polymers. Anal Chim Acta. 1996;335(1–2):71–7. [CrossRef].
43. Li T, Chen S, Li H, Li Q, Wu L. Preparation of an ion-imprinted fiber for the selective removal of $Cu^{2+}$. Langmuir. 2011;27(11):6753–8. [CrossRef].
44. Yoshizako K, Hosoya K, Iwakoshi Y, Kimata K, Tanaka N. Porogen imprinting effects. Anal Chem. 1998;70(2):386–9. [CrossRef].
45. El Ouardi Y, Giove A, Laatikainen M, Branger C, Laatikainen K. Benefit of ion imprinting technique in solid-phase extraction of heavy metals, special focus on the last decade. J Environ Chem Eng. 2021;9(6):106548. [CrossRef].
46. Xu J, Pu Z, Xu X, Wang Y, Yang D, Zhang T, et al. Simultaneous adsorption of Li(I) and Rb(I) by dual crown ethers modified magnetic ion imprinting polymers. Appl Organom Chemis. 2019;33(3):e4778. [CrossRef].
47. Naeimi H, Nejadshafiee V, Masoum S. Highly efficient copper-imprinted functionalized mesoporous organosilica nanocomposites as a recyclable catalyst for click synthesis of 1,2,3-triazole derivatives under ultrasound irradiation: Multivariate study by factorial design of experiments. RSC Adv. 2015;5(20):15006–16. [CrossRef].

48. Chia HL, Jacob J, Boey FYC. The microwave radiation effect on the polymerization of styrene. J Polym Sci A Polym Chem. 1996;34(11):2087–94. [CrossRef].
49. Huang YS, Takada E, Konno S, Huang CS, Kuo MH, Chang RF. Computer-aided tumor diagnosis in 3-D breast elastography. Comput Methods Programs Biomed. 2018;153:201–9. [CrossRef].
50. Yuan G, Tu H, Liu J, Zhao C, Liao J, Yang Y, et al. A novel ion-imprinted polymer induced by the glycylglycine modified metal-organic framework for the selective removal of Co(II) from aqueous solutions. Chem Eng J. 2018;333:280–8. [CrossRef].
51. Yang L, Li S, Sun C. Selective adsorption and separation of Cs(I) from salt lake brine by a novel surface magnetic ion-imprinted polymer. J Dispers Sci Technol. 2017;38(11):1547–55. [CrossRef].
52. Huang Y, Wang R. Highly effective and low-cost ion-imprinted polymers loaded on pretreated vermiculite for lithium recovery. Ind Eng Chem Res. 2019;58(27):12216–25. [CrossRef].
53. Dong C, Shi H, Han Y, Yang Y, Wang R, Men J. Molecularly imprinted polymers by the surface imprinting technique. Eur Polym J. 2021;145:110231. [CrossRef].
54. Huang Y, Wang R. Green recovery of lithium from water by a smart imprinted adsorbent with photo-controlled and selective properties. Chem Eng J. 2019;378:122084. [CrossRef].
55. Guo M, Ye J, Zheng C, Meng J. Dual-recognition membrane adsorbers combining hydrophobic charge-induction chromatography with surface imprinting via multicomponent reaction. J Chromatogr A. 2022;1668:462918. [CrossRef].
56. He H, Ye S, Zhang W, Li S, Nie Z, Xu X, et al. Synthesis of magnetic mesoporous silica adsorbents by thiol-ene click chemistry with optimised lewis base properties through molecular imprinting for the rapid and effective capture of Pb(II). Chem Eng J. 2024;489:151294. [CrossRef].
57. Xu S, Lu H, Zheng X, Chen L. Stimuli-responsive molecularly imprinted polymers: Versatile functional materials. J Mater Chem C. 2013;1(29):4406. [CrossRef].
58. Kanekiyo Y, Naganawa R, Tao H. pH-responsive molecularly imprinted polymers. Angew Chem Int Ed. 2003;42(26):3014–6. [CrossRef].
59. Gonzato C, Courty M, Pasetto P, Haupt K. Magnetic molecularly imprinted polymer nanocomposites via surface-initiated RAFT polymerization. Adv Funct Mater. 2011;21(20):3947–53. [CrossRef].
60. Imin P, Imit M, Adronov A. Supramolecular functionalization of single-walled carbon nanotubes (SWNTs) with a photoisomerizable conjugated polymer. Macromolecules. 2012;45(12):5045–50. [CrossRef].
61. Meudtner RM, Hecht S. Helicity inversion in responsive foldamers induced by achiral halide ion guests. Angew Chem Int Ed. 2008;47(26):4926–30. [CrossRef].
62. Mizoguchi K, Ida J, Matsuyama T, Yamamoto H. Straight-chained thermo-responsive polymer with high chelating group content for heavy metal ion recovery. Sep Purif Technol. 2010;75(1):69–75. [CrossRef].
63. Qin L, He XW, Zhang W, Li WY, Zhang YK. Macroporous thermosensitive imprinted hydrogel for recognition of protein by metal coordinate interaction. Anal Chem. 2009;81(17):7206–16. [CrossRef].
64. Li Z, Tian H, Yuan Y, Yin X, Wei X, Tang L, et al. Metal-ion-imprinted thermo-responsive materials obtained from bacterial cellulose: Synthesis, characterization, and adsorption evaluation. J Mater Chem A. 2019;7(19):11742–55. [CrossRef].
65. Hoai NT, Yoo DK, Kim D. Batch and column separation characteristics of copper-imprinted porous polymer micro-beads synthesized by a direct imprinting method. J Hazard Mater. 2010;173(1–3):462–7. [CrossRef].
66. Cai X, Li J, Zhang Z, Yang F, Dong R, Chen L. Novel $Pb^{2+}$ ion imprinted polymers based on ionic interaction via synergy of dual functional monomers for selective solid-phase extraction of $Pb^{2+}$ in water samples. ACS Appl Mater Interfaces. 2014;6(1):305–13. [CrossRef].
67. Barciela-Alonso MC, Plata-García V, Rouco-López A, Moreda-Piñeiro A, Bermejo-Barrera P. Ionic imprinted polymer based solid phase extraction for cadmium and lead pre-concentration/determination in seafood. Microchem J. 2014;114:106–10. [CrossRef].
68. Zhu LY, Zhu ZL, Qiu YL, Zhang RH. Synthesis of As(V)-Cr(III) co-imprinted polymer and its adsorption performance for arsenate species. Sep Sci Technol. 2014;49(10):1584–91. [CrossRef].
69. Elsayed NH, Alenazi DAK, Alnahdi KM, Alshareef SA, Al-Anazi M, Alshammari NAH, et al. Tailored ion-imprinted polymer for europium(III) recovery: A cellulose-based click chemistry approach. J Water Process Eng. 2025;76:108061. [CrossRef].

70. Kolb HC, Sharpless KB. The growing impact of click chemistry on drug discovery. Drug Discov Today. 2003;8(24):1128–37. [CrossRef].
71. Killops KL, Campos LM, Hawker CJ. Robust, efficient, and orthogonal synthesis of dendrimers via thiol-ene "click" chemistry. J Am Chem Soc. 2008;130(15):5062–4. [CrossRef].
72. Kolb HC, Finn MG, Sharpless KB. Click chemistry: Diverse chemical function from a few good reactions. Angew Chem Int Ed. 2001;40(11):2004–21. [CrossRef].
73. Li ZA, Yu G, Hu P, Ye C, Liu Y, Qin J, et al. New azo-chromophore-containing hyperbranched polytriazoles derived from $AB_2$ monomers via click chemistry under copper(I) catalysis. Macromolecules. 2009;42(5):1589–96. [CrossRef].
74. Chen L, Xu S, Li J. Recent advances in molecular imprinting technology: Current status, challenges and highlighted applications. Chem Soc Rev. 2011;40(5):2922–42. [CrossRef].
75. Murray M, Charlesworth D, Swires L, Riby P, Cook J, Chowdhry BZ, et al. Faraday communications. Microwave synthesis of the colloidal poly(*N*-isopropylacrylamide) microgel system. Faraday Trans. 1994;90(13):1999. [CrossRef].
76. Zhu X, Chen J, Zhou N, Cheng Z, Lu J. Emulsion polymerization of methyl methacrylate under pulsed microwave irradiation. Eur Polym J. 2003;39(6):1187–93. [CrossRef].
77. Lu JM, Ji SJ, Chen NY, Sun ZR, Zhu XL, Shi WP, et al. Third-order nonlinear optical properties of polyureas and polyimide synthesized by microwave irradiation. J Appl Polym Sci. 2003;89(10):2611–7. [CrossRef].
78. Yu R, Xiang L, Geng M, Ya S, Zeb S, Liu Z, et al. Microwave-assisted synthesis of three dimensional superhydrophilicity ion imprinted polymer based on POSS/SBA-15 for copper ion adsorption in environmental water. Sep Purif Technol. 2025;377:134445. [CrossRef].
79. Wang J, Li Z. Enhanced selective removal of Cu(II) from aqueous solution by novel polyethylenimine-functionalized ion imprinted hydrogel: Behaviors and mechanisms. J Hazard Mater. 2015;300:18–28. [CrossRef].
80. Wu HG, Ju XJ, Xie R, Liu YM, Deng JG, Niu CH, et al. A novel ion-imprinted hydrogel for recognition of potassium ions with rapid response. Polym Adv Technol. 2011;22(9):1389–94. [CrossRef].
81. Su H, Ren H, Maimaitikelimu X, Xu J, Bian F, Wang H. Molecularly and ionically imprinted polymers-based chemical sensors in chemical assays. Chem Eng J. 2024;499:156315. [CrossRef].
82. Song X, Li C, Xu R, Wang K. Molecular-ion-imprinted chitosan hydrogels for the selective adsorption of silver(I) in aqueous solution. Ind Eng Chem Res. 2012;51(34):11261–5. [CrossRef].
83. Wang J, Li X. Ion-imprinted composite hydrogels with excellent mechanical strength for selective and fast removal of $Cu^{2+}$. Ind Eng Chem Res. 2013;52(2):572–7. [CrossRef].
84. Yu P, Zhou G, Yang R, Li Y, Zhang L, Sun L, et al. Green synthesis of ion-imprinted macroporous composite magnetic hydrogels for selective removal of nickel (II) from wastewater. J Mol Liq. 2021;344:117963. [CrossRef].
85. Wang J, Li J. $Cu^{2+}$ adsorption onto ion-imprinted composite hydrogels: Thermodynamics and mechanism studies. Polym Bull. 2015;72(9):2143–55. [CrossRef].
86. Liu YQ, Ju XJ, Zhou XL, Mu XT, Tian XY, Zhang L, et al. A novel chemosensor for sensitive and facile detection of strontium ions based on ion-imprinted hydrogels modified with guanosine derivatives. J Hazard Mater. 2022;421:126801. [CrossRef].
87. Huang K, Li B, Zhou F, Mei S, Zhou Y, Jing T. Selective solid-phase extraction of lead ions in water samples using three-dimensional ion-imprinted polymers. Anal Chem. 2016;88(13):6820–6. [CrossRef].
88. Guan Y, Enock K, Zhou B, Qi Z, Nadeem MS, Chen J, et al. High-efficiency removal of $Cu^{2+}$, $Zn^{2+}$, and $Mg^{2+}$ from contaminated water using a conductive hydrogel based on gellan Gum/$Ti_3C_2$ MXene/PEDOT-S: H/Aluminum oxide silicate composite. Chem Eng Sci. 2026;332:124091. [CrossRef].
89. Earwood J, Snider P, Henke L, Deng B. Recovery of neodymium (III) from mine waste by chitosan-based ion imprinted polymeric hydrogels. Sep Purif Technol. 2025;361:131356. [CrossRef].
90. Li Z, Li C, Liu X, Cao L, Li P, Wei R, et al. Continuous electrical pumping membrane process for seawater lithium mining. Energy Environ Sci. 2021;14(5):3152–9. [CrossRef].
91. Huang Y, Wang R. An efficient lithium ion imprinted adsorbent using multi-wall carbon nanotubes as support to recover lithium from water. J Clean Prod. 2018;205:201–9. [CrossRef].
92. Zhao H, Liang Q, Yang Y, Liu W, Liu X. Magnetic graphene oxide surface lithium ion-imprinted material towards lithium extraction from salt lake. Sep Purif Technol. 2021;265:118513. [CrossRef].

93. Qi D, Jin D, Tu Y, Zhou Z, Du C, Ren Z. Synthesis of lithium ion-imprinted polymers for selective recovery of lithium ions from salt lake brines. Sep Purif Technol. 2024;340:126661. [CrossRef].
94. Jamoussi B, Chakroun R, Al-Mur BA, Halawani RF, Aloufi FA, Chaabani A, et al. Design of a new phthalocyanine-based ion-imprinted polymer for selective lithium recovery from desalination plant reverse osmosis waste. Polymers. 2023;15(18):3847. [CrossRef].
95. Yang J, Qu G, Liu C, Zhou S, Li B, Wei Y. An effective lithium ion-imprinted membrane containing 12-crown ether-4 for selective recovery of lithium. Chem Eng Res Des. 2022;184:639–50. [CrossRef].
96. Luo X, Guo B, Luo J, Deng F, Zhang S, Luo S, et al. Recovery of lithium from wastewater using development of Li ion-imprinted polymers. ACS Sustainable Chem Eng. 2015;3(3):460–7. [CrossRef].
97. Yu C, Lu J, Dai J, Dong Z, Lin X, Xing W, et al. Bio-inspired fabrication of Ester-functionalized imprinted composite membrane for rapid and high-efficient recovery of lithium ion from seawater. J Colloid Interface Sci. 2020;572:340–53. [CrossRef].
98. Prigyai N, Trakulmututa J, Bunchuay T, Sangtawesin T. Gamma radiation synthesized POSS crown ether polymers for efficient and selective lithium recovery from seawater. Chem Eng J Adv. 2025;24:100924. [CrossRef].
99. Liang C, Zhang X, Liu W, Song X, Sun S, Fu D, et al. Thermo-responsive ion imprinted polymer on the surface of magnetic carbon nanospheres for recognizing and capturing low-concentration lithium ion. Miner Eng. 2023;201:108210. [CrossRef].
100. Zavahir S, Riyaz NS, Elmakki T, Tariq H, Ahmad Z, Chen Y, et al. Ion-imprinted membranes for lithium recovery: A review. Chemosphere. 2024;354:141674. [CrossRef].
101. Lu J, Qin Y, Wu Y, Meng M, Yan Y, Li C. Recent advances in ion-imprinted membranes: Separation and detection via ion-selective recognition. Environ Sci Water Res Technol. 2019;5(10):1626–53. [CrossRef].
102. Hou B, Feng Q, Guo K, Wang Y, Fan J, Kong Y, et al. Investigation of imprinted polymers for lithium-ion recovery from low-grade brine: Preparation, application, and evaluation. Environ Sci Technol. 2026;60(19):13782–95. [CrossRef].
103. Meouche W, Branger C, Beurroies I, Denoyel R, Margaillan A. Inverse suspension polymerization as a new tool for the synthesis of ion-imprinted polymers. Macromol Rapid Commun. 2012;33(10):928–32. [CrossRef].
104. Shao H, Li C, Ma C, Sun L, Chen R, Cheng R, et al. An ion-imprinted material embedded carbon quantum dots for selective fluorometric determination of lithium ion in water samples. Microchim Acta. 2017;184(12):4861–8. [CrossRef].
105. Sun D, Zhou T, Lu Y, Yan Y, Liu C, Che G. Ion-imprinted antifouling nanocomposite membrane for separation of lithium ion. Korean J Chem Eng. 2022;39(9):2482–90. [CrossRef].
106. Ke J, Li X, Zhao Q, Hou Y, Chen J. Ultrasensitive quantum dot fluorescence quenching assay for selective detection of mercury ions in drinking water. Sci Rep. 2014;4:5624. [CrossRef].
107. Zhou Z, Kong D, Zhu H, Wang N, Wang Z, Wang Q, et al. Preparation and adsorption characteristics of an ion-imprinted polymer for fast removal of Ni(II) ions from aqueous solution. J Hazard Mater. 2018;341:355–64. [CrossRef].
108. Chaipuang A, Phungpanya C, Thongpoon C, Watla-Iad K, Inkaew P, Machan T, et al. Synthesis of copper(II) ion-imprinted polymers via suspension polymerization. Polym Adv Technol. 2018;29(12):3134–41. [CrossRef].
109. Fei JJ, Wu XH, Sun YL, Zhao LY, Min H, Cui XB, et al. Preparation of a novel amino functionalized ion-imprinted hybrid monolithic column for the selective extraction of trace copper followed by ICP-MS detection. Anal Chim Acta. 2021;1162:338477. [CrossRef].
110. Yu Z, Dai J, Yan Y, Hu H. Ion-imprinted polymers supported by $SiO_2$ with a chitosan incorporated sol-gel process for selective separation of Pb(II) and Cu(II) system. In: Proceedings of the 2011 International Symposium on Water Resource and Environmental Protection; 2011 May 20–22; Xi'an, China. Piscataway, NJ, USA: IEEE; 2011. p. 2921–4. [CrossRef].
111. He HX, Gan Q, Feng CG. An ion-imprinted silica gel polymer prepared by surface imprinting technique combined with aqueous solution polymerization for selective adsorption of Ni(II) from aqueous solution. Chin J Polym Sci. 2018;36(4):462–71. [CrossRef].
112. Urbanová J, Beliančínová K, Pipíška M, Frišták V, Ďuriška L, Feng Y, et al. Immobilization of ion-imprinted polymers on biochar for selective lithium ion recovery. E3S Web Conf. 2025;667:02005. [CrossRef].

113. Cui Y, Du W, Zhao H, Kang W, Liu X, Yang Y. A novel recyclable surface ion-imprinted graphene aerogels for high selective adsorption of lithium in salt lake brine. Surf Interfaces. 2025;56:105574. [CrossRef].
114. Alshuiael SM, Al-Ghouti MA. Development of a novel tailored ion-imprinted polymer for recovery of lithium and strontium from reverse osmosis concentrated brine. Sep Purif Technol. 2022;295:121320. [CrossRef].
115. Lyu D, Märker K, Zhou Y, Zhao EW, Gunnarsdóttir AB, Niblett SP, et al. Understanding sorption of aqueous electrolytes in porous carbon by NMR spectroscopy. J Am Chem Soc. 2024;146(14):9897–910. [CrossRef].
116. Han N, Li Y, Peng H, Gao R, He Q, Miao Z, et al. Adsorption of $Li^+$ by imprinted capacitor deionization—A new method for selective recovery of valuable lithium in acidic solutions. Desalination. 2023;565:116820. [CrossRef].
117. Roobavannan S, Choo Y, Truong DQ, Han DS, Shon HK, Naidu G. Seawater lithium mining by zeolitic imidazolate framework encapsulated manganese oxide ion sieve nanomaterial. Chem Eng J. 2023;474:145957. [CrossRef].
118. Yu Z, Mao Z, Guo S, Li Y, Cheng X, Li C, et al. Adsorption-responsive bionic photothermal ion pump for reversible seawater lithium extraction. Nat Commun. 2025;16(1):8825. [CrossRef].
119. Han Y, Ma J, Liu D, Yang Y, Zhang T, Wang M, et al. Microenvironment-modulating adsorption enables highly efficient lithium extraction under natural pH conditions. ACS Nano. 2024;18(12):9071–81. [CrossRef].
120. Zhang W, Wu M, Xin Y, Liu H, Li F, Fa Y. Comparative analysis of seawater uranium extraction materials: Toward the development of bio-based and biomimetic materials. Coord Chem Rev. 2025;534:216589. [CrossRef].
121. Li Y, Zheng Y, Ahamd Z, Zhu L, Yang J, Chen J, et al. Strategies for designing highly efficient adsorbents to capture uranium from seawater. Coord Chem Rev. 2023;491:215234. [CrossRef].
122. Wu Y, Xie Y, Liu X, Li Y, Wang J, Chen Z, et al. Functional nanomaterials for selective uranium recovery from seawater: Material design, extraction properties and mechanisms. Coord Chem Rev. 2023;483:215097. [CrossRef].
123. Zhang D, Liu L, Zhao B, Wang X, Pang H, Yu S. Highly efficient extraction of uranium from seawater by polyamide and amidoxime co-functionalized MXene. Environ Pollut. 2023;317:120826. [CrossRef].
124. Zhang L, Yang S, Qian J, Hua D. Surface ion-imprinted polypropylene nonwoven fabric for potential uranium seawater extraction with high selectivity over vanadium. Ind Eng Chem Res. 2017;56(7):1860–7. [CrossRef].
125. Yuan Y, Meng Q, Faheem M, Yang Y, Li Z, Wang Z, et al. A molecular coordination template strategy for designing selective porous aromatic framework materials for uranyl capture. ACS Cent Sci. 2019;5(8):1432–9. [CrossRef].
126. Zhao Y, Li J, Wu S, Cheng H. Ion-imprinted guanidine-functionalized zeolite molecular sieves enhance the adsorption selectivity and antibacterial properties for uranium extraction. RSC Adv. 2022;12(24):15470–8. [CrossRef].
127. Monier M, Elsayed NH. Selective extraction of uranyl ions using ion-imprinted chelating microspheres. J Colloid Interface Sci. 2014;423:113–22. [CrossRef].
128. Yuan Y, Yang Y, Ma X, Meng Q, Wang L, Zhao S, et al. Molecularly imprinted porous aromatic frameworks and their composite components for selective extraction of uranium ions. Adv Mater. 2018;30(12):e1706507. [CrossRef].
129. Zuo B, Wang R, Zuo J, Abdelfattah W, Helal MH, Yan G, et al. Thermally-switchable adsorbent for selective uranium extraction from wastewater. Chem Eng J. 2024;500:156484. [CrossRef].
130. Tang L, Ren S, Zhang T, Wei X, Li M, Yin X, et al. $UO_2^{2+}$-imprinted thermoresponsive hydrogel for accumulation of uranium from seawater. Chem Eng J. 2021;425:130589. [CrossRef].
131. Yang X, Liu W, Han P, You Y, Lv J, Zhang X, et al. Antimicrobial ion-imprinted chitosan-derived hydrogel with quaternary ammonium and thermoresponsive components for $UO_2^{2+}$ adsorption. Int J Biol Macromol. 2024;275(Pt 2):133532. [CrossRef].
132. Preetha CR, Gladis JM, Rao TP, Venkateswaran G. Removal of toxic uranium from synthetic nuclear power reactor effluents using uranyl ion imprinted polymer particles. Environ Sci Technol. 2006;40(9):3070–4. [CrossRef].
133. Endrizzi F, Rao L. Chemical speciation of uranium(VI) in marine environments: Complexation of calcium and magnesium ions with $[(UO_2)(CO_3)_3]^{4-}$ and the effect on the extraction of uranium from seawater. Chem A Eur J. 2014;20(44):14499–506. [CrossRef].
134. Singh DK, Mishra S. Synthesis and characterization of $UO_2^{2+}$-ion imprinted polymer for selective extraction of $UO_2^{2+}$. Anal Chim Acta. 2009;644(1–2):42–7. [CrossRef].
135. Cheng G, Zhang A, Zhao Z, Chai Z, Hu B, Han B, et al. Extremely stable amidoxime functionalized covalent organic frameworks for uranium extraction from seawater with high efficiency and selectivity. Sci Bull. 2021;66(19):1994–2001. [CrossRef].

136. Huang YC, Wang CZ, Wu QY, Lan JH, Nie CM, Chen SS, et al. Theoretical exploration of the synergistic effect of phosphate and amidoxime for uranium recovery from seawater. Inorg Chem. 2024;63(52):24685–96. [CrossRef].
137. Cao M, Wang Y, Feng L, Zhao S, Wang H, Liu T, et al. Ion-imprinted nanocellulose aerogel with comprehensive optimized performance for uranium extraction from seawater. Chem Eng J. 2023;475:146048. [CrossRef].
138. Mo H, Chen T, Jiang C, Wang Z, Meng X, Wu F, et al. Combining synergistic interaction and ion imprinting to improve adsorption capacity for selective uranium extraction from seawater. Radiochim Acta. 2025;113(2):113–24. [CrossRef].
139. Kusumkar VV, Galamboš M, Viglašová E, Daňo M, Šmelková J. Ion-imprinted polymers: Synthesis, characterization, and adsorption of radionuclides. Materials. 2021;14(5):1083. [CrossRef].
140. Su Y, Wenzel M, Seifert M, Weigand JJ. Surface ion-imprinted brewer's spent grain with low template loading for selective uranyl ions adsorption from simulated wastewater. J Hazard Mater. 2022;440:129682. [CrossRef].
141. Meng H, Li Z, Ma F, Wang X, Zhou W, Zhang L. Synthesis and characterization of surface ion-imprinted polymer based on $SiO_2$-coated graphene oxide for selective adsorption of uranium(VI). RSC Adv. 2015;5(83):67662–8. [CrossRef].
142. Wang R, Sun R, Lin Y, Wang Y, Ding Z, Sun C. Mechanism insights into uranyl ion adsorption interactions with functional groups for uranium extraction from seawater. Chem Eng Sci. 2026;323:123262. [CrossRef].
143. Wang Y, Jiang Y, Zhang Y, Liu X, Sun S, Qin S, et al. Construction of amidoxime-functionalized magnetic hydroxyapatite with enhanced uranium extraction performance from aqueous solution and seawater. Chemosphere. 2023;343:140257. [CrossRef].
144. Anirudhan TS, Nima J, Divya PL. Adsorption and separation behavior of uranium(VI) by 4-vinylpyridine-grafted-vinyltriethoxysilane-cellulose ion imprinted polymer. J Environ Chem Eng. 2015;3(2):1267–76. [CrossRef].
145. Gan J, Zhang L, Wang Q, Xin Q, Xiong Y, Hu E, et al. Phosphorylation improved the competitive U/V adsorption on chitosan-based adsorbent containing amidoxime for rapid uranium extraction from seawater. Int J Biol Macromol. 2023;238:124074. [CrossRef].
146. Zhu J, Zhao L, Song D, Yu J, Liu Q, Liu J, et al. Graphene oxide based ion-imprinted polymers for selective uranium adsorption from seawater. Appl Surf Sci. 2023;640:158378. [CrossRef].
147. Yan B, Ma C, Gao J, Yuan Y, Wang N. An ion-crosslinked supramolecular hydrogel for ultrahigh and fast uranium recovery from seawater. Adv Mater. 2020;32(10):e1906615. [CrossRef].
148. Fasihi J, Ammari Alahyari S, Shamsipur M, Sharghi H, Charkhi A. Adsorption of uranyl ion onto an anthraquinone based ion-imprinted copolymer. React Funct Polym. 2011;71(8):803–8. [CrossRef].
149. Wang J, Li J, Li H, Ding L. Modulated ion recognition by thermosensitive ion-imprinted hydrogels with IPN structure. Mater Lett. 2014;131:9–11. [CrossRef].
150. Wang JJ, Liu F. Thermoresponsive ion-imprinted hydrogels with interpenetrating network structure for removal of heavy metal ions. Adv Mater Res. 2013;643:83–6. [CrossRef].
151. Zhong X, Sun Y, Zhang Z, Dai Y, Wang Y, Liu Y, et al. A new hydrothermal cross-linking ion-imprinted chitosan for high-efficiency uranium removal. J Radioanal Nucl Chem. 2019;322(2):901–11. [CrossRef].
152. Ling C, Liu X, Yang X, Hu J, Li R, Pang L, et al. Uranium adsorption tests of amidoxime-based ultrahigh molecular weight polyethylene fibers in simulated seawater and natural coastal marine seawater from different locations. Ind Eng Chem Res. 2017;56(4):1103–11. [CrossRef].
153. Sun W, Feng L, Zhang J, Lin K, Wang H, Yan B, et al. Amidoxime group-anchored single cobalt atoms for anti-biofouling during uranium extraction from seawater. Adv Sci. 2022;9(10):e2105008. [CrossRef].
154. Butler KT, Davies DW, Cartwright H, Isayev O, Walsh A. Machine learning for molecular and materials science. Nature. 2018;559(7715):547–55. [CrossRef].
155. Abney CW, Mayes RT, Saito T, Dai S. Materials for the recovery of uranium from seawater. Chem Rev. 2017;117(23):13935–4013. [CrossRef].
156. Chen L, Wang X, Lu W, Wu X, Li J. Molecular imprinting: Perspectives and applications. Chem Soc Rev. 2016;45(8):2137–211. [CrossRef].
157. Stuart MA, Huck WT, Genzer J, Müller M, Ober C, Stamm M, et al. Emerging applications of stimuli-responsive polymer materials. Nat Mater. 2010;9(2):101–13. [CrossRef].
158. Park J, Gill GA, Strivens JE, Kuo LJ, Jeters RT, Avila A, et al. Effect of biofouling on the performance of amidoxime-based polymeric uranium adsorbents. Ind Eng Chem Res. 2016;55(15):4328–38. [CrossRef].

159. Liu J, Chen J, Liu S, Li T, Chen Y, Chen L, et al. Mechanical training drives structural remodeling of zwitterionic hydrogels. Mater Horiz. 2025;12(18):7473–85. [CrossRef].